

# The Impact of Lipid Constraints on Model Membranes

## Dissertation

zur Erlangung des Doktorgrades der Naturwissenschaften  
(Dr. rer. nat.)

der

Naturwissenschaftlichen Fakultät II  
Chemie, Physik und Mathematik

der Martin-Luther-Universität  
Halle-Wittenberg,

vorgelegt von

Herrn Matthias Hoffmann  
geb. am 9. April 1995 in Gotha



**First Reviewer**

Prof. Dr. Dariush Hinderberger  
MLU Halle-Wittenberg  
Institute of Physical Chemistry  
Von-Danckelmann-Platz 4  
06120 Halle (Saale)  
Germany

**Second Reviewer**

Prof. Dr. Heinz-Jürgen Steinhoff  
Universität Osnabrück  
Institute of Physics  
Barbarastrasse 7  
49076 Osnabrück  
Germany

Day of public defense: 10.02.2022



Ich erkläre an Eides statt, dass ich die hier vorliegende Arbeit selbstständig und ausschließlich unter Nutzung der angegebenen Hilfsmittel und Quellen angefertigt habe.

Alle Textstellen, die wörtlich oder sinngemäß aus Veröffentlichungen entnommen sind, habe ich als solche kenntlich gemacht.

Ich versichere weiterhin, dass ich diese Arbeit an keiner anderen Institution eingereicht habe.

Mir ist bekannt, dass bei Angabe falscher Aussagen die Prüfung als nicht bestanden gilt, und versichere mit meiner Unterschrift die Richtigkeit dieser Angaben. Ich erkenne alle rechtlichen Grundlagen an.

---

Matthias Hoffmann

---

Datum

## Abstract

What are the main influences governing the behavior of lipids within lipid model membranes? This question concerns nearly all membrane-related biochemical and biophysical research. However, in many cases the consequences of structural variations within the involved lipids or the impact of exogenous molecules, that are introduced during the study, are not addressed. This thesis aims at giving answers to this main question in the context of some exemplary model systems.

To address different possibilities in influencing lipid behavior and the varying complexity of well-established lipid model membranes, this thesis is divided into two main projects: the study of (i) the impact of an intramolecular change within the lipids in monolayers at the air/water interface and of (ii) the effect of three amphiphilic copolymers on lipid bilayers, consisting of either a simple model lipid or myelin-like complex lipid mixtures, during the formation of polymer-encapsulated nanodiscs.

In the first project, the model lipid 1,2-dipalmitoyl-*sn*-glycero-3-phosphocholine (DPPC), which contains two fatty acids esterified to the glycerol backbone, was compared with its monoether analogue 1-palmitoyl-2-*O*-hexadecyl-*sn*-glycero-3-phosphocholine (PHPC) bearing a fatty acid and a long-chain alkyl ether. The study of lipid monolayers containing one of both lipids revealed differences in the lipids' chain tilt angles, hydration of their headgroups and carbonyl groups, and altered ordering of carbonyl-near chain segments. These differences were attributed to a rearrangement of the glycerol backbone at the air/water interface induced by substituting just one ester bond by an ether linkage. Langmuir monolayers of mixtures of both lipids showed non-ideal mixing behavior despite their similarity.

In the second part of this thesis, the influences of two anionic polymers and one zwitterionic polymer on the model lipid 1,2-dimyristoyl-*sn*-glycero-3-phosphocholine (DMPC) and complex myelin-like lipid mixtures were characterized. The studied polymers affected the temperature-dependent behavior of DMPC and changed the water accessibility in different positions of the bilayer as well as the rotational freedom of the lipids as can be concluded from continuous wave electron paramagnetic resonance (CW EPR) spectroscopical results.

The formation of myelin-like nanodiscs was complicated by the complex lipid mixtures containing natural lipids and cholesterol. Nevertheless, solubilization could be achieved. Two styrene-based copolymers were able to solubilize myelin-like liposomes without pronounced preferences for distinct lipids. Similar effects as in DMPC nanodiscs were found in this system by application of CW EPR spectroscopy, that are additional constraints caused by the polymers onto lipid order and mobility both in the membrane core and the carbonyl-near chain segment. Addition of a bilayer-stacking model protein induced association of nanodiscs encapsulated by poly-(styrene-*co*-maleic acid) (SMA) indicating a possible use of these nanodiscs as a model system for the human myelin sheath.

## Kurzdarstellung

Was sind die Haupteinflüsse auf das Verhalten von Lipiden in Lipidmodellmembranen? Die Antwort auf diese Frage betrifft fast alle biochemischen und biophysikalischen Untersuchungen, in denen Lipidmembranen von Bedeutung sind. Trotz der Vielzahl an möglichen Einflüssen, hervorgerufen durch strukturelle Unterschiede der Lipide oder die Zugabe von membranassoziierten Fremdmolekülen, werden diese häufig nicht im Detail betrachtet. Das Ziel dieser Dissertation ist es, die Wirkung verschiedener Faktoren auf eine Auswahl an Lipidmodellmembranen zu untersuchen. Um den vielfältigen Einflussmöglichkeiten und der unterschiedlichen Komplexität verschiedener Modellsysteme gerecht zu werden, ist diese Arbeit in zwei Projekte aufgeteilt. Die Projekte behandeln (i) den Einfluss einer molekularen Änderung innerhalb der Lipidmoleküle auf deren Monoschichten an der Wasser-Luft-Grenzfläche und (ii) den Einfluss von drei amphiphilen Copolymeren auf Lipiddoppelschichten eines Modelllipids und zwei myelinartiger, komplexer Lipidmischungen in polymergestützten Lipidnanodiscs.

Im ersten Teil dieser Arbeit wurden das Modelllipid 1,2-Dipalmitoyl-*sn*-glycero-3-phosphocholin (DPPC), das zwei veresterte Fettsäureketten trägt, und dessen einfach verethertes Analogon 1-Palmitoyl-2-*O*-hexadecyl-*sn*-glycero-3-phosphocholin (PHPC) in Lipidmonoschichten an der Wasser-Luft-Grenzfläche miteinander verglichen und Unterschiede in der Lipidordnung und -hydratation gefunden. Diese Unterschiede zwischen DPPC und PHPC konnten durch eine Umordnung des Glycerol-Rückgrates erklärt werden. Gemischte Monoschichten beider Lipide verhielten sich trotz deren Ähnlichkeit nicht ideal.

Im zweiten Projekt wurde der Einfluss von zwei anionischen und einem zwitterionischen Copolymer auf das Modelllipid 1,2-Dimyristoyl-*sn*-glycero-3-phosphocholin (DMPC) und auf komplexe, myelinartige Lipidmischungen untersucht. Aus Ergebnissen der Elektronenspinresonanz-Spektroskopie bei kontinuierlicher Mikrowelleneinstrahlung (CW EPR) ging hervor, dass die drei Polymere das temperaturabhängige Verhalten von DMPC, die Penetration der Doppelschicht durch Wasser und die Rotationsfreiheit der Lipide in zwei untersuchten Positionen innerhalb der Membran beeinflussten.

Im Vergleich zu DMPC war die Nanodiscbildung von myelinähnlichen Lipidmischungen durch enthaltene natürliche Lipide und Cholesterol erschwert. Trotzdem konnten myelinartige Nanodiscs ohne Bevorzugung bestimmter Lipide mithilfe zweier styrolbasierter Copolymere erzeugt werden. Auch in diesem System waren zusätzliche Einschränkungen der Lipidordnung und -mobilität in der Mitte der Membran und dem Kettensegment nahe den Carbonylgruppen mit Hilfe der CW EPR Spektroskopie nachweisbar. Die Zugabe eines Modellproteins, das in der Myelinscheide die Membranen aneinanderbindet, sorgte für eine Assoziation von Nanodiscs, die durch Poly-(styrol-co-maleinsäure) (SMA) gebildet wurden, was eine Verwendung dieser als Modellsystem für die menschliche Myelinscheide ermöglichen könnte.

# Table of Contents

1	Publication List .....	1
2	Introduction.....	4
3	Theory .....	8
3.1	Methods.....	8
3.1.1	Infrared reflection absorption spectroscopy (IRRAS).....	8
3.1.2	Continuous wave electron paramagnetic resonance (CW EPR) spectroscopy .....	9
3.2	Ether Lipids .....	10
3.3	Nanodiscs.....	12
3.3.1	Nanodiscs in the context of commonly used lipid model systems.....	12
3.3.2	The formation of nanodiscs.....	14
3.3.3	Nanodiscs in protein research.....	16
4	Results .....	18
4.1	Overview over the published papers .....	18
4.1.1	The impact of a single ether bond within the lipid on the behavior of its monolayer at the air/water interface .....	18
4.1.2	The influence of different polymers on DMPC nanodiscs .....	19
4.1.3	Mimicking the human myelin sheath with myelin-like nanodiscs.....	20
4.2	Publications .....	21
5	Discussion .....	60
6	Conclusions and Outlook.....	66
7	References .....	69
8	List of Abbreviations and Symbols .....	77
8.1	Abbreviations.....	77
8.2	Symbols.....	78
9	Acknowledgments .....	79
10	Academic Curriculum Vitae.....	80

# 1 Publication List

[P1] M. Hoffmann, S. Drescher, C. Ihling, D. Hinderberger and C. Schwieger

**An Azidolipid Monolayer – Transitions, Miscibility, and UV Reactivity Studied by Infrared Reflection Absorption Spectroscopy<sup>1</sup>**  
*Langmuir* **2020**, 36, 43, 12804-12815

The research for this publication was mainly performed during my Master's thesis supervised by C. Schwieger and D. Hinderberger. In short, I was responsible for all measurements and data evaluation besides mass spectrometric (MS) experiments. S. Drescher and K. Gruhle synthesized the studied azidolipid. The MS experiments, their interpretation, and reviewing was done by C. Ihling. C. Schwieger, S. Drescher, and D. Hinderberger supervised the whole project. During my doctorate research, I completed the experiments mainly including IRRAS and MS measurements and wrote the paper draft. In addition, I contributed to the reviewing process which was done by all authors.

[P2] M. Hoffmann, S. Drescher, C. Schwieger and D. Hinderberger

**Influence of a Single Ether Bond on Assembly, Orientation, and Miscibility of Phosphocholine Lipids at the Air-Water Interface**  
*Phys. Chem. Chem. Phys.* **2021**, 23, 5325-5339

For this publication, I performed the major part of sample preparation and data analysis. I planned the experiments and contributed to the conceptualization of the work. In addition, I wrote the publication draft and assisted in all reviewing and editing steps during the publication process. S. Drescher and K. Gruhle synthesized the ether lipid PHPC. S. Drescher also contributed to the writing and review process and added valuable advice to data interpretation. C. Schwieger and D. Hinderberger supervised the project. C. Schwieger performed further experiments and contributed to data analysis. He also wrote all software scripts used for evaluations and took part in writing and editing. D. Hinderberger, additionally, supervised all steps of research and the publication process.

---

<sup>1</sup> [P1] will not be shown in full text in this thesis to avoid overlap with my Master's thesis, where most of the results are already published.

[P3] J. Eisermann, M. Hoffmann, F. A. Schöffmann, M. Das, C. Vargas, S. Keller and D. Hinderberger

**Molecular-level interactions of nanodisc-forming copolymers dissected by EPR spectroscopy<sup>2</sup>**

*Macromol. Chem. Phys.* **2021**, 222, 2100051.

In this project, I contributed to planning of experiments. Furthermore, I mostly prepared the studied samples. J. Eisermann, F. A. Schöffmann, and I performed all experiments. J. Eisermann and F. A. Schöffmann were responsible for conducting and evaluating the CW EPR spectroscopic measurements, while I did the other experiments and the respective evaluations. M. Das and C. Vargas synthesized the studied polymers. J. Eisermann, F. A. Schöffmann, and I wrote the publication and all authors were involved in reviewing during the publication process. S. Keller and D. Hinderberger supervised the work.

[P4] M. Hoffmann, J. Eisermann, F. A. Schöffmann, M. Das, C. Vargas, S. Keller and D. Hinderberger

**Influence of Different Polymer Belts on Lipid Properties in Nanodiscs Characterized by CW EPR Spectroscopy**

*BBA Biomembranes* **2021**, 1863 (10), 183681.

In this work, I was responsible for planning and conducting all experiments besides CW EPR measurements. I prepared samples and performed dynamic light scattering (DLS) and differential scanning calorimetry (DSC) experiments as well as the respective data evaluation. In addition, I contributed to electron microscopy sample preparation and imaging. Additionally, A. Rother helped with the electron microscopy. F. A. Schöffmann and J. Eisermann performed CW EPR measurements and data evaluation to which I contributed partly. The paper draft was written by J. Eisermann, F. A. Schöffmann, and me. F. A. Schöffmann, J. Eisermann, D. Hinderberger, and I contributed to the reviewing process. M. Das and C. Vargas synthesized and purified the used polymers. S. Keller and D. Hinderberger supervised the work.

---

<sup>2</sup> [P3] will not be shown in full text in this thesis to avoid overlap with the future dissertation of F. A. Schöffmann.

[P5] M. Hoffmann, D. Haselberger, T. Hofmann, L. Müller, K. Janson, A. Meister, M. Das, C. Vargas, S. Keller, P. L. Kastritis, C. Schmidt and D. Hinderberger

**A Nanoscale Model System for the Human Myelin Sheath**

*Biomacromolecules* **2021**, accepted for publication.

For this publication, I was responsible for a major part of planning of the work. I performed experiments and evaluated the results. Furthermore, I supervised D. Haselberger in his Master's thesis while he performed experiments and interpretations. In detail, the first experiments and the concluding measurements were conducted by me. D. Haselberger did sample preparation, DLS, size exclusion chromatography (SEC), DSC, and CW EPR experiments under my supervision and high-performance liquid chromatography (HPLC) measurements under the supervision of L. Müller. A. Rother and I performed electron microscopy. Data evaluation and interpretation were done by D. Haselberger and me. The evaluation steps done with the CW EPR data were conducted exclusively by me. I wrote the paper draft and all authors contributed to the reviewing process prior to publication. T. Hofmann was responsible for MS measurements under supervision of C. Schmidt. K. Janson, A. Meister, and P. L. Kastritis were involved in TEM measurement and interpretation and had major impact on the microscopy experiments shown in this publication. M. Das and C. Vargas synthesized, purified, and characterized the used polymers under the supervision of S. Keller. D. Hinderberger supervised the whole work and contributed to all stages of planning, writing and reviewing of the paper.

The results presented in this thesis are mainly published in [P2], [P4], and [P5]. In the remaining two publications, [P1] and [P3], I participated in all phases of research and writing either during my Master's thesis or during my doctorate. Both of these publications are listed here and contribute as groundwork to this thesis but are not reprinted within this thesis or discussed in detail.

## 2 Introduction

How are the properties of supramolecular lipid assemblies affected by molecular changes of single components? In modern research, a variety of lipid model systems are applied to mimic the behavior of natural membranes.<sup>1-4</sup> They can be as elementary as detergent micelles or as complex as nanodiscs encapsulated by amphiphilic molecules.<sup>1-5</sup> To be suitable for studying biomolecules, such as proteins, the utilized systems have to be as nature-like as possible, while they can still be handled efficiently. Despite such model systems being used for decades, some molecular properties of the lipids, such as lipid order and hydration, are still not well understood. To increase knowledge in the field of supramolecular lipid assemblies and constraints affecting them, different model systems with increasing complexity are characterized for this dissertation.

In the first presented project, the effect of substituting one ester group of the lipid molecule with an ether bond on the supramolecular assembly is studied in a well-known model system. The lipids used here are 1,2-dipalmitoyl-*sn*-glycero-3-phosphocholine (DPPC) and its *sn*-2 ether analogue 1-palmitoyl-2-*O*-hexadecyl-*sn*-glycero-3-phosphocholine (PHPC). Both molecules differ in their molecular structure as can be seen in **Figure 2.1**. While both lipid chains in DPPC are connected to the headgroup via ester bonds, PHPC possesses one ester bond in *sn*-1 and an ether bond in *sn*-2 position. In the current work, both lipids are compared within lipid monolayers at the air/water interface. The model system of such Langmuir monolayers is well suited for studying lipids due to highly advanced methods being available for manipulation and observation of the whole assembly.<sup>6-7</sup> Because the lipids are situated

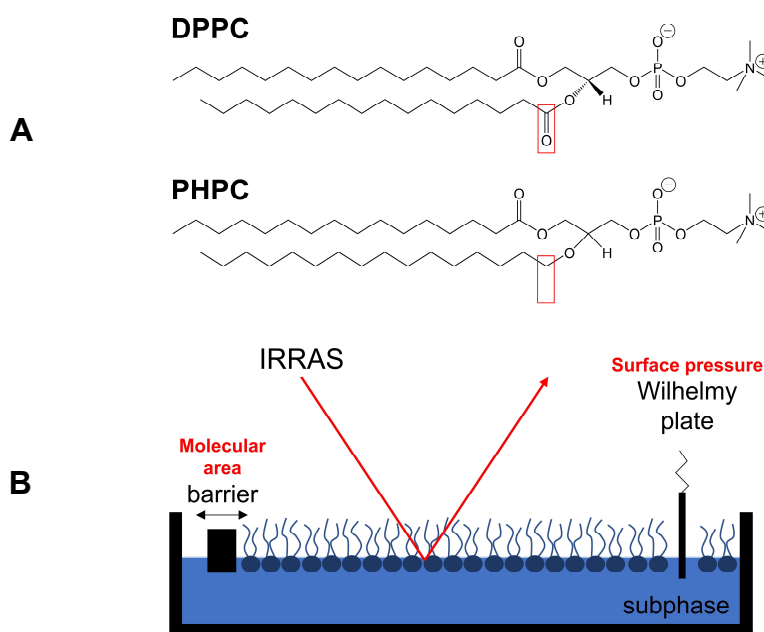


**Figure 2.1.** **A**, chemical structures of the ester lipid DPPC and the monoether lipid PHPC used in this thesis (the main structural difference is marked red), and **B**, schematical representation of a lipid monolayer at the air/water interface in the IRRAS measurement setup.

at the interface between air and water, they can be easily compressed or expanded while being investigated by e.g. infrared reflection absorption spectroscopy (IRRAS)<sup>6-7</sup> (as is depicted in **Figure 2.1B**) and epi-fluorescence microscopy.<sup>6</sup>

In the second part of this thesis, a model system of increased complexity is presented consisting of polymer/lipid nanodiscs.<sup>5,8-9</sup> In these particles, the lipid bilayer membrane is encapsulated by amphiphilic copolymers that form the rim of the disc and shield the hydrophobic chains of the lipids from surrounding water molecules.<sup>5,10</sup> To characterize the effect of different polymers on the encapsulated lipids is the goal of this part of my studies.

The nanodisc technique is promising for biochemical research because of the capability of the copolymers to solubilize natural membranes including lipids and proteins without the need for detergents.<sup>5,10-11</sup> Most of the published work focusses on the basic research of polymers, e.g. by solubilizing simple model lipids,<sup>8,12-13</sup> or on solubilizing cell membranes for protein research.<sup>11,14</sup> First, the interactions between the polymers and small molecules including model lipids are not understood completely despite this knowledge being essential for more complex studies with proteins involved. This thesis aims at contributing to the field of research by studying the interactions between three amphiphilic copolymers and the model lipid 1,2-dimyristoyl-*sn*-glycero-3-phosphocholine (DMPC).

Published nanodisc research is mostly done in a bottom-up approach, *i.e.*, by solubilizing model compounds, or a top-down approach, that is by solubilizing complex natural membranes. A further part of this thesis presents the solubilization of artificial liposomes consisting of natural lipids resembling the lipid composition of the cytosolic membrane leaflet of human myelin. This approach fits in between both usually applied procedures. Therefore, it ensures an appropriately accessible handling of the samples while avoiding over-simplification of the natural system of interest. For this, the human myelin sheath is mimicked with polymer/lipid nanodiscs containing natural brain lipids in a nature-like composition.

Both aspects of the polymer-encapsulated nanodisc research have in common that different constraints are exerted onto the lipids by other molecules rather than due to molecular changes within the lipids compared to the study of PHPC and DPPC. By splitting the research of polymer/lipid interactions into two parts, an unambiguous interpretation of (i) the impact of the nanodisc-forming polymers on simple systems such as DMPC membranes and (ii) changes caused by increased complexity of nature-like membranes was ensured.

Observation of DMPC solubilization presents several advantages over other lipids, in the first place:

- DMPC contains the phosphocholine (PC) headgroup which is highly abundant in most natural membrane systems<sup>15-16</sup> and zwitterionic without the formation of intermolecular hydrogen bonds.<sup>17</sup>
- Nanodisc formation by polymers is known to depend on lipid chain length and the degree of saturation, that is, short-chained and saturated lipids are

solubilized at lower temperatures than unsaturated lipids with long chains.<sup>8</sup> DMPC with its short, saturated chains, hence, is well suited for such solubilization experiments.

- The main transition temperature of DMPC was found to be approximately 23 °C.<sup>18</sup> At this temperature, the lipid membrane changes its fluidity and lateral order together with other parameters abruptly due to a phase transition between two adjacent mesophases of this liquid crystalline molecule.<sup>19</sup> Therefore, both the gel phase and the liquid crystalline phase can be observed near room temperature with methods sensitive for these properties.

The focus of the first lipid nanodisc study lies in unraveling the interactions between DMPC and three nanodisc-forming polymers, that are poly-(styrene-co-maleic acid) (SMA),<sup>8-9</sup> poly-(diisobutylene-*alt*-maleic acid) (DIBMA),<sup>13</sup> and poly-(styrene-co-maleimide sulfobetaine) (SMA-SB). The main method used here is continuous wave electron paramagnetic resonance (CW EPR) spectroscopy. Applying spin labeled lipids bearing the unpaired electron either at the chain termination or near the headgroup this method allows determination of lipid order and hydration at the center of the bilayer or near the carbonyls, respectively.<sup>20-23</sup> By varying the temperature during the experiments, the properties of different lipid phases are therefore readily observed. In the second study, the lipids occurring in natural human myelin were solubilized to form nanodiscs. The preparation of a suitable model system for the myelin sheath allows the study of all its major components (lipids and proteins) in an accessible system for research. Therefore, myelin-like nanodiscs could contribute to future studies regarding pathological conditions in diseases connected to demyelination processes, for instance. Since the lipid composition of the cytosolic leaflet of the human myelin membrane is mimicked, a high amount of cholesterol (37–44 %) has to be included as well as natural, unsaturated phospholipids with various chain lengths.<sup>24</sup> The heterogeneity of these membranes enables a variety of interactions between the lipids themselves and with other molecules such as the amphiphilic copolymers. For membranes of such a complexity, the preparation of nanodiscs in the first place is challenging.

With the knowledge gained from literature and the first part of this project, we were able to prepare myelin-like nanodiscs from SMA and SMA-SB and to study their lipid composition, lipid properties, and the natural function of the myelin basic protein (MBP) in these systems. To gain insight into the nanodiscs' properties it was necessary to use a variety of different methods such as dynamic light scattering (DLS), analytical high performance liquid chromatography (HPLC), mass spectrometry (MS), differential scanning calorimetry (DSC), transmission electron microscopy (TEM), and CW EPR spectroscopy. The combination of these techniques allowed a detailed characterization of the prepared nanodiscs.

The aim of this dissertation is to study different constraints exerted onto two types of lipid model membranes of increasing complexity. For this, Langmuir monolayers of lipids at the air/water interface were used as the first model system to unravel the effect

of a small structural change within the lipid molecules on the monolayer. In the second part of this work, amphiphilic copolymers were added to liposomes of (i) the model lipid DMPC and (ii) a myelin-like mixture containing natural lipids. The impact of these extrinsic molecules was subsequently studied in the thus formed lipid nanodiscs.

This cumulative thesis consists of six chapters. Prior to this introduction, a list of publications is presented containing all papers relevant for this thesis and the detailed author contributions. Next, this introduction is shown followed by a theoretical chapter, which briefly summarizes the methodological basics including helpful references to literature. The main focus of the theoretical chapter lies on introducing the studied systems to the reader, that are ether lipids and the rather new model system of polymer/lipid nanodiscs. The fourth chapter contains an overview over the published papers as well as reprints of the original papers. The results of the publications are then discussed in detail in the fifth chapter. The final part of this thesis draws conclusions and presents an outlook in the field of research.

## 3 Theory

### 3.1 Methods

In this work, a variety of methods, fitting to the type of studied model system, were used. In the case of lipid monolayers, isothermal surface pressure measurements during monolayer compression, IRRAS, and epi-fluorescence microscopy were applied. For liposomes and lipid nanodiscs, DLS, electron microscopy, DSC, HPLC, MS, and CW EPR spectroscopy were used. In this chapter, IRRAS and CW EPR spectroscopy are presented briefly as main methods for the respective projects.

#### 3.1.1 Infrared reflection absorption spectroscopy (IRRAS)

In the research of lipid monolayers, IRRAS has proven to be a well-suited method for studying lipids at the air/water interface.<sup>25</sup> Due to the scope of this thesis, the theory and application of IRRAS will be presented only as an overview. For detailed theoretical and experimental considerations, I refer to the extensive literature (e.g. references 7, 25-26).

IRRAS is based on focusing an IR beam on a reflecting surface and collecting the light after reflection and passing through a part of the sample. In the case of Langmuir monolayers, the reflecting plane is the interface between air and water including the monolayer. The data collected is the reflectance-absorbance ( $RA$ ) which is defined as

$$RA = -\lg \left( \frac{R}{R_{\text{ref}}} \right) \quad (3.1)$$

with  $R$  being the reflectivity of the film-covered interface containing all kinds of infrared (IR) spectroscopic information and  $R_{\text{ref}}$  being the reflectivity of the pure subphase surface. In contrast to typical IR absorption spectra,  $RA$  can be positive or negative depending on polarization and angle of the incoming IR light and orientation of the absorbing molecules at the interface.<sup>27</sup> By simulating the spectral intensities in IRRA spectra of lipid monolayers collected at various angles of incidence and both s- and p-polarization, the film thickness and the orientation of parts of the interfacial molecules can be obtained.<sup>28-30</sup> In biophysical studies of lipid monolayers, this approach is promising because it enables the characterization of the lipids<sup>25-26</sup> and even interactions between lipids and guest molecules, such as proteins adsorbed to the monolayer.<sup>7,25,31-32</sup> While being able to study the orientation of molecular moieties and the thickness of monolayers, IRRAS provides additional spectral information on the monolayer. IRRA spectra contain all molecular properties typically accessible by IR spectroscopy.<sup>26,31</sup> Regarding lipids, this is mostly the phase state and hydration of the different molecular moieties, *i.e.*, the hydrophobic chains, the glycerol backbone, and the headgroup.<sup>19,25-26</sup> Furthermore, observation of ion binding, protein adsorption, or even protein folding is possible.<sup>7,32-34</sup>

### 3.1.2 Continuous wave electron paramagnetic resonance (CW EPR) spectroscopy

In the second part of this work, the studied lipids were suspended in aqueous buffer solutions and, thus, were not observable by interfacial methods such as IRRAS. In the here used lipid nanodiscs and liposomes, the method of choice for characterizing the lipid ordering and hydration was CW EPR spectroscopy. For the theory and various applications of CW EPR spectroscopy an extensive number of publications is available. Therefore, I will only give a short introduction into the method. For a detailed discussion of CW EPR spectroscopic basics, I refer to the already published knowledge (see for example references 35-37).

As implied by the name of the method, electron paramagnetic resonance spectroscopy is the spectroscopic characterization of paramagnetic molecules.<sup>35-38</sup> To achieve absorption of light, as is typically done in spectroscopy, several requirements have to be met. These include the existence of an absorbing species (in this case an unpaired electron), the existence of differently populated states of the electron spin that are not degenerate, and an energy input via microwave irradiation with the energy corresponding to possible transitions between the non-degenerate states.<sup>38</sup> The latter is also called resonance condition which has to be fulfilled for a successful absorption of light. In EPR spectroscopy, the spacing between two adjacent spin states differing by an electron spin quantum number of  $\Delta m_s \pm 1$  depends on the external magnetic field due to the Zeeman effect and the properties of the unpaired electron and moieties adjacent to it, for example polarity and electronic structure.<sup>35-36</sup> All of these properties are covered by the spin Hamiltonian. The main elements of the spin Hamiltonian affecting the spacing between spin ground state and excited state for nitroxide radicals, which are used in this work, are the electron Zeeman interaction, spin-orbit interactions, hyperfine interactions, and electron-electron interactions.<sup>37-38</sup> From interactions between the electron spin and surrounding moieties or other molecules, several conclusions can be drawn regarding the structure and dynamics of the molecule bearing the unpaired electron.<sup>35-39</sup>

In this thesis, the unpaired electrons had to be introduced into the studied systems by adding stable radicals. The here used nitroxide radicals are stable due to their cyclic structure with methyl groups (or parts of the lipid chain) directly adjacent to the nitroxide moiety.<sup>40-41</sup> For detailed information on nitroxide radicals, I refer to chapter 3 of reference 40 and chapters 1, 3, and 5 of reference 41. These radicals degrade slowly<sup>40-41</sup> if stored correctly and can be introduced into studied model systems either directly by adding small molecules bearing the unpaired electron or by linking the nitroxide radicals covalently to molecules already present in the system of interest.<sup>41</sup> The latter approach enables, for example, the study of lipid model systems with minimal disturbance of the lipid bilayer. With that in mind, two different spin probes were used in this work which are based on a long chain phosphocholine lipid. The introduction of spin labeled lipids enables the observation of lipid properties such as hydration and rotational freedom with CW EPR spectroscopy.<sup>20-23,41</sup> For several lipid

model systems, spin label studies were performed in the last decades.<sup>20,22-23,42</sup> In this work, this approach will be applied to a new model system that is the polymer/lipid nanodisc.

### 3.2 Ether Lipids

Most of the natural lipid membranes consist of mainly ester lipids and cholesterol.<sup>16,24,43</sup> In some environments, however, ether lipids have evolved that possess several advantages over ester lipids. In Archaea, living in extreme environments, ether lipids are the main constituents of the lipid membranes due to their superior temperature, pH, and mechanical stability compared to ester lipids.<sup>44-46</sup> Chemically, ether lipids are not easily degraded by phospholipases, which remove lipid chains at their ester bond.<sup>47</sup> In extreme environments with low or high pH, ester bonds can also be catalytically cleaved, which is additionally accelerated by high temperatures.<sup>48-49</sup>

Besides monopolar ether lipids bearing two chains connected to one headgroup, bipolar tetraether lipids (TELs) are abundant in the membranes of Archaea.<sup>44</sup> These lipids consist of two long chains connected to headgroups on either side. Therefore, TELs span the whole membrane and enhance its mechanical stability.<sup>46</sup> Another effect caused by the existence of TELs is the exceptionally low ion permeability of the membrane.<sup>46</sup>

Archaea in extreme environments are able to adjust their membrane lipid composition according to the ambient temperature.<sup>46</sup> Thus, they tolerate a wide range of temperatures. The lipid composition of the membrane is adjusted while maintaining its liquid crystalline state by introducing longer chains, higher degrees of saturation, or by transition from monopolar ether lipids to TELs with increasing temperature.<sup>46</sup>

In most mammalian cells, ether lipids are less abundant.<sup>43</sup> However, in some mammalian membranes they are enriched. An unbalanced ratio between ether and ester lipids can be connected to pathological conditions. In tumors, for example, the ether lipid content is increased, which therefore may be used as a diagnostical marker for some tumors in the future.<sup>50</sup> Furthermore, in lipid membranes of various human tissues, especially in brain and heart membranes, ether lipids are present in form of plasmalogens.<sup>51-52</sup>

Plasmalogens are lipids that contain one ether linkage to a long-chain enol instead of an esterified fatty acid.<sup>51-52</sup> Within their lipid environments, plasmalogens modulate the bilayer's properties including fluidity and ordering and are even known to be oxidized preferentially instead of diacyl lipids.<sup>51-52</sup> In addition, the oxidation products of plasmalogens are not able to propagate further lipid oxidation, *i.e.*, they terminate the oxidation process. Thus, they are thought to function as sacrificial antioxidants within the membrane.<sup>51</sup> Hence, a deficiency in plasmalogens alters the bilayer's capability of withstanding oxidative stress. Some neurodegenerative diseases may even be connected to loss of plasmalogens in the human brain.<sup>51-52</sup>

Despite being substantial for a variety of organisms, the differences between ether and ester lipids are not fully understood yet. In this work, the model lipids DPPC and PHPC

are studied. Therefore, this chapter aims at elaborating on both of these lipids in the following.

DPPC and PHPC differ in their *sn*-2 linkage between glycerol and the hydrophobic chain. Lewis *et al.* studied the temperature dependent phase behavior of both lipids in aqueous suspension.<sup>53</sup> They found that, despite their quite similar structure, DPPC and PHPC form completely different gel phases at low temperatures.<sup>53</sup> DPPC as diester lipid forms crystalline ( $L_c$ ), lamellar gel ( $L_{\beta'}$ ), and rippled ( $P_{\beta'}$ ) gel phases below its main transition temperature ( $T_m$ ).<sup>53</sup> PHPC, in contrast, presents chain interdigitation below  $T_m$ .<sup>53</sup> The formation of an interdigitated gel phase ( $L_{\beta I}$ ) has to be the result of the single ether bond substituting an ether linkage.

Interdigitation of lipids can be the result of several structural changes, for example in lipids bearing the chains in position 1 and 3 instead of 1 and 2 on the glycerol backbone or by addition of surface active small molecules which penetrate the headgroup region.<sup>54-56</sup> In general, the formation of interdigitated lipid membranes depends on the balance of interactions between lipid chains, headgroups, and with the surrounding water and can be induced by the introduction of hydrophilic chain terminations (as was done *e.g.* in [P1]) or a size mismatch between headgroup and chains, for instance.<sup>56</sup> In the case of ether lipids, the headgroup is probably of comparable size as in ester lipids and no other modifications are present. To unravel the cause of chain interdigitation in PHPC among other ether lipids, Lewis *et al.* measured IR spectroscopy of liposomal systems.<sup>53</sup>

At first glance, DPPC and PHPC showed a similar temperature-dependent behavior in aqueous suspension. Both lipids presented their main phase transition from gel phase to liquid crystalline phase in a similar temperature range (DPPC  $T_m = 41.6$  °C, PHPC  $T_m = 44.4$  °C).<sup>53</sup> The overall chain order behaved similarly in both lipids' membranes but differences in the hydration and ordering of their polar regions were observed.<sup>53</sup> The authors discussed hydration and environmental polarity of the carbonyl and the phosphate groups, respectively, and observed additional ordering defects in the methylene groups adjacent to the ester or ether group of the ether lipids.<sup>53</sup> It was observed that the hydration of the carbonyl and phosphate groups were increased in ether lipids when compared to the ester lipid DPPC. The wavenumbers of both the carbonyl stretching vibration and the antisymmetric phosphate stretching vibrational band were decreased,<sup>53</sup> which are sensitive to hydrogen bonded water molecules.<sup>57-58</sup> This is somewhat unexpected because ether lipids seem to have more apolar glycerol regions when compared with ester lipids. However, Lewis *et al.* attributed the effects they observed to a change in the orientation of the glycerol backbone of the lipids.<sup>53</sup> While typical ester lipids such as DMPC and DPPC contain a glycerol part oriented approximately perpendicular to the bilayer plane,<sup>59-60</sup> the glycerol backbone of the ether lipid PHPC (together with other studied ether lipids) has to be aligned approximately parallel to the bilayer plane.<sup>53</sup> This interpretation was supported by the IR spectroscopic findings and further explains a possible size mismatch between headgroup and chain volume that could be responsible for the observed chain interdigitation at low temperatures.<sup>56</sup>

It can be concluded that the differences between simple ester and ether lipids in aqueous suspensions are known. However, a similar approach has not been made in other model systems. While some ether lipids were already investigated in Langmuir monolayers at the air/water interface, the authors of these studies did not measure hydration effects.<sup>61-62</sup> By evaluating x-ray grazing incidence diffraction data, Brezesinski *et al.* concluded that the studied ether lipids were comparable to the structurally related ester lipid.<sup>62</sup> However, they found that the ether lipids occupied a smaller area and exhibited a decreased chain tilt angle than the ester lipids at the air/water interface.<sup>62</sup> From the observed data it was suggested that in Langmuir monolayers the glycerol backbone of the ether lipids is presumably also oriented differently than in ester lipid monolayers.<sup>62</sup> With the methods used in this study, the authors could not verify this further.

As can be summarized here, the influence of a small change on the molecular scale can have a tremendous impact on the supramolecular assembly formed by the molecules. Comparing the model compounds of ester and ether lipids, their small structural difference causes a different phase behavior of their suspensions in water.<sup>53</sup> In this model system the influence of the ether linkage was investigated before but the behavior of these lipids at the air/water interface is not fully understood. To enhance the basic knowledge of this influence, this question will be addressed in this thesis using monolayer techniques such as IRRAS and epi-fluorescence microscopy.

### 3.3 Nanodiscs

#### 3.3.1 Nanodiscs in the context of commonly used lipid model systems

In recent years, a variety of model systems was used to mimic natural membranes for protein studies.<sup>3,63-64</sup> Depending on the stability of the membrane proteins, the natural lipids surrounding the proteins have to be included or can be substituted by short-chain detergents or amphiphilic polymers (amphipols).<sup>3,65-66</sup> For some techniques, the model system of liposomes is used due to its native lipid content and accessibility.<sup>3,64,67</sup> However, solution nuclear magnetic resonance (NMR) spectroscopy, for instance, benefits significantly from small lipid assemblies.<sup>68-69</sup> Hence, different model systems have been used for a number of membrane proteins.

The simplest of all lipid models is the sole use of detergents. In this case, the detergents assemble to micelles that can surround hydrophobic parts of proteins or other guest molecules.<sup>66</sup> Caused by the shielding of the hydrophobic moieties membrane proteins are able to remain folded in an aqueous environment.<sup>66</sup> If the model has to be more natural, bilayer phospholipids can be mixed with short-chain phospholipids or single-chain detergents.<sup>64,70</sup> The combination of different lipid geometries allows additional shape anisotropy. Here, the cylindrical lipids prefer to form planar layers, while the cone-shaped detergents or short-chain lipids cover the bilayer rim.<sup>64,70</sup> This results in lipid assemblies of a disc shape with the bilayer core being shielded by detergents.<sup>64,70</sup> These so-called bicelles contain more natural lipids and provide a bilayer structure for membrane proteins.<sup>64,70</sup>

An alternative to detergents is the use of amphiphilic polymers or amphipols. These polymers belt the membrane protein's hydrophobic parts directly without involvement of detergents in the final particle.<sup>65,71</sup> Direct extraction of membrane proteins from lipid bilayers, however, is often not possible with amphipols.<sup>72</sup> Thus, detergents are commonly used to facilitate solubilization and, subsequently, are substituted by amphipols.<sup>72</sup> As a consequence, protein/amphipol complexes contain no or only few lipid molecules. Therefore, they may be useful for some experiments and proteins but they do not resemble natural membranes.

To this end, the discussed methods involve exogenous molecules that are tolerated only by stable membrane proteins. More labile proteins are denaturated by these molecules which are, hence, not suitable in every case.<sup>66,71</sup>

In the last decades, other possibilities of shielding the hydrophobic center of lipid bilayers were explored. The two main methods that emerged are (i) the use of amphiphilic proteins<sup>73-75</sup> and (ii) the use of amphiphilic copolymers<sup>5,9,63</sup> that both can encircle natural lipids and proteins.

In the first case, several proteins are available which stabilize the bilayer membrane.<sup>75</sup> Their advantage is their low dispersity and broad applicability.<sup>75</sup> The main class of proteins commonly used to stabilize the lipids are called membrane scaffold proteins (MSPs).<sup>74-75</sup> MSPs consist of amphiphilic helices being able to surround the bilayer's core in a belt-like manner.<sup>74-75</sup> They can be optimized in size for various diameters of the formed nanodiscs and are commonly used in combination with synthetic lipids as well as natural lipids.<sup>75</sup> However, MSP-based nanodiscs have three major disadvantages: (i) some biochemical techniques (NMR or IR spectroscopy for instance) are not able to discriminate between the MSP and incorporated membrane proteins, (ii) in preparation protocols for protein-based nanodiscs detergents are involved<sup>73-75</sup> that could denaturize membrane proteins, and (iii) MSPs are expensive and not easily accessible.

To overcome the limitations of protein-encapsulated nanodiscs, the use of polymers was investigated. In this thesis, polymer-based nanodiscs are studied. For clarity, they will be called nanodiscs or polymer/lipid particles (xLPs with x being SMA, DIBMA, or SMA-SB) in this work. Nowadays, a variety of amphiphilic copolymers is known to solubilize membrane proteins in combination with surrounding lipids (for examples see references 5, 13, 76-78). In contrast to the already discussed methods, these polymers are able to solubilize their targets directly from natural membranes without the use of detergents.<sup>5,13</sup> They are commercially available in large quantities and do not interfere with most of the commonly used biochemical assays.<sup>5,13,63</sup> Currently, research effort goes into developing polymers that are compatible with high concentrations of divalent cations and that are capable of efficient but mild solubilization.<sup>13,63</sup> In the following, this technique will be introduced in detail.

### 3.3.2 The formation of nanodiscs

To form polymer-encapsulated nanodiscs, amphiphilic copolymers are necessary. The frequently used polymers have in common that they contain a random or alternating sequence of hydrophilic and hydrophobic monomers.<sup>13,79</sup> The polymers' properties can be adjusted further by changing the ratio or sequence of the monomers, *i.e.*, by making them more hydrophilic or hydrophobic, or by varying the them.<sup>13,76-80</sup>

To optimize the polymers used in lipid solubilization, in-depth knowledge of the mechanism of solubilization is necessary. From combined bulk and monolayer studies, it was concluded that the solubilization of lipid bilayers proceeds via three steps, that are depicted in **Figure 3.1**: (a) the binding of the polymer to the lipid bilayer, (b) the insertion of the polymer into the bilayer, and (c) the fragmentation of the former lipid assembly into nanodiscs.<sup>8</sup> In each of these steps the solubilization efficiency can be modulated by changing the polymer's and lipids' properties.

During the binding phase, the main interactions influencing the amount of bound polymer are the electrostatic interactions between the lipid headgroups and the polymer, and the hydrophobic interactions between the hydrophobic monomer units and the lipid chains.<sup>8,79</sup> The latter one can only occur if the electrostatic interactions are attractive or if repulsive interactions are overcome. When the polymer is bound, the hydrophobic moieties can penetrate the lipid bilayer.<sup>8</sup> The insertion of polymeric side chains is most efficient with planar aromatic groups such as the phenyl ring in styrene monomers.<sup>8,81</sup> In the last phase of the solubilization, the fragmentation into

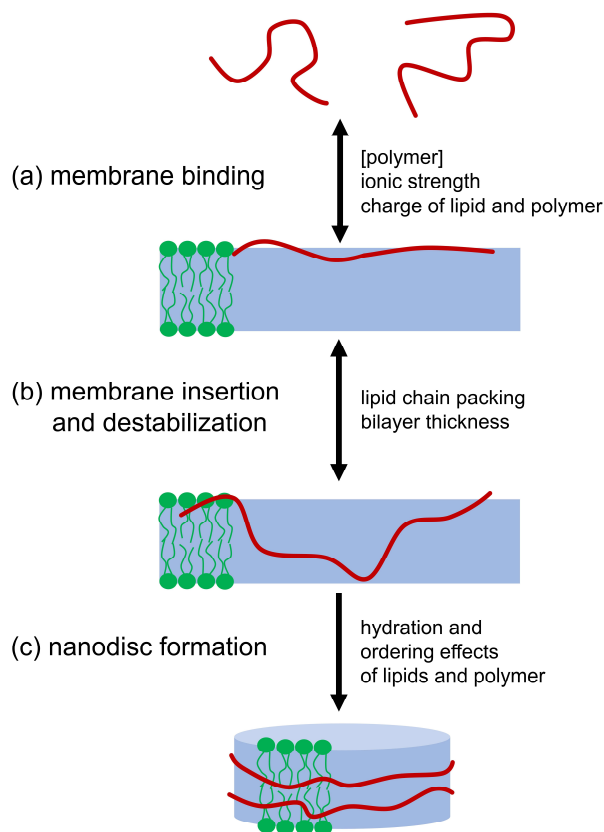


**Figure 3.1.** Schematic representation of the formation of nanodiscs in three steps. This figure is recreated from reference 8. The main parameters governing the respective formation step are: (a) the concentration of the polymer and charged lipids (in case of SMA and DIBMA mainly of anionic lipids repelling the polymer), and ionic strength; (b) the lipid chain order and the membrane thickness; and (c) entropic and enthalpic differences between the second state (polymer inserted in membrane) and nanodiscs.

nanodiscs, the preference of the polymer for either a hydrophobic lipid environment within the bilayer or a mixed hydrophobic/hydrophilic environment at the rim of a nanodisc plays a major role.<sup>8,81</sup>

As the hydrophilic monomer in these polymers, maleic acid is most commonly used. In SMA, which is the best studied polymer, the maleic acid is polymerized with styrene as the hydrophobic monomer (see **Figure 3.2**). Different ratios between both monomers and different chain lengths are described in the literature.<sup>79-80,82</sup> Despite being negatively charged, as are most natural lipid membranes, SMA exerts a high solubilization efficiency.<sup>5,8,79</sup> This is most likely due to its capability to insert its phenyl rings in between the lipid chains during solubilization and in the stable nanodisc.<sup>8,81</sup> However, the simple insertion of SMA into the lipid bilayer is accompanied by a strong disrupting effect on the lipids which is, thus, a major disadvantage of the polymer.<sup>13,83</sup> To overcome this influence of SMA, DIBMA has been developed (see **Figure 3.2**).<sup>13</sup> This polymer contains no aromatic monomers and, hence, does not exhibit an equally strong membrane-disrupting effect.<sup>13</sup> Following the mechanism of solubilization, new polymers are developed optimizing their properties, *i.e.* their charge (for example SMA-SB, a zwitterionic copolymer derived from SMA), polydispersity, hydrophilic/hydrophobic ratio, and their compatibility with divalent cations to list a few characteristics influencing suitability for lipid solubilization and applicability for protein studies.<sup>13,76-78,82</sup> Finally, the interactions between polymers and lipids can be manipulated simply by the polymer/lipid ratio. In contrast to MSP-based nanodiscs, of which the size is mainly defined by the protein's length, the diameter of polymer/lipid nanodiscs can be adjusted by changing the polymer/lipid ratio, that is, an excess of polymer forms small discs while lower amounts of polymers form larger discs.<sup>5,13,84</sup> However, in many cases, this adjustment cannot be reasonably made due to a required polymer excess for suitable solubilization of natural or nature-like membranes.

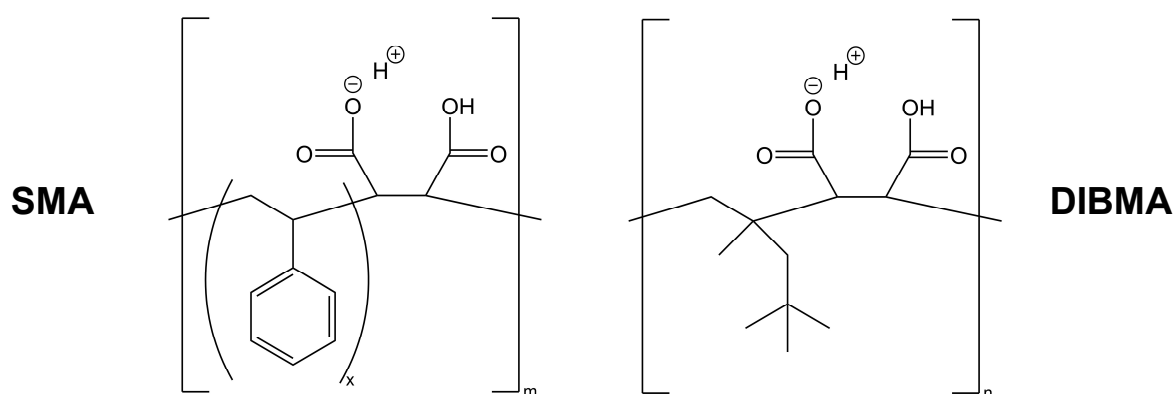


**Figure 3.2.** The two most commonly used polymers in membrane solubilization: poly-(styrene-co-maleic acid) (SMA) and poly-(diisobutylene-*alt*-maleic acid) (DIBMA). In literature, a variety of different SMA copolymers is used with differing maleic acid content, polymer length, or monomer sequence control.<sup>79,82</sup> In this thesis SMA with  $x = 2.2$  and  $m \approx 8$  and DIBMA with  $n \approx 37$  are used.<sup>81</sup>

Besides the polymers, the lipids have a huge impact on the solubilization efficiency.<sup>81,85</sup> In the first phase of the solubilization, the charges of the lipids' headgroups affects the binding of the polymer.<sup>8,79</sup> This effect is mostly screened by adding large amounts of salt to weaken the coulombic repulsion between lipids and polymer.<sup>11,81</sup> The lipid chains mainly influence the insertion of the polymeric side chains into the bilayer. It was found that the bilayer thickness and the lateral density have a strong impact on the insertion.<sup>8</sup> While a thin bilayer containing lipids with short chains is readily solubilized, long-chain lipids are more resistant to nanodisc formation.<sup>8</sup> The lateral density within the bilayer is modulated mainly by the lipid's phase state and the degree of unsaturation of the chains.<sup>8</sup> Therefore, solubilization efficiency is increased, when defects in lipid order are present, which are, e.g., the coexistence of gel phase and liquid crystalline phase directly at the  $T_m$  of the bilayer.<sup>8</sup> Unsaturated lipids, in addition, hinder the formation of nanodiscs despite forming bilayers of lower order. This is thought to be caused by the increased lateral density induced by the double bonds.<sup>8</sup> For the same reason, cholesterol integrated between the lipid chains has a strong decreasing effect on solubilization efficiency.<sup>86</sup>

### 3.3.3 Nanodiscs in protein research

Polymer-encapsulated nanodiscs are a versatile tool in protein research. They are used to stabilize membrane proteins in their native lipid environment and allow detergent-free protein purification.<sup>5,13</sup>

The major advantage of using amphiphilic copolymers to solubilize natural membranes is their ability to directly form nanodiscs of natural membranes.<sup>5,13</sup> Thus, the native lipid mixture is maintained during solubilization and a variety of proteins are solubilized as well. The formed nanodiscs are compatible with commonly used purification and characterization techniques.<sup>5,13</sup>

Since detergents are not needed for keeping the membrane proteins folded, the risk of denaturizing the proteins during purification is minimized. Once the proteins are incorporated in nanodiscs with surrounding lipids, the polymers as amphiphilic molecules are not able to penetrate the bilayer. This is due to the monomer sequence which is random but not statistical, *i.e.*, the sequence does not contain adjacent maleic acid units.<sup>5,79,82</sup>

The ability to purify and stabilize membrane proteins without the addition of disturbing small molecules was appreciated by many researchers in the last years and is probably the main driving force in polymer design and characterization.

Amphiphilic copolymers exert mild solubilization properties towards membrane proteins by initially maintaining the membranes native lipid content. However, the lipid composition within the nanodiscs is not static. Polymer/lipid particles are known to exchange their lipids frequently and much faster than liposomes.<sup>87-90</sup> Thus, the lipid content of the nanodiscs during solubilization and after purification, *i.e.*, separating the protein-filled nanodiscs from nanodiscs without proteins and other membrane fractions, is not necessarily identical. However, this property of the nanodiscs enables systematic design of the lipid composition of protein-containing nanodiscs in theory.

As mentioned before, polymer/lipid nanodiscs are excellently suited for most biochemical and biophysical observations.<sup>5,13</sup> The absence of external proteins enables the use of common methods for protein characterization, that average the whole sample's properties, such as circular dichroism (CD) spectroscopy, ultraviolet- (UV), or IR spectroscopy. In some cases, several proteins can be discriminated by using isotopic labeling techniques. However, complete isotopic labeling is not suitable for whole proteins. The adjustment of the nanodiscs' diameters allows both solution NMR spectroscopy (small (< 30 nm), fast tumbling nanodiscs) and solid-state NMR spectroscopy (large nanodiscs (> 40 nm) suitable for magnetic alignment) to be measured for protein characterization.<sup>78</sup> Regarding CD- and UV spectroscopy, styrene-containing copolymers show absorption in the UV range of typical protein absorption.<sup>13</sup> Therefore, for methods detecting at those wavelengths, aliphatic copolymers are more promising.

In some cases, the nanodisc technique is excellently suited for protein research due to its unique properties, such as the bilayer exhibiting no curvature or being stackable. One of these systems is the human myelin sheath. In this case, the use of nanodiscs allows protein research in a native-like system consisting of stacked lipid bilayers. In this dissertation, this point is addressed by preparing a nanodisc-containing model system for the human myelin sheath and studying its lipid properties.

## 4 Results

### 4.1 Overview over the published papers

The publications presented in this thesis intend to increase the understanding of basic principles causing the properties of supramolecular lipid assemblies. For this, two different approaches were made involving the simple model system of lipid monolayers at the air/water interface and polymer-encapsulated nanodiscs as a model of higher complexity.

The fractionation of this work allows unambiguous discussion of: (i) the influence of chemical modification of the lipids, (ii) the impact of amphiphilic polymers on a simple model lipid, and (iii) the interactions between complex, myelin-like mixtures of lipids and the same polymers.

All published papers aim towards elucidating some factors affecting the lipid properties, *i.e.*, hydration, lipid order and mobility, phase behavior, or lipid composition, within two selected model systems, which are frequently used in modern research.

As mentioned before, [P1] and [P3] are not shown and discussed in detail in this thesis.

#### 4.1.1 The impact of a single ether bond within the lipid on the behavior of its monolayer at the air/water interface

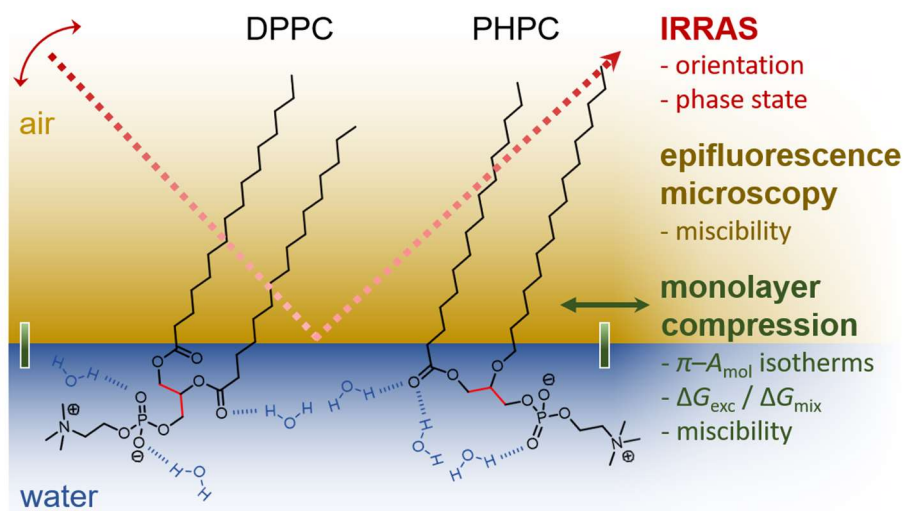


**Figure 4.1.** Differences between DPPC and PHPC as observed in this study presented together with the methodical approach (image taken from [P2]).

Ether lipids are highly abundant in some niche environments in nature. They are the main constituents of the membranes of extremophile organisms withstanding the challenges of their extreme environments.<sup>44-46</sup> Compared to ester lipids, which are much more abundant in other biological systems, ether lipids contain at least one alkyl chain instead of an acyl chain. This somewhat small molecular change can lead to differences in the orientation of the whole molecule when comparing ester and ether lipids, as was shown in aqueous suspensions.<sup>53</sup>

In this project, the two structurally related lipids DPPC and PHPC are studied in monolayers at the air/water interface as is schematically presented in **Figure 4.1**. Both lipids differ in their *sn*-2 lipid chain containing either an ester (DPPC) or an ether linkage (PHPC) to the glycerol backbone.

In the first part of this study, monolayers of pure DPPC or PHPC were characterized, respectively. To this end, compression isotherms were measured with parallel collection of IRRA spectra or fluorescence micrographs. The ether linkage in PHPC turned out to induce a glycerol orientation parallel to the air/water interface, which resembled the findings in liposomes. Contrary to the expected decrease in polarity because of substitution of a carbonyl with a methylene group, the glycerol rearrangement was connected to a higher degree of hydration of the remaining carbonyl group and a lower order in methylene segments directly adjacent to the ester bond.

In the second chapter of the paper, mixed monolayers containing DPPC and PHPC were observed by compression isotherms and following thermodynamic analyses of the isotherms, IRRAS, and epi-fluorescence microscopy. The measured isotherms presented unexpected additional plateaus or kinks at surface pressures above the transition from the liquid expanded to the liquid condensed phase. Applying the mentioned methods, this was attributed to a non-ideal miscibility of PHPC and DPPC. The observed non-ideal miscibility is probably the result of geometrical differences between both lipids and the additional plateau could be caused by changes in hydration of the headgroups following the lipid main transition.

#### **4.1.2 The influence of different polymers on DMPC nanodiscs**

In recent years, polymer-encapsulated nanodiscs have frequently been used as lipid model membranes.<sup>5,63</sup> In biochemical research, amphiphilic copolymers, such as SMA or DIBMA, are used to purify and characterize membrane proteins that could be denaturated by detergents in alternative purification protocols (for examples see references 14, 91-92). However, the study of proteins requires in-depth knowledge of the lipid properties within the used nanodiscs and, thus, interactions between the commonly used polymers and the lipids.

The goal of this project is to study the influence of the three different copolymers SMA, DIBMA, and SMA-SB on DMPC as a model lipid that is commonly used in nanodisc research.<sup>13,78,80,82</sup> DMPC renders the observation of two lipid mesophases near room temperature possible and is easily solubilized by all three polymers. Furthermore, the use of such a simple lipid model molecule enables detailed interaction studies without influences of complex lipid mixtures as are occurring in natural membranes.

The main methods of determining the impact of the polymers on DMPC are DSC and CW EPR spectroscopy. The combination of both techniques allows observation of the temperature-dependent phase behavior of DMPC calorimetrically as well as on the molecular scale using different lipid spin probes. To this end, spin-labeled lipids bearing a doxyl group at the chain end or near the carbonyl groups, respectively, were used to

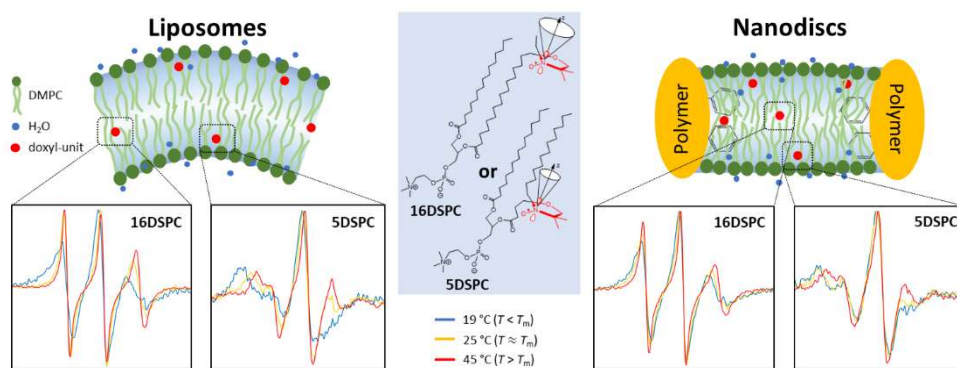


**Figure 4.2.** Overview over spectroscopical differences between DMPC liposomes and DMPC nanodiscs as observed by CW EPR spectroscopy of 5- and 16DSPC and the derived model containing hydration and lipid order (this picture is taken from [P4]).

unravel the impact of the polymers on the center of the bilayer and the region adjacent to the headgroup, separately.

Addition of all polymers in amounts sufficient for complete lipid solubilization did not alter the main transition temperature of DMPC substantially. However, all polymers increased the segmental order parameter and had an impact on water penetration into the bilayer at both observed positions as is depicted schematically in **Figure 4.2**.

#### 4.1.3 Mimicking the human myelin sheath with myelin-like nanodiscs

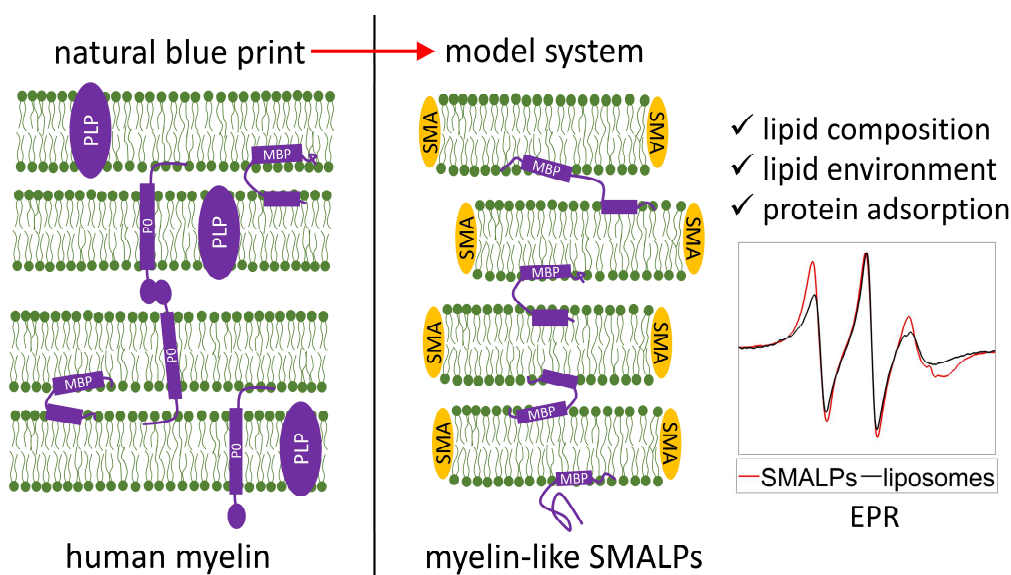


**Figure 4.3.** Concept of mimicking the human myelin sheath with polymer-encapsulated nanodiscs containing natural lipids as applied in this study (schematic overview taken from [P5]).

In the third part of this thesis, the influence of the same three amphiphilic copolymers as in [P3] and [P4] is studied on lipid bilayers resembling the cytosolic leaflets of myelin in either the central nervous system (CNS) or the peripheral nervous system (PNS). Mimicking the myelin membrane enables research of a nature-like system of utmost complexity in an accessible way. Polymer-encapsulated nanodiscs are well-suited for this kind of study due to their low curvature and ability to build up stacks that could

resemble the compacted myelin sheath. To this end, the preparation of myelin-like nanodiscs has to be achieved in the first place. However, the solubilized liposomes contain a variety of unsaturated and negatively charged phospholipids as well as a high amount of cholesterol.<sup>24</sup> The complex lipid composition of these membranes hinders efficient solubilization and is therefore thought to be exceptionally difficult to solubilize.<sup>5,86</sup>

The goal of this project, hence, was to solubilize myelin-like liposomes and study the resulting nanodiscs regarding their lipid composition and lipid properties. In addition, their use to mimic the human myelin sheath was explored by investigating the interaction between the myelin basic protein (MBP) with myelin-like nanodiscs.

Solubilization of myelin-like liposomes could be achieved with SMA and SMA-SB and the lipid composition was studied using HPLC and MS. The results of both methods suggest a rather unspecific solubilization by both polymers without preference for distinct lipid headgroups or chain compositions. Furthermore, CW EPR spectroscopy revealed only small changes in hydration of the used lipid spin probes because of solubilization by SMA or SMA-SB. However, differences in the rotational mobility of the lipids between myelin-like liposomes and nanodiscs could be observed: the polymers restricted the lipids' motion in the center of the bilayer while enabling more isotropic rotation near the headgroup.

In human myelin, a variety of proteins contributes to a compaction of the lipid multilayer.<sup>93-94</sup> To probe this requirement in mimicking the whole myelin sheath, we introduced bovine MBP (bMBP)<sup>95-97</sup> into the nanodisc system to induce stacking of the discs. With myelin-like SMALPs, DLS and CW EPR revealed aggregation of the nanodiscs with lipid/protein interactions being involved. Consequently, we interpreted this result as strong evidence for a native-like stacking of the bilayers. SMA-SBLPs were able to interact with bMBP when containing the PNS lipid composition, which may be caused by the higher abundance of negatively charged lipids, that are preferred binding partners of the positively charged bMBP. For clarity, the main results regarding polymer/lipid- and lipid/protein interactions are depicted in **Figure 4.3** which is taken from the publication.

## 4.2 Publications

In this chapter, the three main publications contributing to this thesis are presented. To avoid overlap with other dissertations and my own Master's thesis, the publications [P1] and [P3] are not shown here as is also described in the list of publications. However, both papers provide the basis for interpretations and comparisons included in the publications shown here.

## **Influence of a single ether bond on assembly, orientation, and miscibility of phosphocholine lipids at the air–water interface**

Matthias Hoffmann, Simon Drescher, Christian Schwieger and Dariush Hinderberger

*Phys. Chem. Chem. Phys.* **2021**, *23*, 5325-5339

DOI: [10.1039/D0CP06520J](https://doi.org/10.1039/D0CP06520J)

Reproduced by permission of the PCCP Owner Societies.


 Cite this: *Phys. Chem. Chem. Phys.*, 2021, **23**, 5325

# Influence of a single ether bond on assembly, orientation, and miscibility of phosphocholine lipids at the air–water interface†

 Matthias Hoffmann,<sup>ab</sup> Simon Drescher,<sup>id cd</sup> Christian Schwieger<sup>id \*b</sup> and Dariush Hinderberger<sup>id \*ab</sup>

How does a small change in the structure of a phospholipid affect its supramolecular assembly? In aqueous suspensions, the substitution of one ester linkage in **DPPC** (1,2-dipalmitoyl-*sn*-glycero-3-phosphocholine) by an ether linkage alters its phase behaviour completely. To unravel the effect of replacing a phospholipid's ester linkage by an ether linkage in lipid monolayers, we characterized pure monolayers of the model lipid **DPPC** and its *sn*-2 ether analogue **PHPC** (1-palmitoyl-2-*O*-hexadecyl-*sn*-glycero-3-phosphocholine) as well as mixtures of both by measurements of surface pressure–molecular area ( $\pi$ - $A_{\text{mol}}$ ) isotherms. In addition, we used infrared reflection absorption spectroscopy (IRRAS) to study lipid condensation, lipid chain orientation, headgroup hydration, and lipid miscibility in all samples. Mixed monolayers consisting of **DPPC** and **PHPC** were studied further using epifluorescence microscopy. Our results indicate a strong influence of the *sn*-2 ether linkage on headgroup hydration and ordering effects in the regions of the apolar chains and the headgroups. Both effects could originate from changes in glycerol conformation. Furthermore, we observed a second plateau in the  $\pi$ - $A_{\text{mol}}$  isotherms of **DPPC**/**PHPC** mixtures and analysis of the mixed  $\pi$ - $A_{\text{mol}}$  isotherms reveals a non-ideal mixing behaviour of both lipids which may be caused by conformational differences in their headgroups.

 Received 17th December 2020,  
 Accepted 16th February 2021

DOI: 10.1039/d0cp06520j

rsc.li/pccp

## Introduction

In nature, ether lipids are highly abundant in Archaea.<sup>1</sup> Many representatives of this domain of life are extremophiles, needing extraordinarily stable membranes to withstand their extreme habitat conditions, *e.g.* at extremely low pH, high temperature, or high ionic strength.<sup>1</sup> To maintain a functional membrane structure, ester lipids are not suitable. In this environment, chemically more stable ether lipids as well as membrane-spanning bipolar tetraether lipids (TELS), also known as bolaamphiphiles,<sup>2</sup> have evolved.<sup>3,4</sup> On the other hand, different types of ether lipids were also found in mammalian cells. Here, an unbalanced ratio of

ether lipids to ester lipids is presumably connected to *e.g.* neurodegenerative diseases or cancer.<sup>5,6</sup>

In biophysics of lipids, it is well known that ether and ester lipids exhibit different phase behaviours. In aqueous suspensions of some ether lipids, a complex thermotropic polymorphism is observed.<sup>7</sup> When comparing 1,2-dipalmitoyl-*sn*-glycero-3-phosphocholine (**DPPC**) with its mono- or di-ether derivatives, namely 1-palmitoyl-2-*O*-hexadecyl-*sn*-glycero-3-phosphocholine (**PHPC**, see Scheme 1 for chemical structures) and 1,2-di-*O*-hexadecyl-*sn*-glycero-3-phosphocholine (**DHPC**), respectively, significant differences in gel phase structures are found. While **DPPC** forms crystalline ( $L_c$ ), lamellar gel ( $L_\beta'$ ), and rippled gel ( $P_\beta'$ ) phases at temperatures below the main transition temperature ( $T_m$ ) of

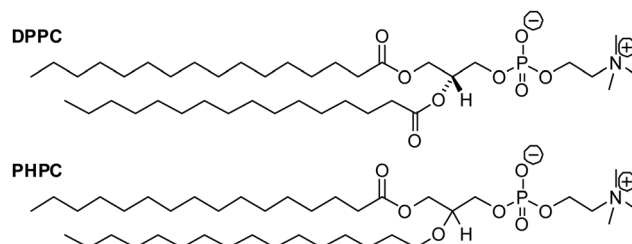
<sup>a</sup> Institute of Chemistry, Martin Luther University (MLU) Halle-Wittenberg, Von-Danckelmann-Platz 4, 06120 Halle (Saale), Germany.  
 E-mail: dariush.hinderberger@chemie.uni-halle.de

<sup>b</sup> Interdisciplinary Research Center HALOmem, MLU Halle-Wittenberg, Charles Tanford Protein Center, Kurt-Mothes-Str. 3a, 06120 Halle (Saale), Germany

<sup>c</sup> Institute of Pharmacy, MLU Halle-Wittenberg, Wolfgang-Langenbeck-Str. 4, 06120 Halle (Saale), Germany

<sup>d</sup> Phospholipid Research Center, Im Neuenheimer Feld 515, 69120 Heidelberg, Germany

† Electronic supplementary information (ESI) available: Synthetic details, further IRRAS data, simulation of IRRAS spectra, further PCA results and thermodynamic data. See DOI: 10.1039/d0cp06520j



Scheme 1 Chemical structure of **DPPC** (top) and **PHPC** (bottom).

41.6 °C, **PHPC** and **DHPC** form a lamellar interdigitated gel phase  $L_{\beta I}$  (and **DHPC** an additional  $L_{\beta}$  phase between 34.8 and 43.9 °C) at temperatures below  $T_m$ .<sup>7</sup> In **PHPC** and **DHPC**, one or two small changes in the region linking the alkyl chain and headgroup, *i.e.* the glycerol backbone, cause major structural modifications of their supramolecular assemblies in comparison with **DPPC**. Lewis *et al.* studied the reasons for the differences between these otherwise structurally identical lipids extensively using infrared (IR) spectroscopy and isotopic labeling.<sup>7</sup> They concluded that the exchange of at least one ester bond with an ether bond induces a conformational change of the involved glycerol backbone, altered hydration of the remaining carbonyl moiety, and conformational changes of the adjacent chain segment.<sup>7</sup> Hence, a change in glycerol orientation caused by as little as the substitution of one ester bond with an ether bond enables the lipid to preferably aggregate in a lipid gel phase showing alkyl chain interdigitation at temperatures below  $T_m$ . Consequently, in aqueous suspensions the effects of ether bonds on lipid properties are understood quite well.

In contrast, differences between **DPPC** and **PHPC** in Langmuir monolayers are far less studied and understood. Surface pressure–molecular area ( $\pi$ - $A_{mol}$ ) isotherms of **DPPC**, **PHPC**, and **DHPC** were already measured and characterized by fluorescence microscopy and X-ray diffraction.<sup>8–10</sup> Brezesinski *et al.* observed a decreased chain tilt angle of **DHPC** and **PHPC**, in comparison to **DPPC**. Moreover, the lateral lipid density of both ether lipids is increased compared to **DPPC** monolayers.<sup>8</sup> They predicted a change in glycerol conformation to be responsible for these differences and the hydration of the headgroup to change.<sup>8</sup> However, this remains speculation until now and little is known about structure, conformation, and hydration of the glycerol backbone of ether lipids in monolayers.

Here, we first investigate the phase behaviour, lipid conformation, and hydration of **DPPC** and **PHPC** monolayers, respectively. We present  $\pi$ - $A_{mol}$  isotherms combined with infrared reflection absorption (IRRA) spectra to detect how monolayers of both lipids differ in their molecular changes caused by compression of the monolayer. We evaluate the chain order parameter ( $S(CH_2)$ ) and the order parameter of the phosphate group ( $S(PO_2^-)$ ) by performing a least square minimization of both methylene stretching vibrational bands and the antisymmetric phosphate stretching vibrational band, respectively. To characterize the hydration of the carbonyl moiety of both lipids, we use principal component analysis (PCA).

In the second part of this study, we report the characterization of mixed monolayers of **DPPC** and **PHPC**, in particular their miscibility at the air–water interface, by epifluorescence microscopy using a rhodamine-labelled lipid, the Gibbs phase rule, and calculation of the excess Gibbs energy of mixing ( $\Delta G_{exc}$ ) and the Gibbs energy of mixing ( $\Delta G_{mix}$ ).<sup>11,12</sup> In addition, we present IRRA spectra of mixtures of **PHPC** and **DPPC-*d*<sub>62</sub>**, bearing fully deuterated alkyl chains, to characterize their miscibility spectroscopically.

## Experimental

### Materials

1,2-Dipalmitoyl-*sn*-glycero-3-phosphocholine (**DPPC**) was purchased from Genzyme Pharmaceuticals (Cambridge, MA, USA)

and used without further purification. 1-Palmitoyl-2-O-hexadecyl-*sn*-glycero-3-phosphocholine (**PHPC**) was synthesized as described in the ESI.† **DPPC** bearing perdeuterated acyl chains (**DPPC-*d*<sub>62</sub>**) was purchased from Avanti Polar Lipids Inc. (Alabaster, AL, USA). The fluorescent dye 1,2-dipalmitoyl-*sn*-glycero-3-phosphoethanolamine-*N*-(lissamine rhodamine B sulfonyl) (ammonium salt) (**Rh-DPPE**) was obtained from Life Technologies GmbH (Darmstadt, Germany). The solvents chloroform and methanol (HPLC-grade) were obtained from Carl Roth (Karlsruhe, Germany).

### Methods

**Sample preparation.** All used lipids were dissolved in chloroform/methanol (9/1, v/v). Mixtures of phospholipids were prepared by mixing different amounts of appropriate lipid stock solutions using glass syringes (Hamilton Bonaduz, Bonaduz, Switzerland). For storage, solvents were then removed in a gentle stream of nitrogen. Directly prior to experiments, the lipids and lipid mixtures were dissolved again in chloroform/methanol.

**Monolayer preparation.** All  $\pi$ - $A_{mol}$  isotherms were measured on a rectangular Teflon trough (78.3 × 6.8 cm<sup>2</sup> Riegler & Kirstein, Potsdam, Germany) except for compression isotherm measurements with parallel IRRAS detection. The Langmuir trough was equipped with a Wilhelmy sensor and filled with H<sub>2</sub>O (MilliQ Millipore water with a specific resistance of  $\rho = 18.2$  M $\Omega$  cm). After the trough was filled with water, the freshly dissolved lipids or lipid mixtures were carefully spread on the surface with a glass syringe (Hamilton Bonaduz, Bonaduz, Switzerland). The solvents were allowed to evaporate for at least 10 min prior to each measurement.

**Monolayer compression.** All shown  $\pi$ - $A_{mol}$  isotherms were compressed at the air–water interface by Teflon barriers moving at a compression speed of 2 Å<sup>2</sup> (molecule min)<sup>-1</sup>. During the measurements, 40 points per seconds were averaged. In all measurements, the temperature of subphase and monolayer was kept constant (accuracy  $\Delta T \pm 0.2$  K) through a coupled water-cooling system operated at 20 °C. Each isotherm was measured at least three times, from which one representative isotherm is shown.

**Analysis of Langmuir isotherms.** From each measured isotherm, the monolayer compressibility  $C_S$  was evaluated:

$$C_S = -\frac{1}{A_{mol}} \left( \frac{dA_{mol}}{d\pi} \right)_T, \quad (1)$$

to determine the transition surface pressure  $\pi_{plateau}$  from the maximal value of  $C_S$ .

The mixing behaviour of the lipids was studied as follows. Thermodynamically, the Gibbs energy of mixing  $\Delta G_{mix}$  describes whether the components of a mixture are miscible or not. It can be split in an ideal and an excess, *i.e.* non-ideal, term:

$$\Delta G_{mix} = \Delta G_{id} + \Delta G_{exc}. \quad (2)$$

$\Delta G_{id}$  only depends on entropy, specifically on mixture composition, that is the mole fraction  $x_i$ , and temperature. This value is

always negative, which means that, ideally, all components are miscible regardless of composition:

$$\Delta G_{\text{id}} = RT \sum_i x_i \ln(x_i). \quad (3)$$

However, demixing can occur. Deviations from ideal behaviour are included in  $\Delta G_{\text{exc}}$ . In two-dimensional systems such as Langmuir monolayers, deviations from ideal mixing are associated with an excess areas  $A_{\text{exc}}$ .

$$\Delta G_{\text{exc}} = \int_0^\pi A_{\text{exc}}(\pi) d\pi \quad (4)$$

with

$$A_{\text{exc}}(\pi) = A_{\text{mol,measured}}(\pi) - \sum_i x_i A_{\text{mol},i}(\pi). \quad (5)$$

The integration of (4) was conducted from  $\pi = 0 \text{ mN m}^{-1}$ , starting in the gaseous/liquid-expanded (LE) transition region. Combination of  $\Delta G_{\text{id}}$  and  $\Delta G_{\text{exc}}$  results in:

$$\Delta G_{\text{mix}} = RT \sum_i x_i \ln(x_i) + \int_0^\pi A_{\text{exc}}(\pi) d\pi. \quad (6)$$

**Infrared reflection absorption spectroscopy (IRRAS).** According to a procedure described elsewhere,<sup>13,14</sup> IRRAS experiments were performed on a Bruker Vector 70 FT-IR spectrometer equipped with an A511 reflection unit (Bruker Optics, Ettlingen, Germany), a liquid nitrogen-cooled MCT detector, and a Langmuir trough system (Riegler & Kirstein, Potsdam, Germany). The trough system consists of a rectangular sample trough ( $30 \times 6 \text{ cm}^2$ ) and a small circular reference trough ( $r = 3 \text{ cm}$ ). Surface pressure in the sample trough was detected with a Wilhelmy sensor using a filter paper as the pressure probe. During the measurements, the filling levels of both troughs were kept equal and constant by means of an automated, laser-reflection-controlled pumping system connected to a reservoir of  $\text{H}_2\text{O}$ . Prior to collection of each monolayer IRRAS spectrum, a spectrum of the pure subphase was measured with identical conditions to ensure best comparability and effective water vapor compensation.

Two general types of experiments were performed in this work: (i) IRRAS measurements at constant angle of incidence and polarization during compression of the monolayer and (ii) angle- and polarization-dependent IRRAS measurements to reveal orientations of different molecular moieties. For (i), IRRAS spectra were collected at a constant angle of incidence  $\varphi = 60^\circ$  and with s-polarized IR light. 1000 single interferograms were collected, averaged, and, subsequently, Fourier-transformed with a zero-filling factor of 2 to obtain one spectrum with a nominal spectral resolution of  $2 \text{ cm}^{-1}$ . Here, five of these individual spectra were averaged to obtain one final spectrum to ensure excellent signal to noise ratio. For (ii), we varied both, angle of incidence ( $25^\circ$  to  $70^\circ$  in increments of  $3^\circ$ ) and polarization (s- and p-polarization) of the incoming IR beam. Either 1000 (s-polarized IR light) or 2000 (p-polarized IR light) interferograms were averaged and Fourier-transformed with the same parameters as described above. At least three of the resulting

spectra were averaged to acquire the shown spectra. The  $\pi$ - $A_{\text{mol}}$  isotherms of **DPPC** and **PHPC**, respectively, were halted at four different surface pressures at 3, 10, 20, and  $30 \text{ mN m}^{-1}$  and sets of polarization- and angle-dependent IRRAS spectra were measured at each pressure, which allows comparison of different compression states of both lipids.

Simulation and fitting of the experimental angle- and polarization-dependent IRRAS spectra was conducted as explained in detail elsewhere.<sup>15–17</sup>

**Principal component analysis (PCA).** The goal of a principal component analysis (PCA) is to unravel subtle changes or relations in large datasets and to simplify the data. To this end, the intercorrelated variables of the data are transformed into principal components (PCs), which are orthogonal and linear combinations of the original variables. For further mathematical details, we refer to the literature.<sup>18</sup>

In this work, we present PCA of several IR-bands of **DPPC** and **PHPC** in monolayers, as measured with IRRAS. All spectra used in the PCA were measured in s-polarization at angles of incidence of the IR beam ranging from  $25^\circ$  to  $70^\circ$ . Since the band shape of s-polarized IRRAS spectra is independent of orientation of the absorbing group, they can be used directly for PCA.<sup>19</sup> The aim of this analysis is to correlate spectral changes with the phase state of the lipid and to obtain information about differences between both lipid species. We have chosen the spectral range of the carbonyl stretching vibrational band ( $1700$ – $1775 \text{ cm}^{-1}$ ) due to its sensitivity to hydration of the polar–apolar interfacial region of the lipids.<sup>20</sup>

We measured IRRAS spectra of the pure  $\text{H}_2\text{O}$  subphase directly before collecting the monolayer spectra with identical measurement parameters. These water reference spectra were subtracted from each spectrum to reduce spectral contributions of the water vapor vibrational–rotational bands. The subtraction factor was determined by minimizing the variance of the second derivative of the spectrum in the spectral range of  $3500$ – $4000 \text{ cm}^{-1}$ . Since our aim was PCA of the carbonyl bands, which overlap with the water deformation band  $\gamma(\text{H}_2\text{O})$ , we additionally subtracted simulated water absorption bands of the measured monolayer to ensure minimal spectral contributions of the  $\gamma(\text{H}_2\text{O})$  band. Both subtractions were performed with home-written MATLAB scripts (MathWorks Inc., Natick, MA, USA).

Prior to PCA, a linear baseline was subtracted from the pre-treated spectra and vector normalization of the carbonyl bands of all spectra was conducted. This ensures exclusion of major intensity differences between the bands from the PCs. The PCA was performed using the princomp function of MATLAB (MathWorks Inc., Natick, MA, USA).

**Epifluorescence microscopy.** As described previously,<sup>13</sup> fluorescence images of monolayers being composed of **DPPC**, **PHPC**, and their mixtures, respectively, were recorded with an Axio Scope A1 Vario epifluorescence microscope (Carl Zeiss MicroImaging, Jena, Germany). Imaging was conducted during compression of the monolayer, which was performed as described before, allowing full control of the pressure status when the images were taken. A Teflon-coated trough ( $26.6 \times 9.9 \text{ cm}^2$ ) equipped with a

Wilhelmy balance (Riegler & Kirstein, Potsdam, Germany) was mounted below the microscope on an  $x$ - $y$ - $z$  stage (Märzhäuser, Wetzlar, Germany), which was controlled by a MAC5000 system (Ludl Electronic Products, Hawthorne, NY, USA). During measurements, a home-built Plexiglas hood covered the film balance. The microscope was equipped with a mercury short arc reflector lamp HXP 120 C, a long working distance objective (50 $\times$  magnification, LD EC Epiplan-NEOFLUAR), and a filter/beam splitter combination, which was appropriate for the used Rhodamine dye (all components from Carl Zeiss MicroImaging, Jena, Germany).

To measure fluorescence, 0.2 mol% Rh-DPPE was added to the lipid solutions, before spreading the monolayers. This fluorescence dye partitions preferentially in lipid LE phases, which leads to a brightness contrast in phase separated monolayers.<sup>12,21</sup>

## Results and discussion

The aim of this study is to compare monolayers of pure **DP**PC and **PH**PC, respectively, and to characterize their miscibility. First, we show how both lipids self-organize individually at the air–water interface using IRRAS parallel to measurements of the respective  $\pi$ - $A_{\text{mol}}$  isotherms. Secondly, we present insights into mixed monolayers of **DP**PC and **PH**PC by measuring  $\pi$ - $A_{\text{mol}}$  isotherms as a basis for subsequent thermodynamic analyses, and by performing epifluorescence measurements and IRRAS of the mixed monolayers.

### Monolayers of pure **DP**PC and pure **PH**PC

To answer the question whether a small change in chemical structure—that is replacing one ester linkage between the glycerol and the *sn*-2 chain with an ether linkage—leads to measurable changes in lipid behaviour in monolayers, we performed  $\pi$ - $A_{\text{mol}}$  isotherm measurements.

As can be seen in Fig. 1, there are only small differences between  $\pi$ - $A_{\text{mol}}$  isotherms of **DP**PC and **PH**PC. The only noteworthy differences are (i) the slightly increased phase transition pressure of **PH**PC (6.05  $\text{mN m}^{-1}$  for **PH**PC vs. 4.42  $\text{mN m}^{-1}$  for **DP**PC at 20  $^{\circ}\text{C}$ ), as derived from the maxima in monolayer compressibility (see Fig. 1B) and (ii) the overall higher compressibility of **PH**PC in the liquid-condensed (LC) phase compared to **DP**PC, as deduced from the decreased slope of the isotherm in the LC phase region. An increased transition pressure of **PH**PC, as measured in this work, is in accordance with literature reports,<sup>10</sup> while the difference in LC phase compressibility could be due to different pressure-dependent ordering of either lipid. A spectroscopic IRRAS analysis was coupled to the isotherm measurements, with the aim to obtain more detailed insights into the organization of the lipids in the monolayer and to detect structural differences between **DP**PC and **PH**PC.

Both lipids were previously characterized in aqueous suspensions using IR spectroscopy.<sup>7,22</sup> It was concluded that the main spectroscopic differences between both lipid bilayers are due to different orientations of the glycerol backbones. This effect seems to result in different hydration of the carbonyl moieties as well as conformational changes in adjacent methylene segments.<sup>7,22</sup>

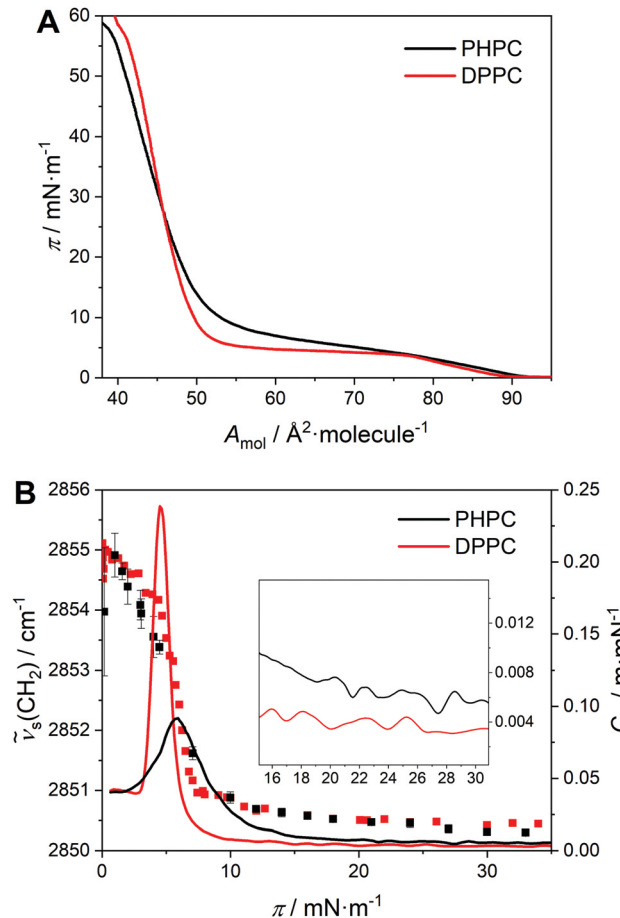


Fig. 1 Langmuir isotherms and IRRAS data of pure **DP**PC and **PH**PC monolayers. (A)  $\pi$ - $A_{\text{mol}}$  isotherms of **DP**PC (red) and **PH**PC (black) at 20  $^{\circ}\text{C}$ ; (B)  $\nu_{\text{s}}(\text{CH}_2)$  frequency (scattered data) and compressibility (solid lines) of pure **DP**PC (red) and **PH**PC (black) monolayers at 20  $^{\circ}\text{C}$  plotted over surface pressure. The inset shows a magnification of  $C_{\text{s}}$  in the LC phase (from 15 to 31  $\text{mN m}^{-1}$ ).

Furthermore, from X-ray diffraction data and  $\pi$ - $A_{\text{mol}}$  isotherms of both lipids, Brezesinski *et al.* suggested different glycerol orientations in monolayers as well.<sup>8</sup> In our study, we consequently first evaluated chain ordering and headgroup hydration in monolayers from IRRAS data.

For evaluating the order in the apolar lipid chain region, both symmetric and antisymmetric  $\text{CH}_2$  stretching vibrations were measured and simulated (see Fig. S1 and S2, ESI $^{\dagger}$ ). Further details of the simulation procedure can be found elsewhere.<sup>15–17</sup> The band positions of both  $\text{CH}_2$  stretching vibrations are indicative of the *trans/gauche* ratio in alkyl chains.<sup>19,23</sup> Therefore, they are widely used to monitor phase transitions connected to chain melting. Simulation of angle- and polarization-dependent IRRAS bands allows evaluating the order parameter  $S(\text{CH}_2)$  of the whole all-*trans* chain if the orientation of the transition dipole moment is known. This order parameter can be translated into hydrocarbon chain tilt angle. The wavenumbers of  $\nu_{\text{s}}(\text{CH}_2)$  and  $\nu_{\text{as}}(\text{CH}_2)$  measured in this study are shown in Fig. 1B ( $\nu_{\text{s}}(\text{CH}_2)$  as a function of surface pressure) and, additionally, in Fig. S1 and S2 (ESI $^{\dagger}$ ) together with the simulation results. The derived order

**Table 1** Summarized spectral parameters of pure **DPPC** and **PHPC** monolayers

	$\pi/\text{mN m}^{-1}$	$S(\text{CH}_2)$	$\theta/^\circ$	$\nu_{\text{as}}(\text{PO}_2^-)^a/\text{cm}^{-1}$	$S(\text{PO}_2^-)^b$
<b>DPPC</b>	3	0.16	— <sup>c</sup>	1225.2	−0.18
	10	0.68	27.3	1226.0	— <sup>d</sup>
	20	0.71	26.1	1225.2	−0.21
	30	0.73	25.3	1224.0	−0.22
<b>PHPC</b>	3	0.05	— <sup>c</sup>	1220.9	−0.28
	10	0.68	27.5	1223.3	−0.22
	20	0.75	24.0	1224.8	−0.22
	30	0.84	19.4	1224.1	−0.28

<sup>a</sup> Obtained by simulating the  $\nu_{\text{as}}(\text{PO}_2^-)$  region including overlapping  $\text{CH}_2$  wagging band progressions. <sup>b</sup> Simulated with the axis defined parallel to the transition dipole moment of  $\nu_{\text{as}}(\text{PO}_2^-)$  ( $\alpha = 0^\circ$ ).<sup>17</sup> <sup>c</sup> Not determined because lipid chains are not all-*trans* in the liquid-expanded (LE) phase. <sup>d</sup> It was not possible to fit the experimental phosphate band with  $\alpha = 0^\circ$ .

parameters of the lipid chains as well as the resulting chain tilt angles in the LC phase are plotted in Fig. S3 (ESI<sup>†</sup>) and included in Table 1. To interpret changes in  $\nu_s(\text{CH}_2)$  and, hence, changes in the *trans/gauche* ratio, we plotted  $\nu_s(\text{CH}_2)$  versus  $\pi$  during monolayer compression in Fig. 1B (scattered data). We only show the frequency of  $\nu_s(\text{CH}_2)$  because  $\nu_{\text{as}}(\text{CH}_2)$  contains overlapping contributions from  $\text{CH}_3$  group vibrations and a Fermi resonance band.<sup>24</sup>

Our data suggest that the *trans/gauche* ratio of both lipids is similar since  $\nu_s(\text{CH}_2)$  are identical at similar  $\pi$ . We also found a comparably disordered LE phase in both lipid monolayers, which becomes more ordered after phase transition to the LC phase. Directly after phase transition, at 10  $\text{mN m}^{-1}$ ,  $S(\text{CH}_2)$  of both lipids are similar. However, during further compression, differences between **DPPC** and **PHPC** arise as **PHPC** forms more ordered monolayers above 20  $\text{mN m}^{-1}$ . In the LC phase, the chains of both lipids are in all-*trans* conformation as concluded from the  $\text{CH}_2$  stretching frequencies (see Fig. 1B, scattered data).<sup>19,24</sup> Therefore, we calculated the tilt angle  $\theta$  of the fully stretched lipid chains, which is also shown in Table 1. **PHPC** possesses a smaller tilt angle with respect to the surface normal than **DPPC**, which is in excellent accordance with X-ray data.<sup>8</sup> In addition,  $\theta$  of **PHPC** decreases further during LC phase compression as opposed to **DPPC**. This continuous film reorganization upon **PHPC** LC phase compression explains the higher compressibility of **PHPC** as compared to **DPPC** in the condensed phase as shown in Fig. 1B (inset, solid lines).

Additional interpretation of deformation bands of the methylene groups is typically conducted to get insights into ordering effects of the chains and to elucidate coupling with other moieties. Evaluation of the  $\text{CH}_2$  scissoring vibrational band ( $\delta(\text{CH}_2)$ ) enables us to detect the geometry of the lipid unit cell in the monolayer.<sup>19,23</sup> For the two studied lipids, we found the frequency of the  $\delta(\text{CH}_2) = 1468.9 \text{ cm}^{-1}$  (at 30  $\text{mN m}^{-1}$ ) for both **DPPC** and **PHPC** in the LC phase (see Fig. S4, ESI<sup>†</sup>) while this band is not visible in the fluid LE phase. This band position in the LC phase is indicative of a hexagonal lattice, which is again in accordance with X-ray diffraction data.<sup>8,19</sup> During LC phase compression, the value slightly decreases, but no difference between both lipids could be detected. Another methylene

deformation band, the  $\text{CH}_2$  wagging band progressions, will be discussed later in this work in combination with the antisymmetric phosphate vibration.

Headgroup vibrations of the characterized lipids contain information on ion binding and hydration of their polar moieties. Typical IRRA bands originating from headgroup vibrations of both lipids are the carbonyl stretching vibrational band  $\nu(\text{C}=\text{O})$  and the antisymmetric phosphate stretching vibrational band  $\nu_{\text{as}}(\text{PO}_2^-)$ . Both are shown in Fig. 2. As can be seen directly, a small frequency decrease of the  $\nu(\text{C}=\text{O})$  band from **DPPC** to **PHPC** was found that is significantly less pronounced than the shift found in the bulk system.<sup>7,22</sup> As opposed to aqueous suspensions, where complete subtraction of solvent spectra is possible, IRRA spectra inherently contain subphase contributions. Thus, the negative  $\nu(\text{C}=\text{O})$  overlaps with the positive water deformation band ( $\nu(\text{H}_2\text{O})$ , see Fig. 2A), which could hinder a direct band interpretation and shifts the  $\text{C}=\text{O}$  band minima to higher wavenumbers. To circumvent this issue, we simulated the water absorption bands for each spectrum and subtracted them from the original data to yield spectra that are

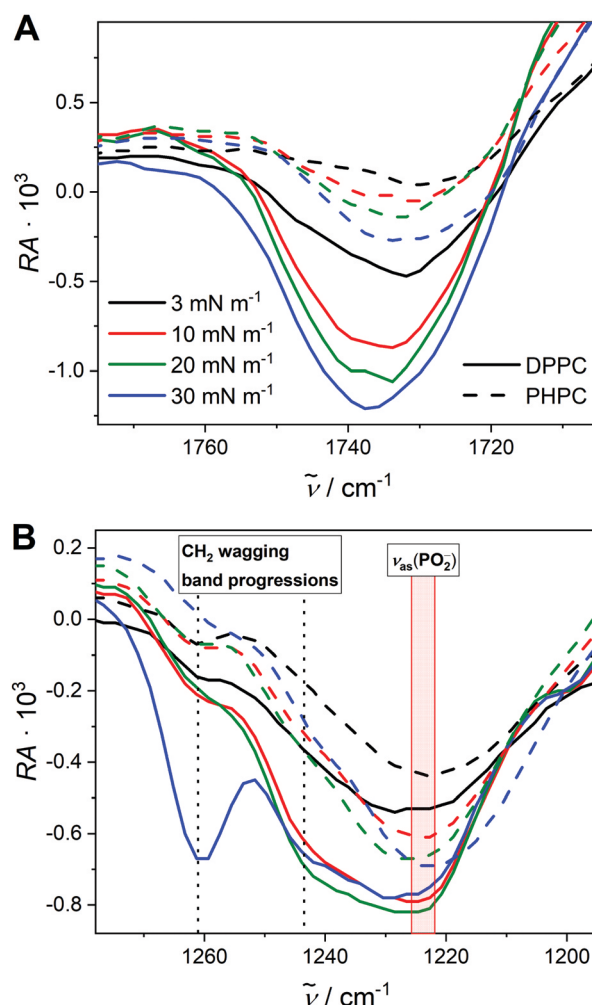


**Fig. 2** Headgroup vibrations of pure **PHPC** (dashed lines) and **DPPC** (solid lines) monolayers at 20 °C and at different surface pressure as indicated. (A)  $\nu(\text{C}=\text{O})$  band, (B)  $\nu_{\text{as}}(\text{PO}_2^-)$  region including  $\text{CH}_2$  wagging band progressions as indicated.

nearly free from water absorptions (see Experimental). Subsequently, we performed PCA of the corrected carbonyl bands to analyse a large dataset of spectra recorded at various pressures and angles for both lipids.

The frequency of  $\nu(\text{C}=\text{O})$  can be interpreted in terms of hydration of the carbonyl group.<sup>7,20,22</sup> In general, increasing hydration shifts the band centre to lower wavenumbers. However, it is not possible to derive the number of bound water molecules directly without knowing the exact absorption coefficients of the dehydrated, monohydrated, and dihydrated species, respectively. In addition, hydrogen bonding by more water molecules and stronger hydrogen bonding are indiscernible from IRRAS frequency shifts.<sup>25</sup> Still, in aqueous suspensions, different subcomponents of the  $\nu(\text{C}=\text{O})$  band are interpreted as different hydration states of the carbonyl group containing distinct numbers of bound water molecules.<sup>20</sup> The spectra shown in Fig. 2A are therefore indicative of differences in hydration of the headgroups between both lipids. However, a more precise analysis is necessary due to different influence of the overlapping  $\gamma(\text{H}_2\text{O})$  band on the  $\text{C}=\text{O}$  bands of both lipids. In contrast to IR measurements of aqueous suspensions, we are not able to detect whether two or three subcomponents<sup>22</sup> are included in the lipids' carbonyl stretching vibrational band because of the overlap of the  $\nu(\text{C}=\text{O})$  band with the water deformation band.

Using IRRAS, we evaluated the  $\nu(\text{C}=\text{O})$  bands of both pure lipid monolayers at four distinct surface pressures, namely at  $3 \text{ mN m}^{-1}$  in the LE phase and at 10, 20, and  $30 \text{ mN m}^{-1}$  in the LC phase. For each surface pressure, we performed angle- and polarization-dependent IRRAS measurements that allow fitting the data to unravel conformational differences between both lipids and subtraction of the water absorption bands, which only depend on monolayer thickness, monolayer refractive index, and the quality of the used polarizer. The latter was determined empirically from all measurements with the used polarizer to be  $\Gamma = 0.007$ . The monolayer refractive index of

phospholipids is known from literature ( $n = 1.41$ ).<sup>26</sup> Monolayer thickness as the only remaining parameter can be derived from fitting the theoretical subphase water absorption bands to the measured data. After subtracting the simulated water bands from all IRRAS spectra, we conducted a PCA of the vector-normalized carbonyl bands of all s-polarized spectra of both lipids recorded at various angles of incidence ( $25^\circ$ – $70^\circ$ ) and surface pressures. The results of the PCA are shown in Fig. 3 and Fig. S5, S6 (ESI<sup>†</sup>).

The interpretation of spectral PCA is not necessarily straightforward. At first, one must interpret the resulting loadings of the principal components (PCs). PC 1 and PC 2 (Fig. 3A) account for approximately 90% of all variance in the  $\nu(\text{C}=\text{O})$  dataset and, hence, we limit our interpretation to these PCs. The loading of PC 1 reflects a spectral shift of the band minima from high to low frequency. Thus, higher scores on PC 1 are indicative of a higher hydration of the interfacial carbonyls, which is not visible as clearly in the averaged spectra without PCA (compare to Fig. 2A). PC 2, in contrast, seems to result mainly from atmospheric water vapor and experimental noise. It is an advantage of the PCA that these disturbing contributions are separated from the systematic variations mapped through PC 1. To interpret the differences between **DPPC** and **PHPC**, the score of PC 1 *versus* the surface pressure is shown in Fig. 3B as a box plot, where the individual boxes contain contributions of IRRAS spectra measured at various angles of incidence. Fig. 3B shows a clear separation of the scores of **DPPC** and **PHPC** on the PC 1 axis at all examined surface pressures, indicating different hydration of their respective carbonyl moieties. Additionally, within each subset of data, the scores on PC 1 decrease with increasing compression of the monolayer. For both lipids, this shift is most pronounced between 3 and  $10 \text{ mN m}^{-1}$ , corresponding to the LE/LC phase transition. Within the LC phase, this shift is smaller; however, it is more pronounced for **PHPC** than for **DPPC**. This reflects

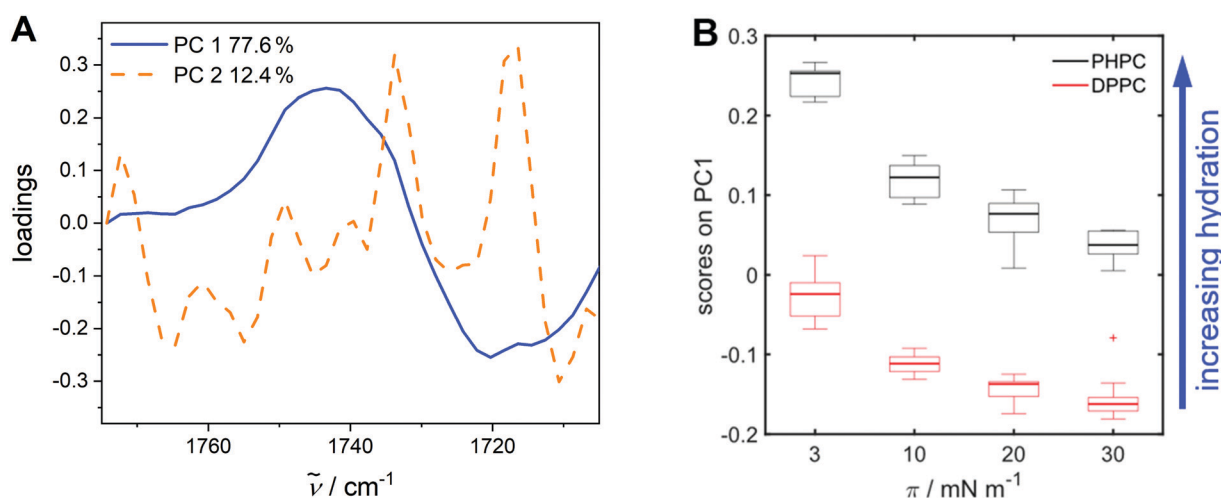


Fig. 3 PCA results of the  $\nu(\text{C}=\text{O})$  band of pure **PHPC** and **DPPC** monolayers at different surface pressures. (A) Loadings of PC 1 (blue) and PC 2 (orange); (B) score on PC 1 *versus* surface pressure  $\pi$  shown as box-whisker-plot. The IRRAS data used in this PCA were measured in the LE phase of both lipids ( $3 \text{ mN m}^{-1}$ ) and in the LC phase ( $10 \text{ mN m}^{-1}$ ,  $20 \text{ mN m}^{-1}$ , and  $30 \text{ mN m}^{-1}$ ) of **DPPC** (red) and **PHPC** (black), respectively. The (+) at  $30 \text{ mN m}^{-1}$  refers to an outlier for **DPPC**.

once more the ongoing ordering of **PHPC** upon LC phase compression corresponding to the chain order parameter and compressibility, respectively, reported above.

The scores of PC 2 versus PC 1 are shown in Fig. S5 (ESI<sup>†</sup>). No systematic changes are visible in the second PC, which matches the assumption of stochastic causes for the PC 2. The angle of incidence  $\varphi$  did not affect the score of any spectrum on PC 1 as can be seen in Fig. S6 (ESI<sup>†</sup>). However, the score of PC 2 depends on the angle of incidence, which, in turn, is due to the dependence of surface reflectivity on  $\varphi$ . This means the reflectivity and, hence, the signal-to-noise ratio increases for s-polarized IR light with increasing angle of incidence.<sup>19</sup>

As can be interpreted from Fig. 3, the PCA yields two results:

- (a) at all surface pressures, the frequency of the  $\nu(\text{C}=\text{O})$  band of **PHPC** is decreased compared to **DPPC** and
- (b) for both lipids, the frequency of the  $\nu(\text{C}=\text{O})$  band increases upon compression.

Since a frequency difference of the carbonyl stretching vibration between **DPPC** and **PHPC** reflects different hydration of the carbonyl group, we conclude that the carbonyl moiety of **PHPC** is either more hydrated (more bound water molecules) or the existing water molecules are bound more tightly to the carbonyls at the interface when compared to **DPPC**. This finding at first glance seems counterintuitive, as the substitution of an ester linkage between the glycerol and the *sn*-2 chain with an ether should result in a slightly more apolar headgroup region in comparison to **DPPC**. However, this seems not to decrease the hydration of the remaining carbonyl, but rather increases it. With respect to the literature, this may be interpreted as a change in glycerol orientation from approximately perpendicular to the water surface in **DPPC** to parallel to the water surface in **PHPC**—similar to findings in aqueous (bulk) suspensions.<sup>7</sup> An altered glycerol orientation in the gel phase of **PHPC** in bulk is connected to the formation of an interdigitated gel phase ( $L_{\beta}I$ ). In contrast, in monolayers an interdigitated arrangement is obviously not possible.

To support this hypothesis, we also evaluated the  $\text{CH}_2$  wagging band progressions (1260–1262 and 1243  $\text{cm}^{-1}$ ) of both lipids in monolayers, which overlap with the antisymmetric phosphate stretching vibrational band,  $\nu_{\text{as}}(\text{PO}_2^-)$  (1221–1226  $\text{cm}^{-1}$ ), of the headgroup.<sup>27</sup> The  $\text{CH}_2$  wagging band progressions are sensitive to single *gauche* conformers near the carbonyl groups of the lipid in the LC phase, because the intensity of the wagging band progressions increases significantly with coupling to the carbonyl group.<sup>24</sup> Adjacent kinks within the alkyl chain, *i.e.* the presence of *gauche* conformers, prevent this coupling resulting in attenuation of the  $\text{CH}_2$  wagging band progressions. No band progressions of the  $\text{CH}_2$  wagging vibration are therefore observed in fluid LE phases.<sup>24</sup> When comparing **PHPC** with **DPPC**, this effect is superimposed by the attenuation of these bands due to removal of one carbonyl group in **PHPC**. However, in **DPPC** bilayers, the  $\text{CH}_2$  wagging band progressions almost exclusively originate from the *sn*-1 chain, since the *sn*-2 chain includes a kink adjacent to the carbonyl group.<sup>7</sup> Therefore, if **PHPC** adopts a similar conformation of the glycerol backbone and the *sn*-1 ester linkage compared to **DPPC**, no or only little attenuation should occur. However, the

$\text{CH}_2$  wagging band progressions are significantly attenuated in bulk, which was considered by Lewis *et al.* as an additional argument for different glycerol orientations when comparing **DPPC** and **PHPC**.<sup>7</sup>

Our results in monolayers, as shown in Fig. 2B, expose an almost complete vanishing of the  $\text{CH}_2$  wagging band progressions of **PHPC** as compared to **DPPC** independent of the lipid phase. This must be caused by the introduction of one or more *gauche* conformers adjacent to the carbonyl moiety of the *sn*-1 chain.<sup>24</sup> Since the glycerol orientation in the LC phase of typical diester phosphocholines does not induce this *gauche* conformer<sup>28</sup> and measured spectra, thus, show significant coupling of carbonyl group and  $\text{CH}_2$  wagging vibrations,<sup>7</sup> we interpret this spectral difference of **PHPC** again in terms of a different glycerol orientation. By comparing our monolayer studies with literature-based knowledge from aqueous suspensions,<sup>7</sup> it becomes obvious that the attenuation of the  $\text{CH}_2$  wagging band progressions is remarkably more pronounced in monolayers than in bilayers. This can be interpreted as the *sn*-1 carbonyl moieties and the *sn*-1 chains having different orientations towards each other in bulk and in the monolayer, respectively. Additionally, all molecules in the monolayer are probably more uniformly arranged when compared to the bulk system, *i.e.*, one adjacent *gauche* conformer is introduced in all molecules in the **PHPC** monolayer.<sup>24</sup> However, these differences are expected because the typical arrangement of lipid molecules in monolayer LC phases is by no means the same as in interdigitated gel phases in bulk. It is remarkable that a change as small as substitution of one carbonyl with a  $\text{CH}_2$  group has a similar effect on the glycerol backbone conformation as changing the whole chain position from *sn*-2 to *sn*-3 and, thus, forcing the glycerol to be oriented parallel to the bilayer surface, as found in 1,3-dipalmitoylglycerophosphocholine (1,3-DPPC,  $\beta$ -DPPC)<sup>29,30</sup> and 1,3-diamidophospholipids, respectively.<sup>31,32</sup>

The absence of  $\text{CH}_2$  wagging band progressions in the LE phase of both lipid monolayers allows direct comparison of the  $\nu_{\text{as}}(\text{PO}_2^-)$  bands. This band of the polar headgroup is sensitive to ion binding as well as hydrogen bonding.<sup>19,23</sup> Since we used deionized water for all experiments, we may neglect contributions from remaining ions. Consequently, frequency shifts of  $\nu_{\text{as}}(\text{PO}_2^-)$  are caused by hydrogen bonding to either water or other lipid molecules. However, the phosphate groups in phosphocholines are known to be proton acceptors while no acidic protons can be donated from phosphocholines (unlike, *e.g.*, phosphoethanolamines).<sup>33</sup> Thus, hydrogen bonds cannot be formed directly with other lipids and must always include hydrating water molecules. In the IRRA spectra of both lipids at 3  $\text{mN m}^{-1}$ ,  $\text{CH}_2$  wagging band progressions are absent as expected, therefore, the frequency of the  $\nu_{\text{as}}(\text{PO}_2^-)$  band could be derived by simulating the spectra using only a single component. The results are summarized in Table 1. From the data it becomes evident that **PHPC** exhibits a lower  $\nu_{\text{as}}(\text{PO}_2^-)$  frequency than **DPPC**. Similar to what we found for the carbonyl stretching vibrational band, this again indicates an increased hydration of the **PHPC** headgroups, *i.e.* the presence of more or stronger bound water molecules.<sup>33,34</sup>

By simulating the  $\nu_{\text{as}}(\text{PO}_2^-)$  region including  $\text{CH}_2$  wagging band progression contributions in the LC phase, it is possible

to calculate the spectral components of these overlapping bands directly (see selected data in Fig. 4 and all spectra in Fig. S7 and S8, ESI†). For simulation, we used literature values for  $\text{CH}_2$  wagging band progression frequencies of **DPPC** in aqueous suspensions as starting parameters<sup>27</sup> and adjusted them in a nonlinear least squares fit. However, the frequencies fitted to our measurements did not deviate more than  $5\text{ cm}^{-1}$  from literature values despite being measured in LC phase monolayers instead of gel phase bilayers. Especially the evaluation of the order parameter  $S(\text{PO}_2^-)$  from  $\nu_{\text{as}}(\text{PO}_2^-)$  is promising as it can be correlated with the headgroup ordering. The determined order parameters of the  $\nu_{\text{as}}(\text{PO}_2^-)$  are shown in Fig. S9 (ESI†) and Table 1.

We simulated  $S(\text{PO}_2^-)$  with respect to the axis defined by the transition dipole moment of  $\nu_{\text{as}}(\text{PO}_2^-)$  ( $\alpha = 0^\circ$ )<sup>17</sup> to evaluate only the orientation of the phosphate group itself.  $S(\text{PO}_2^-)$  of both lipids depends on the lipid phase and our data clearly show differences between **DPPC** and **PHPC**. The phosphate groups of **DPPC** monolayers are less ordered, *i.e.*,  $S(\text{PO}_2^-)$  is smaller when compared to **PHPC**, regardless of the monolayer phase state. While **DPPC** maintains similar  $S(\text{PO}_2^-)$  values over the whole

compression range, **PHPC** shows a jump during phase transition from a higher magnitude of  $S(\text{PO}_2^-)$  in the LE phase to a lower magnitude of  $S(\text{PO}_2^-)$  in the LC phase. Beyond the LE/LC phase transition, both lipids exhibit a decreasing  $S(\text{PO}_2^-)$  during further compression of the condensed monolayer, with **PHPC** covering a larger range of ordering. As can be seen in Fig. S9 (ESI†),  $S(\text{PO}_2^-)$  of **PHPC** decreases significantly during compression of the LC phase. However, this effect should be interpreted cautiously as only three order parameters were measured in this lipid phase.

All the observed differences between **DPPC** and **PHPC** regarding their  $S(\text{PO}_2^-)$  are associated with the different glycerol orientation of both lipids, which must be caused by the comparably small chemical change of the *sn*-2 linkage.

With respect to all the results regarding the phosphate group, we conclude that an increased hydration of the **PHPC** phosphate in the LE phase goes along with a higher degree of headgroup ordering. These effects do not occur in **DPPC** monolayers and may therefore be related to different arrangements of glycerol backbones when **DPPC** and **PHPC** are compared. Presumably, more or strongly bound water molecules

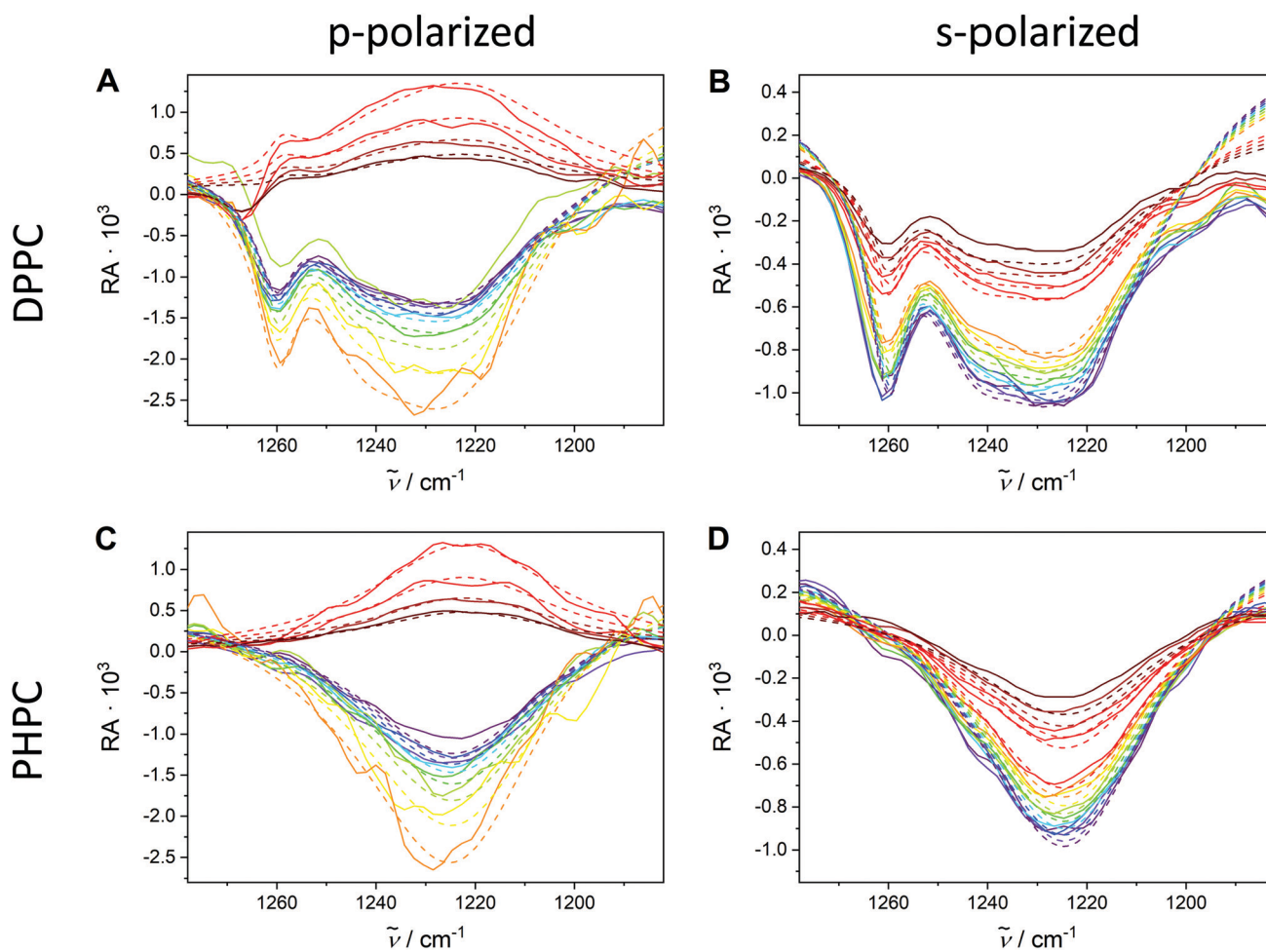
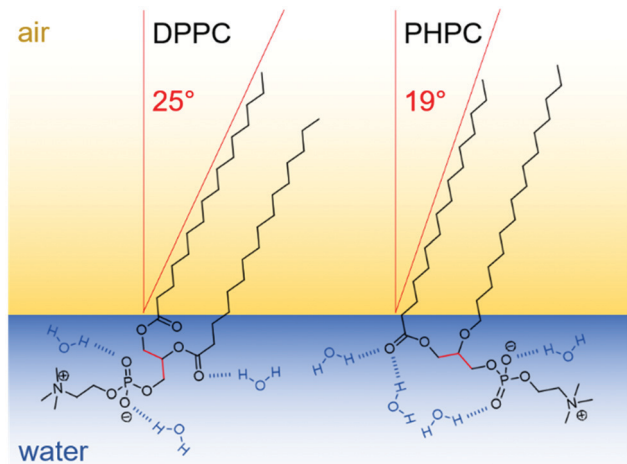


Fig. 4 Selected fits of the antisymmetric phosphate region including  $\text{CH}_2$  wagging band progressions at  $30\text{ mN m}^{-1}$  in the LC phase of pure **DPPC** (A, p-polarized; B, s-polarized) and **PHPC** (C, p-polarized; D, s-polarized).



**Scheme 2** Schematic representation of a possible LC phase orientation of a **DPPC** and a **PHPC** molecule on the air–water interface as deduced from IRRA spectroscopy. The number and orientation of the water molecules and hydrogen bonds, respectively, are schematic and for illustration purposes only.

increase the ordering of the phosphate moiety in **PHPC** monolayers. Furthermore, while in **DPPC** monolayers significant overlapping of  $\text{CH}_2$  wagging band progressions with  $\nu_{\text{as}}(\text{PO}_2^-)$  impede interpretation of separate bands, the corresponding bands in **PHPC** are attenuated to such a degree that they are hardly observable at all. This, firstly, supports our interpretation of a glycerol backbone oriented parallel to the surface and, secondly, allows direct interpretation of the  $\nu_{\text{as}}(\text{PO}_2^-)$  band.

In summary, the substitution of the *sn*-2 ester bond in **DPPC** by an ether bond in **PHPC** leads to:

- a different ordering of the lipid alkyl/acyl chains while maintaining the overall phase behaviour,
- a rearrangement of the glycerol backbone to a presumably parallel orientation with respect to the water surface connected with the introduction of (at least one) *gauche* conformers in the *sn*-1 alkyl chain adjacent to the carbonyl moiety, and
- a higher degree of headgroup ordering combined with increased hydration of both the carbonyl and the phosphate group.

The resulting different molecular orientations of **DPPC** and **PHPC** molecules at the air–water interface are schematically depicted in Scheme 2.

### Mixed monolayers of DPPC and PHPC

In the second part of this study, we focus on the mixing behaviour of **DPPC** and **PHPC** in monolayers at the air–water interface. For this purpose, we measured  $\pi$ - $A_{\text{mol}}$  isotherms of mixed monolayers containing both lipids at different mixing ratios at 20 °C and, simultaneously, performed epifluorescence microscopy of these mixed monolayers. Furthermore, we measured IRRA spectra of the corresponding mixtures of **PHPC** and **DPPC-*d*<sub>62</sub>**, which is the chain-perdeuterated analogue of **DPPC**, to be able to monitor the behaviour of both types of lipids separately.

The  $\pi$ - $A_{\text{mol}}$  isotherms of mixtures containing 90 to 25% **DPPC** and 10 to 75% **PHPC** are shown in Fig. 5A together with

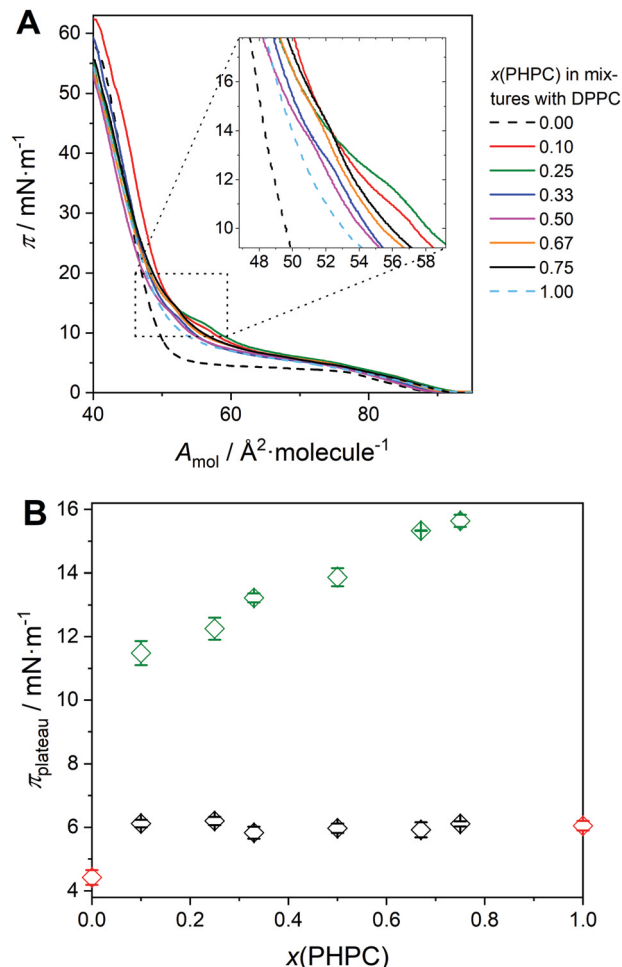


**Fig. 5** Isothermal compression of mixed **DPPC/PHPC** monolayers at 20 °C. (A)  $\pi$ - $A_{\text{mol}}$  isotherms with  $\pi$  range of the upper plateau in the inset, (B) phase diagram with all observed  $\pi_{\text{plateau}}$  (pure lipids are marked in red,  $\pi_{\text{plateau}}$  of the upper plateau is highlighted green).

the isotherms of the pure compounds. In the isotherms of the mixtures, two plateaus or kinks are observable, the upper of which does not exist in isotherms of the pure substances. Therefore, the question arises, whether this plateau is connected to a phase transition or not. By evaluating the compressibility maxima (see Fig. S10, ESI<sup>†</sup>) of all films, the surface pressure values at both plateaus were determined. These values are plotted in Fig. 5B in form of a partial phase diagram and are further shown in Table 2. The midpoint of the lower transition is always located at the transition pressure of pure **PHPC**, whereas the upper plateau pressure increases with increasing **PHPC** content. From measuring compression isotherms alone, it is not possible to answer the three main questions arising from the observation of an additional plateau: (i) what is its origin, (ii) what are the phase states outside the plateaus, and (iii) are both lipids miscible in all occurring phases?

Therefore, we further characterized the phase behaviour of the mixed monolayers by epifluorescence microscopy, using Rh-DPPE as fluorescent dye. The obtained micrographs are shown in Fig. 6 and additional images in Fig. S11–S16 (ESI<sup>†</sup>).

**Table 2** Plateau surface pressures ( $\pi_{\text{plateau}}$ ) of pure and mixed monolayers of **PHPC** and **DPPC**

$x(\text{PHPC})$	$\pi_{\text{plateau}}/\text{mN m}^{-1}$	
0.00	$4.42 \pm 0.23$	
0.10	$6.12 \pm 0.12$	$11.48 \pm 0.38$
0.25	$6.20 \pm 0.13$	$12.25 \pm 0.35$
0.33	$5.83 \pm 0.19$	$13.22 \pm 0.14$
0.50	$5.97 \pm 0.15$	$13.87 \pm 0.28$
0.67	$5.92 \pm 0.24$	$15.33 \pm 0.01$
0.75	$6.11 \pm 0.08$	$15.64 \pm 0.19$
1.00	$6.05 \pm 0.15$	

Typically, Rh-DPPE dissolves readily in LE-phase monolayers while it is excluded from LC-phase domains.<sup>12,21</sup> As can be seen in column (c) of Fig. 6, this is true for a pure **DPPC** monolayer, where LC domains appear black.<sup>21</sup> In contrast, in **PHPC**-containing monolayers, Rh-DPPE can partition into LC domains leading to a lower contrast between the LE and LC phase. Moreover, the shape of **DPPC** and **PHPC** LC domains is remarkably different. Therefore, changes in LC phase composition can be unravelled by contrast and shape of the observed domains in mixed monolayers of **DPPC** and **PHPC**.

First, epifluorescence microscopy of the mixed monolayers enables us to determine, whether (partial) demixing occurs in the LE and/or the LC phase of the mixed monolayers. As it is evident from Fig. 6 and Fig. S12–S15 (ESI<sup>†</sup>), the LE phases of all measured mixtures are uniformly bright. This leads to the conclusion that no phase separation occurs below the lower plateau of the respective mixture. At surface pressures above this plateau, the micrographs of all **DPPC/PHPC** mixtures appear uniformly grey indicating the existence of only one homogeneously mixed phase in between both plateaus (column (e) in Fig. 6). No further changes were detected at the upper plateau of the compression isotherms.

Second, the LE/LC transition of the mixtures, which evidently occurs at the lower plateau, is compared to the LE/LC transition of both pure substances. The LC domain shape of pure **DPPC** and **PHPC** differs significantly (see Fig. 6). While **DPPC** forms characteristic chiral bean or propeller shaped domains, **PHPC**, which is racemic in this study, forms star-like, fractal grey LC domains which do not exhibit chirality.<sup>35</sup>

When both lipids are mixed, nucleation of the LC domains begins with mainly **DPPC**, as can be deduced from the appearance of compact black domains (see column (b) in Fig. 6 as well as Fig. S12–S15, ESI<sup>†</sup>). The dye Rh-DPPE is excluded from these small **DPPC**-rich domains at the onset of the LE/LC transition but, subsequently, partitions into the LC phase while **PHPC** is incorporated. As the LC domains grow in size, **PHPC** joins at the rim of already formed **DPPC**-rich domains with its typical star-like LC domain shape leading to the formation of demixed LC domains (see Fig. 6, column (c)). At the end of the phase transition, the LC phase homogenizes, *i.e.*, both lipids form a mixed LC phase, being embedded in a continuous LE phase (see Fig. 6, column (d)). Mixtures with high **DPPC** content remain in the demixed LC state up to higher surface pressures and their LC phases tend to be

darker because the dye is excluded from **DPPC**-rich domains to a higher extent.

Although these results suggest a co-existence of three phases in the lower plateau (**DPPC**-rich LC phase, 2<sup>nd</sup> LC phase with increased **PHPC** content, and mixed LE phase), these were not stable when the compression was paused and the system was allowed to equilibrate (see Fig. S17, ESI<sup>†</sup>). Likewise, only two phases were observed in the LC/LE transition upon expansion of a mixed **DPPC/PHPC** monolayer ( $x(\text{PHPC}) = 0.1$ ) (see Fig. S17, ESI<sup>†</sup>). We therefore assume that the three phases occurring in the LE/LC transition region upon compression are meta-stable and not in equilibrium, *i.e.*, their appearance is due to a kinetically hindered condensation upon continuous compression.

Yet, the origin of the upper plateau remains uncertain. By means of fluorescence microscopy and with the used Rh-DPPE dye it could not be attributed to a phase transition. To unravel further details of lipid miscibility, we interpret our data by applying the Gibbs phase rule and by calculating the Gibbs energy of mixing,<sup>12</sup> both of which are regularly used in miscibility studies in monolayers.

Although the surface phase rule is frequently used for miscibility studies in Langmuir monolayers,<sup>11,36</sup> in this work application of the Gibbs phase rule is sufficient as shown in Appendix 1. The Gibbs phase rule is given as  $F = C - P + 2$ , where  $F$  denotes the degrees of freedom,  $C$  is the number of components in the monolayer, and  $P$  is the number of phases in the monolayer. It is possible to only discuss the components and phases of the monolayer as long as no lipid exchange between monolayer and bulk phases occurs, which is the case for long-chain phospholipids.<sup>37</sup> With two monolayer components, **DPPC** and **PHPC**, the Gibbs phase rule simplifies to  $F = 4 - P$  or  $P = 4 - F$ , when solved for the number of phases. Thus, by evaluating the degrees of freedom of the studied systems, a prediction of the number of co-existing phases is possible.

Since there must be at least one monolayer phase, maximal three degrees of freedom can exist, which are the surface pressure  $\pi$ , temperature  $T$ , and mole fraction  $x$ . Consequently,  $P$  can vary between one ( $F = 3$ ) and four ( $F = 0$ ).

As evident from Fig. 5, in all phases below, in between, and above the  $\pi_{\text{plateau}}$ ,  $\pi$  and  $x$  and presumably  $T$  (compare Fig. S18, ESI<sup>†</sup>) are degrees of freedom, as they can be varied independently without changing the state of the system. Hence, only one mixed phase would exist in these states. This is consistent with the results of epifluorescence microscopy, which show one uniform phase in the respective surface pressure ranges (Fig. 6, columns (a) and (e) and Fig. S12–S15, ESI<sup>†</sup>) as well as the analysis of  $\Delta G_{\text{mix}}$  discussed below.

In contrast, in the plateaus of the  $\pi$ - $A_{\text{mol}}$  isotherms,  $x$  and  $\pi$  are correlated (Fig. 5B), *i.e.*,  $\pi$  depends on  $x$  and is therefore not a degree of freedom as opposed to  $x$ . Consequently,  $F$  is either one ( $x$ ) or two ( $T, x$ ) and, hence,  $P$  is three or two, respectively. Note that  $\pi$  of the lower plateau seems to be independent of  $x$  due to both pure lipids exhibiting nearly the same LE/LC transition pressure. However, if chain-perdeuterated **DPPC**- $d_{62}$  is used in these mixtures, which has an increased phase transition pressure,<sup>38,39</sup> it can be shown that  $\pi$  of the lower plateau also depends on  $x$  (see below and Fig. S20, ESI<sup>†</sup>).

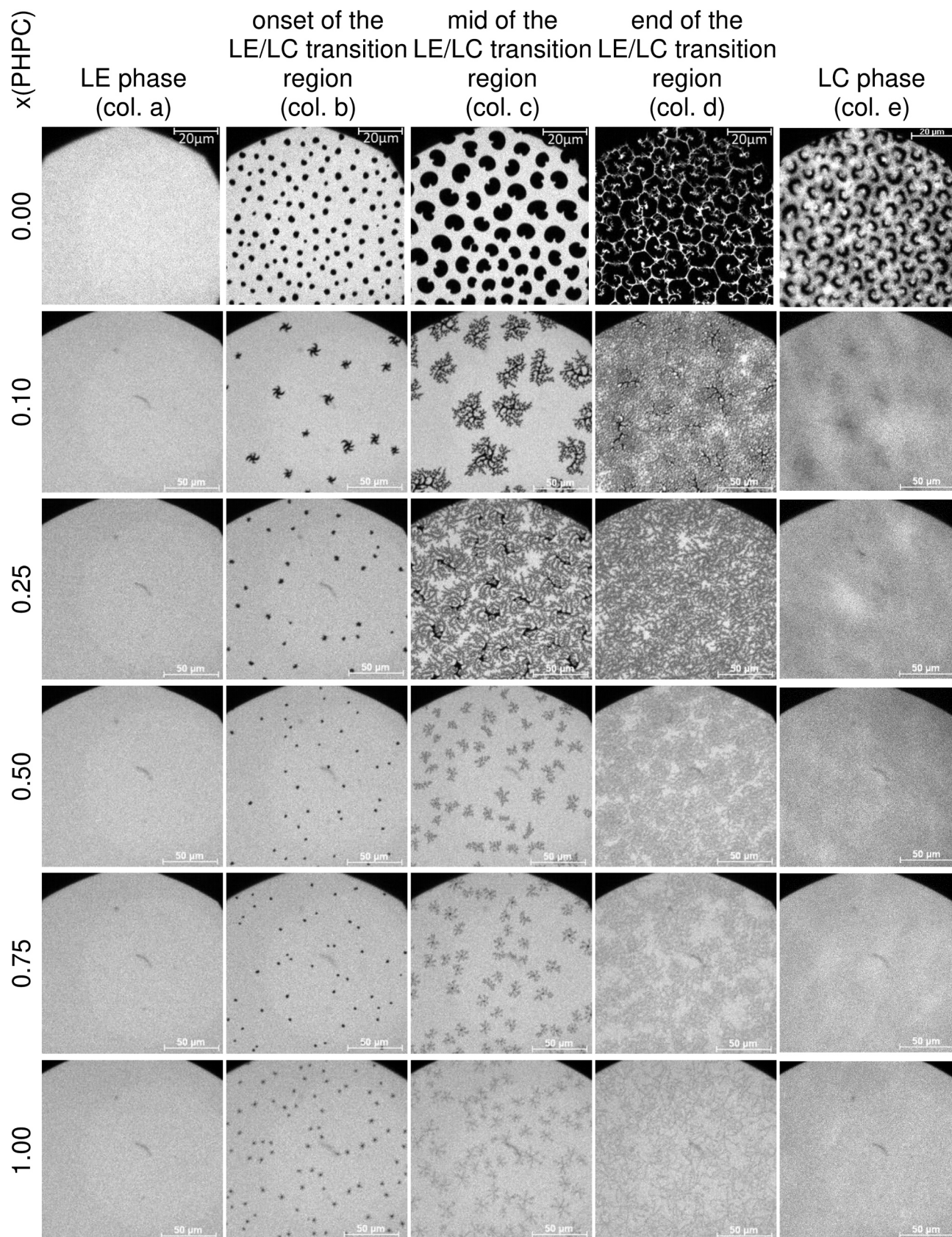


**Fig. 6** Selected fluorescence micrographs of mixed monolayers of **DPPC** and **PHPC**. The scale bars represent 20  $\mu\text{m}$  in case of **DPPC** and 50  $\mu\text{m}$  in all other micrographs. The micrographs shown here were taken in the LE phase, at different points in the LE/LC transition region as indicated in the column headings, and in the LC phase. A full picture of the fluorescence microscopic characterization is presented in Fig. S11–S16 (ESI<sup>†</sup>).

Interestingly, the epifluorescence micrographs shown in columns (c) and (d) of Fig. 6 and further in Fig. S12–S15 (ESI†) display three apparent phases in the lower plateau of the mixtures, which are not stable (see Fig. S17, ESI†), and are probably the consequence of the continuous compression of the monolayer. Hence, they do not represent the equilibrium state within the LE/LC phase transition and, consequently, cannot be interpreted using the phase rule which is only valid in equilibrium. This means that the number of equilibrium phases in the transition is two and consequently both  $x$  and  $T$  are degrees of freedom, *i.e.*,  $\pi$  depends on  $x$  and on  $T$ . The latter,  $\pi$  depends on  $T$ , was proven exemplarily for one mixture (Fig. S18, ESI†). One can clearly see that the compressibility maxima of the DPPC/PHPC 3:1 monolayer shift linearly to lower surface pressure with decreasing temperature. This shows that the transition exists at different temperatures and, hence,  $T$  is a degree of freedom in the phase transition. This allows the conclusion that beyond the plateaus no phase coexistence occurs.

To further evaluate the thermodynamics of the miscibility of both lipids below, in between, and above the plateaus, one can calculate the Gibbs energy of mixing  $\Delta G_{\text{mix}}$  and the excess Gibbs energy of mixing  $\Delta G_{\text{exc}}$ , which describes the deviations from ideal miscibility.<sup>12</sup> To this end, we compare the observed  $\pi$ - $A_{\text{mol}}$  isotherms with ideal ones, calculated from the pure substances, to yield molecular excess areas  $A_{\text{exc}}$ . The  $A_{\text{exc}}$  are then integrated and values of  $\Delta G_{\text{exc}}$  are calculated. Using the known ideal Gibbs energy of mixing,  $\Delta G_{\text{mix}}$  is then derived. Further information on calculations are given in the Experimental part of this study. The calculated  $\Delta G_{\text{exc}}$  and  $\Delta G_{\text{mix}}$  are included in Table S1 (ESI†) and plotted in Fig. 7.

From these data it can be concluded that at all mixing ratios, DPPC and PHPC are miscible. In the LE phase at  $3 \text{ mN m}^{-1}$ , nearly ideal mixing or complete demixing was observed. As complete mixing has been observed by epifluorescence microscopy, we interpret this result as ideal miscibility of both lipid species in the LE phase. However, positive deviations from an ideal miscibility at  $10 \text{ mN m}^{-1}$  (between both plateaus) and  $30 \text{ mN m}^{-1}$  (above both plateaus), *i.e.* repulsive interactions between both lipids, were observed for the DPPC/PHPC mixtures containing 10% and 75% of PHPC, respectively (Fig. 7A). However, the magnitude of  $\Delta G_{\text{exc}}$  is not sufficient to induce complete phase separation.

Analysis of the  $\pi$ - $A_{\text{mol}}$  isotherms by application of the Gibbs phase rule and evaluation of Gibbs energies of mixing leads to the conclusion that (i) outside both plateaus PHPC and DPPC are miscible and (ii) at least at the lower plateau two phases co-exist in equilibrium. Both conclusions are supported by microscopy data.

To evaluate the miscibility in more molecular detail, again IRRAS spectroscopy was used. IRRAS enables us to discriminate both lipids in mixtures through isotopic labelling, since different nuclear isotopes result in different reduced masses of the vibrating moieties. Hence, a shift is observed in the IR spectra. When mixing PHPC with chain-perdeuterated DPPC- $d_{62}$  it is, thus, possible to compare the surface pressure-dependent change in frequency of  $\nu_{\text{s}}(\text{CH}_2)$  and  $\nu_{\text{s}}(\text{CD}_2)$  and to observe the phase transition pressure

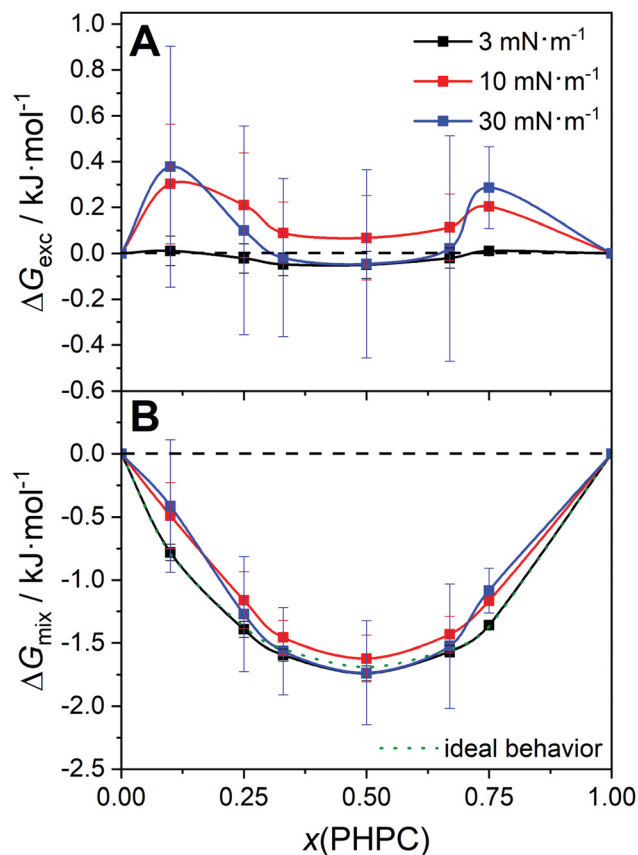


Fig. 7 Thermodynamic parameters  $\Delta G_{\text{exc}}$  (A) and  $\Delta G_{\text{mix}}$  (B) of DPPC/PHPC mixed monolayers as a function of mixture composition at 20 °C (a dashed line at 0  $\text{kJ mol}^{-1}$  in both panels and  $\Delta G_{\text{id}}$  as a green dotted line in B were added for clarity).

of both lipids in their mixtures independently. If both lipids show a condensation (decrease of the methylene stretching vibration wavenumbers) at the same surface pressure during compression, they must be considered miscible. If the LE/LC transition pressure differs between both lipids, they demix at least partially. These measurements can also answer the question whether DPPC and PHPC contribute differently to both transitions observed in the isotherms. Furthermore, it can be deduced whether lipid chain condensation/ordering is involved in the upper plateau, *i.e.*, if this plateau can also be considered as phase transition plateau.

In Fig. 8, the frequencies of  $\nu_{\text{s}}(\text{CH}_2)$  and  $\nu_{\text{s}}(\text{CD}_2)$  are plotted together with the compressibility of the monolayer for the mixture  $x(\text{PHPC}) = 0.75$ , which exhibits positive deviation from ideal mixing behaviour (compare to Fig. 7). The corresponding plots of all other mixing ratios are shown in Fig. S19 (ESI†). Note that the phase transition surface pressure is increased in comparison to the measurements shown in Fig. 5, because of one mixing component being chain-perdeuterated (see Fig. S20, ESI†). Deuteration of the lipids' acyl chains has a significant effect on the phase transition surface pressure as well as the main phase transition temperature in aqueous suspension.<sup>38,39</sup> In all measured mixed monolayers, the lower transition appears to be shifted to higher  $\pi$ -values, that is, no plateau at the pure

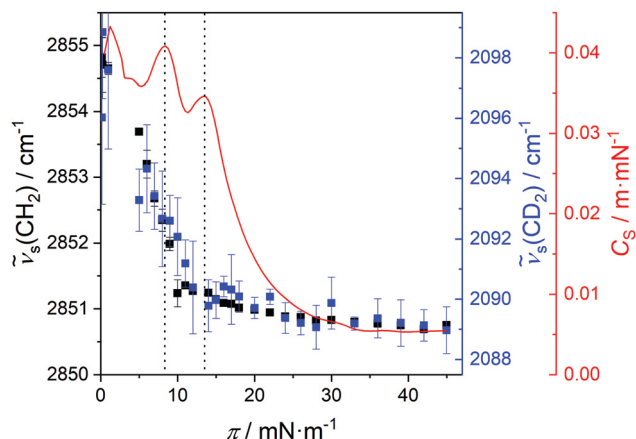


Fig. 8 Comparison of  $\nu_s(\text{CH}_2)$  (black squares) and  $\nu_s(\text{CD}_2)$  (blue squares) during compression of a monolayer of an **PHPC**/**DPPC- $d_{62}$**  mixture ( $\chi(\text{PHPC}) = 0.75$ ) at 20 °C, plotted together with  $C_s$  (red line). (To guide the eye, dotted lines are drawn at both maxima of  $C_s$ , i.e. the  $\pi_{\text{plateau}}$ .)

**PHPC**'s transition pressure is detectable. This is an indication for at least partial miscibility.

Like the band position of the  $\text{CH}_2$  stretching vibrations, also  $\nu_s(\text{CD}_2)$  and  $\nu_{\text{as}}(\text{CD}_2)$  are indicative of the *trans/gauche* ratio in the respective alkyl chains and can therefore be used to detect phase transitions involving chain melting. For the presented  $\chi(\text{PHPC}) = 0.75$  mixture (just like for all other compositions), we found that both lipids undergo a common phase transition and that at the plateau at lower  $\pi$ , a significant frequency shift, i.e. condensation of the lipids, occurs simultaneously. The second transition at higher surface pressure is connected to a comparatively small decrease in  $\text{CH}_2/\text{CD}_2$  stretching vibrational frequencies. This leads to the conclusion that lipid chain condensations have only minor contribution to this second transition. When chain-deuterated **DPPC** is used, the two plateaus are only discernible for mixtures of  $\chi(\text{PHPC}) \geq 0.33$ . In the isotherms of mixtures containing less **PHPC**, both transitions overlay which results in one broadened  $C_s$  curve (compare to Fig. S19, ESI†).

A comparative examination at both methylene stretching vibrational bands ( $\text{CH}_2$  as well as  $\text{CD}_2$ ) and at the phosphate stretching vibrational bands using PCA shows simultaneous transitions of the deuterated and non-deuterated lipid chains but a delayed transition in the phosphate headgroup (Fig. S21 and S22, ESI†). After a concomitant change of the PC 1 scores in all three spectral ranges at the onset of the first plateau, the most pronounced changes in the phosphate vibrations are found at slightly elevated surface pressures, which could correlate with

the surface pressure at the second plateau in the isotherms. In addition, the phosphate stretching vibrations shows another, albeit less pronounced, change in the range between 20 and 30  $\text{mN m}^{-1}$ . This might be correlated with a headgroup re-orientation. In any case, it shows that transitions in the headgroup region may exist that are independent of the chain condensation. However, since we do not have enough complementary data about this transition, we refrain from further speculation about its origin.

By combining the results of all experiments performed in this study regarding miscibility of **DPPC** and **PHPC**, we conclude that there is substantial evidence that the two lipids are miscible in all mixing ratios but might show deviations from ideal miscibility. From IRRAS measurements of mixtures of **PHPC** and **DPPC- $d_{62}$**  it is found that the upper plateau does not involve a significant amount of chain ordering as it would occur in lipid **LE/LC** phase transitions. By employing epifluorescence microscopy, we observed two stable co-existing monolayer phases during the **LE/LC** phase transition in equilibrium (at the lower plateau). However, the nature of the second plateau appearing only in the mixtures of both substances could not be unravelled completely. Our main conclusions on lipid miscibility are summarized in Table 3.

## Conclusions

In this work, we present studies of pure monolayers of the structurally related phospholipids **DPPC** and **PHPC** using  $\pi$ - $A_{\text{mol}}$  isotherms and IRRAS. In addition, we provide a detailed characterization of mixed **DPPC/PHPC** monolayers through their isotherms using epifluorescence microscopy, the Gibbs phase rule, evaluation of thermodynamic mixing parameters, and IRRAS.

The isotherms of both pure lipid monolayers are comparable and differ only slightly in their phase transition pressures and **LC** phase compressibilities. **DPPC** and **PHPC** exhibit comparable alkyl chain *trans/gauche* ratios in their corresponding **LE** and **LC** phases and both form hexagonal, ordered **LC** phases above their **LE/LC** phase transition. We find that the substitution of the ester linkage at the *sn*-2 chain by an ether linkage causes several changes in lipid monolayer organization despite both lipids showing similar  $\pi$ - $A_{\text{mol}}$  isotherms. **PHPC**, when compared to **DPPC**, exhibits:

- a smaller chain tilt angle at surface pressures of 20  $\text{mN m}^{-1}$  and above,
- stronger hydration of the carbonyl group independent of  $\pi$ ,
- stronger hydration of the phosphate group in the **LE** phase,
- increased headgroup ordering, and

Table 3 Summary of results on mixing behaviour of **DPPC** and **PHPC** in monolayers

Method	Main result
$\pi$ - $A_{\text{mol}}$ isotherms	Appearance of two plateaus
Epifluorescence microscopy	Miscibility in both phases, demixing in phase transition, and kinetically hindered mixing after phase transition
Application of the Gibbs phase rule	Miscibility in all non-plateau regions
Evaluation of $\Delta G_{\text{mix}}$	Miscibility in <b>LE</b> and <b>LC</b> phase
IRRAS with <b>DPPC-<math>d_{62}</math></b>	Simultaneous condensation of both lipids, delayed headgroup transition

• strong attenuation of the CH<sub>2</sub> wagging band progressions independent of  $\pi$ .

These findings lead to the conclusion that the glycerol moiety of **PHPC** adopts an orientation parallel to the water surface, which is different from the orientation of the glycerol of **DPPC** or other unsubstituted 1,2-diester phosphocholines. Similar orientational differences have been found in aqueous suspensions of the lipids before.

In the second part of this study, we present plateaus in the  $\pi$ - $A_{\text{mol}}$  isotherms of mixed monolayers containing **DPPC** and **PHPC**, that do not appear in the isotherms of either of the pure lipids. The miscibility studies of mixed monolayers in the full mixing range can be interpreted in terms of non-ideal mixing behaviour; but no demixing occurs neither in the LE nor in the LC phase as detected by epifluorescence microscopy and being confirmed by mixing energy calculations. Further characterization of the mixing behaviour by IRRAS shows that the upper plateau does not involve significant ordering of lipid chains. The cause for existence of the upper plateau remains unclear from our experiments but seems to involve changes in head-group hydration. It is likely to originate from the geometrical differences (for example headgroup re-orientation) found for both pure lipid monolayers.

## Author contributions

Conceptualization M. H., C. S., and D. H.; data curation M. H., S. D., C. S., and D. H.; formal analysis M. H. and C. S.; funding acquisition D. H.; investigation M. H., S. D., and C. S.; methodology S. D. and C. S.; project administration C. S. and D. H.; resources S. D., C. S., and D. H.; software C. S.; supervision S. D., C. S., and D. H.; validation M. H. and C. S.; visualization M. H., S. D., and C. S.; writing – original draft M. H., S. D., C. S., and D. H.; writing – review & editing S. D., C. S., and D. H.

## Conflicts of interest

There are no conflicts to declare.

## Appendix 1

The commonly used surface phase rule in monolayers is given by:<sup>11,36</sup>

$$F = (C_{\text{b}} + C_{\text{m}}) - (P_{\text{b}} + P_{\text{m}}) + 3, \quad (7)$$

with  $F$  degrees of freedom,  $C_{\text{b}}$  and  $C_{\text{m}}$  being bulk and monolayer components, respectively, and  $P_{\text{b}}$  and  $P_{\text{m}}$  being bulk and monolayer phases, respectively.

With  $C_{\text{b}} + C_{\text{m}} = 4$  (water, air, and two lipids) it reduces to:

$$F = 7 - P, \quad (8)$$

with  $P = P_{\text{b}} + P_{\text{m}}$ . Thus,  $F$  can be maximal six and is a subset of  $\{p, T, \pi, x_{\text{monolayer}}, x_{\text{air}}, x_{\text{subphase}}\}$ .

Assuming that bulk and monolayer components do not mix, which is given for a Langmuir monolayer,<sup>37</sup> and that the bulk

phases (air and the aqueous subphase) are always pure, it holds:  $x_{\text{air}} = x_{\text{subphase}} = 1$  (i.e., no degrees of freedom) and  $C_{\text{b}} = P_{\text{b}}$ . Thus, eqn (7) simplifies to:

$$F = C_{\text{m}} - P_{\text{m}} + 3 = 5 - P, \quad (9)$$

where  $F$  is a subset of  $\{p, T, \pi, x_{\text{monolayer}}\}$ . Assuming additionally that the bulk pressure ( $p$ ) does not influence the number of monolayer phases,  $F$  decreases further by one:

$$F = C_{\text{m}} - P_{\text{m}} + 2 = 4 - P, \quad (10)$$

with  $F$  being a subset of  $\{T, \pi, x_{\text{monolayer}}\}$ . Eqn (10) corresponds to the classical Gibbs phase rule applied to an insoluble monolayer (with two lipid monolayer components).

## Acknowledgements

We thank Kai Gruhle (MLU Halle-Wittenberg, Institute of Pharmacy) for his support during the synthesis of **PHPC**. M. H. thanks the Fonds der Chemischen Industrie (FCI) for their support through a Kekulé scholarship.

## References

- J. L. C. M. van de Vossenberg, A. J. M. Driessen and W. N. Konings, *Extremophiles*, 1998, **2**, 163–170.
- J.-H. Fuhrhop and T. Wang, *Chem. Rev.*, 2004, **104**, 2901–2937.
- M. de Rosa, A. Gambacorta and A. Gliozzi, *Microbiol. Rev.*, 1986, **50**, 70–80.
- A. Blume, S. Drescher, G. Graf, K. Kohler and A. Meister, *Adv. Colloid Interface Sci.*, 2014, **208**, 264–278.
- A. Bottelbergs, S. Verheijden, P. P. Van Veldhoven, W. Just, R. Devos and M. Baes, *J. Neuroinflammation*, 2012, **9**, 61.
- D. I. Benjamin, A. Cozzo, X. Ji, L. S. Roberts, S. M. Louie, M. M. Mulvihill, K. Luo and D. K. Nomura, *Proc. Natl. Acad. Sci. U. S. A.*, 2013, **110**, 14912–14917.
- R. N. A. H. Lewis, W. Pohle and R. N. McElhaney, *Biophys. J.*, 1996, **70**, 2736–2746.
- G. Brezesinski, A. Dietrich, B. Struth, C. Böhm, W. G. Bouwman, K. Kjaer and H. Möhwald, *Chem. Phys. Lipids*, 1995, **76**, 145–157.
- G. Brezesinski, A. Dietrich, B. Dobner and H. Möhwald, *Prog. Colloid Polym. Sci.*, 1995, **98**, 255–262.
- P. Mattjus, R. Bittman and J. P. Slotte, *Langmuir*, 1996, **12**, 1284–1290.
- H.-D. Dörfler, *Adv. Colloid Interface Sci.*, 1990, **31**, 1–110.
- A. Blume, *ChemTexts*, 2018, **4**, 3.
- S. W. H. Shah, C. Schwieger, J. Kressler and A. Blume, *Chem. Phys. Lipids*, 2020, **230**, 104918.
- M. Hoffmann, S. Drescher, C. Ihling, D. Hinderberger and C. Schwieger, *Langmuir*, 2020, **36**, 12804–12815.
- C. Schwieger, A. Meister, S. Daum, A. Blume and K. Bacia, *Polymers*, 2017, **9**, 612.
- S. Schrettl, C. Stefaniu, C. Schwieger, G. Pasche, E. Oveisi, Y. Fontana, A. Fontcuberta i Morral, J. Reguera, R. Petraglia, C. Corminboeuf, G. Brezesinski and H. Frauenrath, *Nat. Chem.*, 2014, **6**, 468–476.

- 17 C. Schwieger, B. Chen, C. Tschierske, J. Kressler and A. Blume, *J. Phys. Chem. B*, 2012, **116**, 12245–12256.
- 18 H. Abdi and L. J. Williams, *Wiley Interdiscip. Rev.: Comput. Stat.*, 2010, **2**, 433–459.
- 19 R. Mendelsohn, J. W. Brauner and A. Gericke, *Annu. Rev. Phys. Chem.*, 1995, **46**, 305–334.
- 20 A. Blume, W. Hübner and G. Messner, *Biochemistry*, 1988, **27**, 8239–8249.
- 21 P. Scholtysek, Z. Li, J. Kressler and A. Blume, *Langmuir*, 2012, **28**, 15651–15662.
- 22 R. N. A. H. Lewis, R. N. McElhaney, W. Pohle and H. H. Mantsch, *Biophys. J.*, 1994, **67**, 2367–2375.
- 23 R. Mendelsohn, G. Mao and C. R. Flach, *Biochim. Biophys. Acta*, 2010, **1798**, 788–800.
- 24 R. N. A. H. Lewis and R. N. McElhaney, *Biochim. Biophys. Acta*, 2013, **1828**, 2347–2358.
- 25 A. Dicko, H. Bourque and M. Pézolet, *Chem. Phys. Lipids*, 1998, **96**, 125–139.
- 26 C. R. Flach, A. Gericke and R. Mendelsohn, *J. Phys. Chem. B*, 1997, **101**, 58–65.
- 27 L. Senak, D. Moore and R. Mendelsohn, *J. Phys. Chem.*, 1992, **96**, 2749–2754.
- 28 T. M. Bayerl, R. K. Thomas, J. Penfold, A. Rennie and E. Sackmann, *Biophys. J.*, 1990, **57**, 1095–1098.
- 29 E. N. Serrallach, R. Dijkman, G. H. de Haas and G. G. Shipley, *J. Mol. Biol.*, 1983, **170**, 155–174.
- 30 G. Büldt and G. H. de Haas, *J. Mol. Biol.*, 1982, **158**, 55–71.
- 31 A. Weinberger, R. Tanasescu, C. Stefaniu, I. A. Fedotenko, F. Favarger, T. Ishikawa, G. Brezesinski, C. M. Marques and A. Zumbuehl, *Langmuir*, 2015, **31**, 1879–1884.
- 32 I. A. Fedotenko, C. Stefaniu, G. Brezesinski and A. Zumbuehl, *Langmuir*, 2013, **29**, 9428–9435.
- 33 H. Akutsu, M. Ikematsu and Y. Kyogoku, *Chem. Phys. Lipids*, 1981, **28**, 149–158.
- 34 F. Neuhaus, D. Mueller, R. Tanasescu, C. Stefaniu, P. L. Zaffalon, S. Balog, T. Ishikawa, R. Reiter, G. Brezesinski and A. Zumbuehl, *Soft Matter*, 2018, **14**, 3978–3986.
- 35 P. Krüger and M. Lösche, *Phys. Rev. E: Stat. Phys., Plasmas, Fluids, Relat. Interdiscip. Top.*, 2000, **62**, 7031–7043.
- 36 M. I. Sández Macho, A. Gil Gonzalez and A. Suárez Varela, *J. Colloid Interface Sci.*, 2001, **235**, 241–246.
- 37 R. Smith and C. Tanford, *J. Mol. Biol.*, 1972, **67**, 75–83.
- 38 T. Brumm, C. Naumann, E. Sackmann, A. R. Rennie, R. K. Thomas, D. Kanellas, J. Penfold and T. M. Bayerl, *Eur. Biophys. J.*, 1994, **23**, 289–295.
- 39 N. O. Petersen, P. A. Kroon, M. Kainosho and S. I. Chan, *Chem. Phys. Lipids*, 1975, **14**, 343–349.

## **Influence of Different Polymer Belts on Lipid Properties in Nanodiscs Characterized by CW EPR Spectroscopy**

Matthias Hoffmann, Jana Eisermann, Florian A. Schöffmann, Manabendra Das, Carolyn Vargas, Sandro Keller and Dariush Hinderberger

*BBA Biomembranes* **2021**, 1863 (10), 183681

DOI: [10.1016/j.bbamem.2021.183681](https://doi.org/10.1016/j.bbamem.2021.183681)

This article was published in *BBA Biomembranes*, 1863 (10), M. Hoffmann, J. Eisermann, F. A. Schöffmann, M. Das, C. Vargas, S. Keller and D. Hinderberger, Influence of Different Polymer Belts on Lipid Properties in Nanodiscs Characterized by CW EPR Spectroscopy, 183681, Copyright Elsevier (2021). Reprinted with permission from Elsevier.



## Influence of different polymer belts on lipid properties in nanodiscs characterized by CW EPR spectroscopy

Matthias Hoffmann<sup>a,b,1</sup>, Jana Eisermann<sup>a,c,1</sup>, Florian Arndt Schöffmann<sup>a,b,1</sup>,  
Manabendra Das<sup>d</sup>, Carolyn Vargas<sup>d,e,f,g</sup>, Sandro Keller<sup>d,e,f,g</sup>, Dariush Hinderberger<sup>a,b,\*</sup>

<sup>a</sup> Institute of Chemistry, Physical Chemistry – Complex Self-Organizing Systems, Martin Luther University (MLU) Halle-Wittenberg, Von-Danckelmann-Platz 4, 06120 Halle (Saale), Germany

<sup>b</sup> Interdisciplinary Research Center HALOmem, Charles Tanford Protein Center, MLU Halle-Wittenberg, Kurt-Mothes-Str. 3a, 06120 Halle (Saale), Germany

<sup>c</sup> Department of Chemistry – Molecular Sciences Research Hub, Imperial College London, 82 Wood Ln, W12 0BZ London, United Kingdom

<sup>d</sup> Molecular Biophysics, Technische Universität Kaiserslautern (TUK), Erwin-Schrödinger-Str. 13, 67663 Kaiserslautern, Germany

<sup>e</sup> Biophysics, Institute of Molecular Biosciences (IMB), NAWI Graz, University of Graz, Humboldtstr. 50/III, 8010 Graz, Austria

<sup>f</sup> Field of Excellence BioHealth, University of Graz, Graz, Austria

<sup>g</sup> BioTechMed-Graz, Graz, Austria

### ARTICLE INFO

#### Keywords:

Nanodisc

CW EPR

SMA (styrene/maleic acid)

DIBMA (diisobutylene/maleic acid)

SMA-SB (styrene/maleic sulfobetaine)

### ABSTRACT

With this study we aim at comparing the well-known lipid membrane model system of liposomes and polymer-encapsulated nanodiscs regarding their lipid properties. Using differential scanning calorimetry (DSC) and continuous-wave electron paramagnetic resonance (CW EPR) spectroscopy, we characterize the temperature-dependent lipid behavior within 1,2-dimyristoyl-*sn*-glycero-3-phosphocholine (DMPC) liposomes and nanodiscs made from such liposomes by application of various polymers based on styrene-*co*-maleic acid (SMA), diisobutylene-*alt*-maleic acid (DIBMA), and styrene-*co*-maleic amide sulfobetaine (SMA-SB), a new SMA-derived copolymer containing sulfobetaine side chains. By incorporating a spin label doxyl moiety into the lipid bilayer in position 16 or 5 we were able to study the micropolarity as well as rotational restrictions onto the lipids in the apolar bilayer center and the chain region adjacent to the carbonyl groups, respectively. Our results suggest that all polymers broaden the main melting transition of DMPC, change the water accessibility within the lipid bilayer, and exhibit additional constraints onto the lipids. Independent of the used polymer, the rotational mobility of both spin-labeled lipids decreased with DIBMA exerting less restraints probably due to its aliphatic side chains. Our findings imply that the choice of the solubilizing polymer has to be considered an important step to form lipid nanodiscs which should be included into research of lipid membranes and membrane proteins in the future.

### 1. Introduction

Researchers have access to a variety of model membrane systems for lipid and protein studies [1–4]. One rather new model system consists of polymer-encapsulated nanodiscs, which are also called native nanodiscs or simply polymer/lipid particles. Some polymers such as poly-(styrene-*co*-maleic acid) (SMA) [1,5] or poly-(diisobutylene-*alt*-maleic acid) (DIBMA) [6] are able to directly solubilize membrane lipids from liposomes or even cell lysates [1,2,4,7]. However, research in this field is clearly application-driven, whereas fundamental differences between

nanodiscs and liposomes or among nanodiscs made from different polymers are understood only in part. Most efforts aim towards improving the solubilizing properties of existing polymers [8–12], synthesizing new, more efficient or more gentle polymers [13–15], or facilitating the study of membrane proteins [5,16]. Initial fundamental research has been performed on the influence of the polymer on lipid properties, revealing e.g., a strong impact of SMA on the melting temperature of 1,2-dimyristoyl-*sn*-glycero-3-phosphocholine (DMPC) [6,17]. Moreover, in a previous study, we could verify that the specific structure of the respective polymer affects its interaction pattern with

\* Corresponding author at: Institute of Chemistry, Physical Chemistry – Complex Self-Organizing Systems, Martin Luther University (MLU) Halle-Wittenberg, Von-Danckelmann-Platz 4, 06120 Halle (Saale), Germany.

E-mail address: [dariush.hinderberger@chemie.uni-halle.de](mailto:dariush.hinderberger@chemie.uni-halle.de) (D. Hinderberger).

<sup>1</sup> These authors contributed equally.

<https://doi.org/10.1016/j.bbamem.2021.183681>

Received 13 April 2021; Received in revised form 31 May 2021; Accepted 14 June 2021

Available online 26 June 2021

0005-2736/© 2021 Published by Elsevier B.V.

small guest molecules (in the case at hand, nitroxide radicals), a finding which can be translated to lipid molecules [13]. This aspect highlights the question of how the polymer interacts with different parts of the lipids such as the headgroup, the interfacial carbonyl/glycerol region, and the apolar acyl chains, all of which is not fully understood up to now (see e.g. references [18–21]).

In this work, we employ two spin-labeled lipids (see Scheme 1A) combined with continuous-wave electron paramagnetic resonance (CW EPR) spectroscopy to obtain insights into nanoscopic lipid properties in DMPC liposomes and polymer-encapsulated nanodiscs containing a lipid-bilayer core composed of DMPC that is surrounded by SMA, DIBMA, or poly-(styrene-*co*-maleic amide sulfobetaine) (SMA-SB) (for polymer structures see Scheme 1B). The application of CW EPR spectroscopy in lipid research is well established for liposomes and other membrane model systems [22,23]. Hence, here it will be used to obtain information on the polarity, rotational mobility, and lipid ordering in nanodiscs. The nanoscopic view offered by CW EPR is complemented by dynamic light scattering (DLS), transmission electron microscopy (TEM), and differential scanning calorimetry (DSC). Finally, combination of temperature-dependent CW EPR measurements with DSC provides a broad view on lipid properties and is a promising combination of methods to yield valuable information for future nanodisc research.

## 2. Materials and methods

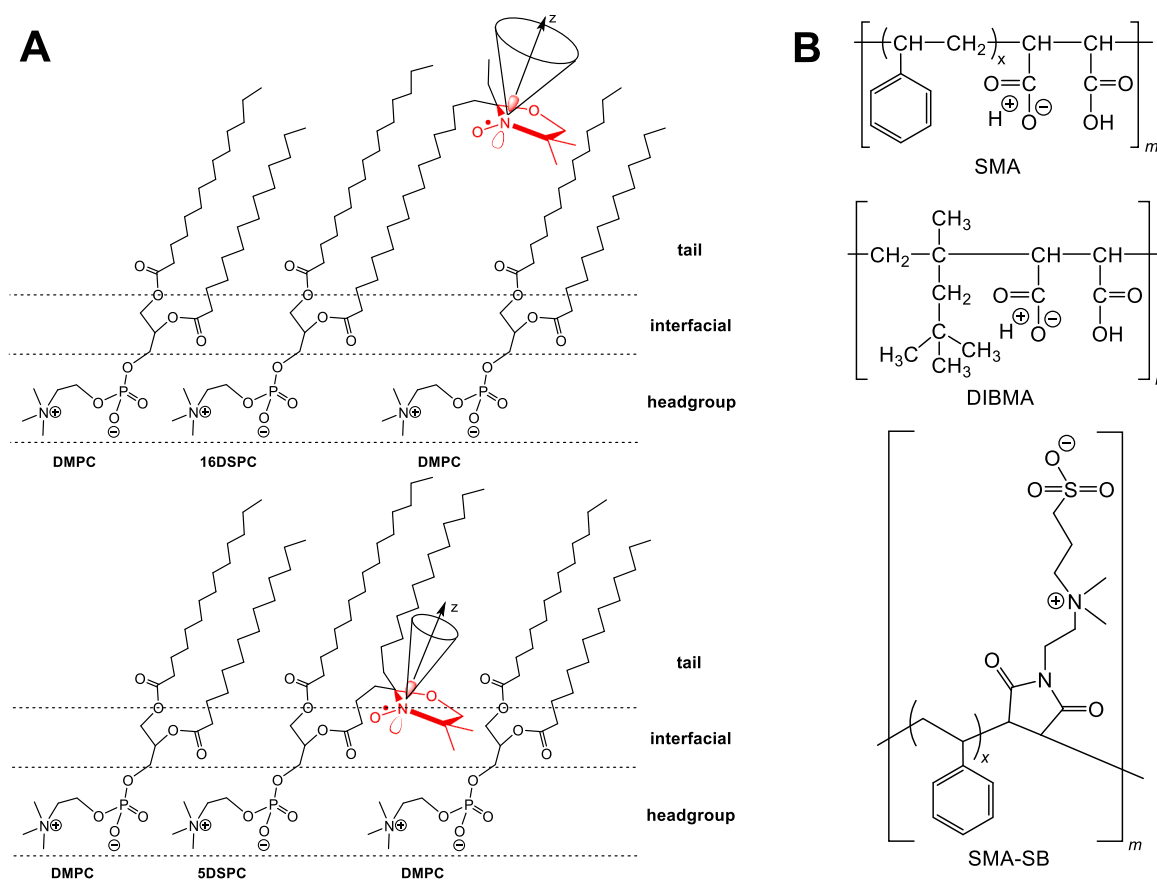
### 2.1. Materials

The three polymers poly-(styrene-*co*-maleic acid) (SMA 2.2:1

hydrolyzed from styrene/maleic anhydride (Xiran SZ30010)), poly-(diisobutylene-*alt*-maleic acid) (DIBMA) and poly-(styrene-*co*-maleic amide sulfobetaine) (SMA-SB) were synthesized as described elsewhere [13]. HPLC-grade chloroform as well as buffer salts were purchased from Carl Roth (Karlsruhe, Germany, Tris buffer salt >99.3% and NaCl >99.7%). The buffer solution was prepared with Millipore MilliQ water with a specific resistance of  $\rho = 18.2 \text{ M}\Omega \text{ cm}$ . 1,2-Dimyristoyl-*sn*-glycero-3-phosphocholine (DMPC) was obtained from Genzyme Pharmaceuticals (Cambridge, MA, USA). 1-palmitoyl-2-stearoyl-(5-doxyl)-*sn*-glycero-3-phosphocholine (5DSPC) and 1-palmitoyl-2-stearoyl-(16-doxyl)-*sn*-glycero-3-phosphocholine (16DSPC) were purchased from Avanti Polar Lipids (Alabaster, AL, USA).

### 2.2. Preparation of polymer solutions and polymer/lipid samples

Polymer solutions were prepared as described in [13]. An appropriate amount of each polymer was dissolved in saline Tris buffer (50 mM Tris, 300 mM NaCl, pH 7.4 in Millipore MilliQ water) to yield mass concentrations of 25 mg/mL (SMA and DIBMA) or 15 mg/mL (SMA-SB) at room temperature followed by heating combined with ultrasonication for 30 min at 70 °C. After cooling down, all three polymer stock solutions were stable for at least two weeks if stored at room temperature. DMPC nanodiscs were prepared as follows: DMPC with added spin label lipid (5DSPC or 16DSPC, 2 mol% of DMPC) was dissolved in chloroform. The solvent was evaporated in a gentle stream of nitrogen to yield a thin dry lipid layer. Tris buffer was added, and the concentration of DMPC was adjusted to somewhat above 1 mM. The lipids were allowed to suspend at 40 °C during ultrasonication of the sample for at least 10 min. The



**Scheme 1.** (A) Structures of 1-palmitoyl-2-stearoyl-(5-doxyl)-*sn*-glycero-3-phosphocholine (5DSPC) and 1-palmitoyl-2-stearoyl-(16-doxyl)-*sn*-glycero-3-phosphocholine (16DSPC) incorporated into a DMPC lipid environment. The rotational mobility of the doxyl unit is represented for both 5DSPC and 16DSPC by a cone with a main axis that is parallel to the z-axis defined for the molecular frame of the doxyl's nitroxide group. (B) Molecular structure of the applied polymers SMA-SB, SMA (both with  $x = 2.2$ ,  $m \approx 8$ ), and DIBMA (with  $n \approx 37$ ).

resulting liposomes were extruded 35 times through a 100 nm polycarbonate membrane. Afterwards, polymer stock solutions were added to the thus prepared large unilamellar vesicles (LUVs) at a polymer/lipid ratio of 1:5 (mol:mol) and a lipid concentration of 1 mM. The molar mass of SMA-SB was estimated to be  $4150 \text{ g mol}^{-1}$  according to full conversion in its synthesis from SMA ( $2700 \text{ g mol}^{-1}$ ). The molar mass of DIBMA amounts to  $8400 \text{ g mol}^{-1}$  [10]. The mixtures of polymers and liposomes were then incubated at  $30^\circ\text{C}$  for 16 h while shaking.

### 2.3. Dynamic light scattering (DLS)

Dynamic light scattering (DLS) experiments were conducted on a Litesizer 500 (Anton Paar, Graz, Austria) with a  $70 \mu\text{L}$  Micro Quartz cuvette. The irradiation wavelength was  $\lambda = 658 \text{ nm}$ , while the detection angle was maintained at  $90^\circ$  (side scattering) at constant temperature of  $20^\circ\text{C}$ . Prior to each measurement, the sample was allowed to equilibrate for at least 1 min. The data obtained from DLS measurements were evaluated in the Kalliope software (Anton Paar).

### 2.4. Transmission electron microscopy (TEM)

TEM samples were prepared by spreading  $5 \mu\text{L}$  of the (polymer-)lipid suspensions (diluted to  $20 \mu\text{M}$  lipid) onto freshly glow discharged grids with carbon support film on copper (Quantifoil Micro Tools, Großlobbichau, Germany). After 30–45 s excess suspension was blotted up using filter paper. The grids were washed three times with MilliQ water.  $5 \mu\text{L}$  of 2% aqueous uranyl acetate solution was placed onto the grid and also blotted up after 1 min. After preparation the samples were dried for at least 24 h. All TEM samples were examined with a Zeiss EM 900 transmission electron microscope (Carl Zeiss Microscopy, Jena, Germany).

### 2.5. Differential scanning calorimetry (DSC)

For DSC, sample preparation was performed as described above using a higher amount of both lipid and polymer (5 mM lipid target concentration in the samples). Prior to all measurements, the samples as well as the reference buffer solution was degassed under vacuum while stirring. DSC measurements were performed using a MicroCal VP-DSC differential scanning calorimeter (MicroCal, Northampton, MA, USA). In all experiments, 5 heating/cooling cycles were measured to assure sample stability and reproducibility from which one representative heating curve (heating rate  $60 \text{ K h}^{-1}$  between  $2$  and  $70^\circ\text{C}$ ) was chosen. Further evaluation of the DSC results involved subtraction of regularly collected buffer/buffer baselines as well as subtraction of offset values, if necessary.

### 2.6. CW EPR spectroscopy

X-band continuous-wave electron paramagnetic resonance (CW EPR) spectroscopic measurements were performed with the Miniscope MS5000 (magnetech, Freiberg Instruments, Freiberg, Germany) benchtop spectrometer. The connection to the H04 temperature control unit (magnetech) allowed the recording of temperature series. All spectra were measured with the following settings: center field position of  $337.5 \text{ mT}$ , field sweep width of  $10 \text{ mT}$ , modulation amplitude of  $0.1 \text{ mT}$  and a microwave power of  $3.63 \text{ mW}$ . For sample preparation,  $10\text{--}15 \mu\text{L}$  of the sample solution were filled into micropipettes (BLAUBRAND intraMark, Wertheim, Germany) and capped with capillary tube sealant (CRITOSEAL Leica, Wetzlar, Germany). Analysis of the recorded CW EPR spectra is based on simulations using MatLab (R2020b, v. 9.9) in combination with the EasySpin toolbox (v. 6.0.0 dev.26) for EPR spectroscopy [24]. Note that all spectra were simulated with a single component using the model of anisotropic Brownian motion with an axial symmetry and orienting potential (see SI for further information) [21,25].

## 3. Results

### 3.1. Preparation of nanodiscs

The general formation of nanodiscs was confirmed with the aid of DLS and TEM, as exemplarily shown in Figs. S1 and S2. From DLS, it is evident that the liposomes were solubilized almost completely yielding SMALPs and SMA-SBLPs in the size range of  $9.4 \pm 2.5 \text{ nm}$  and DIBMALPs of  $16.6 \pm 9.8 \text{ nm}$ . After addition of polymer to the liposomes and incubation, all suspensions appeared clear. SMA and SMA-SB were more efficient in solubilizing DMPC than DIBMA. In samples containing DIBMA-based lipid particles (DIBMALPs), a small fraction of non-solubilized liposomes remained. Interestingly, if applying the same polymer/lipid ratio for all three polymers, DIBMALPs clearly exhibit larger hydrodynamic diameters compared with SMALPs and SMA-SBLPs, which is in accordance with literature reports [6]. In protein research, DIBMALPs with increased hydrodynamic diameter may be useful in solubilizing large protein complexes. TEM observations support the DLS-derived findings. The presence of nanodiscs in each measured sample was confirmed and, in addition, the diameters of the detected nanodiscs correspond in their magnitude to the hydrodynamic diameters determined by DLS (see Fig. S1).

### 3.2. Temperature-dependent measurements of lipid properties in nanodiscs

Temperature-dependent CW EPR spectroscopic (Fig. 1) and differential scanning calorimetric measurements (DSC, Fig. 2, top) of all lipid samples were performed as described above, and we first discuss the DSC data. The DSC trace of the DMPC liposomes was similar to that reported in the literature [26]. While all three polymers had a strong effect on the DSC baseline, no thermotropic transitions as reflected in DSC peaks were observed for polymer-only samples, that is, in the absence of lipid (see Fig. S3). From the results shown in Fig. 2A and B (top), it can be concluded that the lipid main transition broadens when polymer is added, as expected from the resulting decrease in the size of the cooperative unit [6]. In addition, it is evident that all three polymers had an effect on the main transition temperature  $T_m$  of DMPC:  $T_m$  was decreased in SMALPs and DIBMALPs, whereas SMA-SB led to a slight increase in  $T_m$ .

### 3.3. EPR-spectroscopic results

The thermodynamic observations on the phase behavior of DMPC-based model membrane systems was complemented by a nanoscopic view gathered through CW EPR spectroscopy. To this end, we focused on the two spin-labeled lipids 16DSPC and 5DSPC, which allow characterizing the membrane center in the acyl chain region and the region close to the polar headgroup, respectively [22,27–29]. Note, that the spectra of all systems containing 5DSPC showed increased baseline noise, that is decreased signal intensity (compare Fig. 1 and Figs. S4 and S5), due to increased immobilization of the doxyl group corresponding to its position within the membrane when compared to 16DSPC spectra. Based on the position of the doxyl-unit along the fatty acid chain, temperature-dependent changes in the LUVs as well as nanodiscs were found through different simulation parameters (see Fig. 1 and Figs. S4 and S5).

The line shapes of the respective CW EPR spectra reflect the dynamics of the spin label. Three equally spaced sharp lines of similar intensity are associated with an unrestricted reorientational motion of the nitroxide. Upon increasing the spatial restriction on the mobility of the doxyl unit, the similarity of these three lines vanishes, while the apparent hyperfine splitting  $a_{\text{iso,app}}$  increases (further described in the Discussion section and SI), and the line width of the recorded spectral features rises. The CW EPR spectra become more anisotropic with (i) decreasing temperature for LUVs as well as nanodiscs and (ii) from the

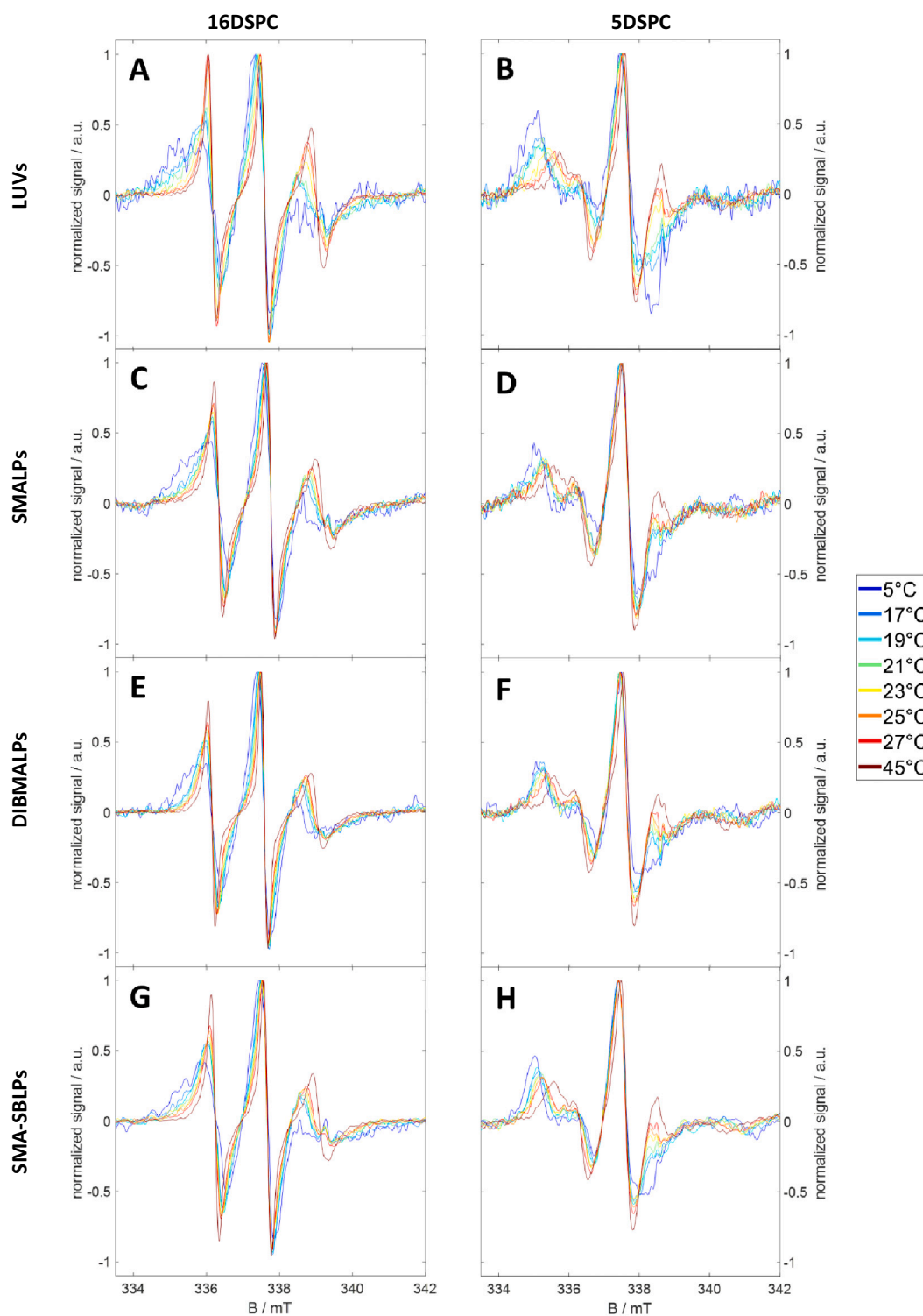


**Fig. 1.** Temperature-dependent CW EPR spectra of 16DSPC (left column) and 5DSPC (right column) incorporated in DMPC LUVs or several polymer-encapsulated nanodiscs; (A/B) LUVs; (C/D) SMALPs; (E/F) DIBMALPs; (G/H) SMA-SBLPs. Here, all spectra are normalized to their maximal intensity (for spectra without normalization see Figs. S4/S5).

position of the doxyl label along the acyl chain: 5DSPC spectra are more anisotropic than 16DSPC spectra. The doxyl unit of 16DSPC is positioned at the end of the acyl chains as compared with 5DSPC that is close to the carbonyl region in the bilayer. Hence, 16DSPC shows higher reorientational mobility and, therefore, more isotropic spectra in all tested DMPC model membrane systems. Note that the CW EPR spectra of LUVs feature more isotropic peaks than those of the three nanodisc

systems [18–21]. A superficial, visual comparison of SMALPs, DIBMALPs, and SMA-SBLPs seems to indicate that the differences in the line shapes of the spin labels are insignificant.

Therefore, we performed spectral simulations using the model of anisotropic Brownian motion with axial symmetry (see SI for further information). Two important parameters that derive from this approach are (i) the rotational correlation time  $\tau_c$  and (ii) the segmental order

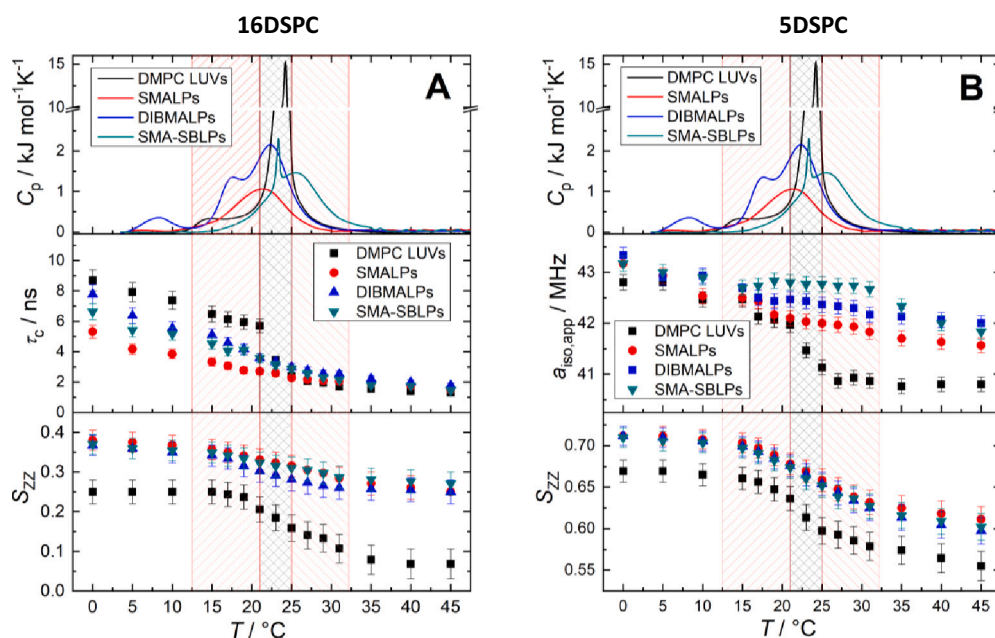


**Fig. 2.** Comparison of the DSC thermograms of DMPC LUVs, SMALPs, DIBMALPs, and SMA-SBLPs with best-fit simulation parameters extracted from CW EPR measurements using (A) 16DSPC and (B) 5DSPC. Shown are the temperature dependencies of the rotational correlation time  $\tau_c$ , the mean apparent isotropic hyperfine coupling value  $a_{\text{iso,app}}$ , and the nitroxide order parameter  $S_{zz}$ .

parameter  $S_{zz}$  for the doxyl unit. The respective values for both parameters at temperatures below (15 °C), around (23 °C), and above (35 °C) the main phase transition temperature  $T_m$  of DMPC are summarized in Tables 1 and 2.

The rotational correlation time  $\tau_c$  is derived from the diffusion tensor elements  $D_{\parallel}$  (motion around the unique axis of the NO-group) and  $D_{\perp}$  (perpendicular to unique axis) as  $\tau_c = \frac{1}{6\sqrt{D_{\parallel}^2 + D_{\perp}^2}}$  and is a simplified measure of the rotational mobility of the doxyl unit. As described above, changes in the spectral line shape reveal fastest motion for 16DSPC inside LUVs. The  $\tau_c$ -values for the three nanodisc system are similar to but slightly higher than for LUVs above  $T_m$ , indicating a more restricted mobility of the nitroxide. The segmental order parameter  $S_{zz}$  correlates with the semi-cone angle  $\beta$  via  $S_{zz} = \frac{1}{2}(3\cos^2\beta - 1)$  [22]. The semi-cone angle confines the wobbling motion of the respective observable segment based on the position of the doxyl-unit along the acyl chain of the lipid. A rigid crystal structure of the membrane would be described by the maximum value of  $S_{zz} = 1$ , whereas a state of maximum disorder would be characterized by its lowest value of  $S_{zz} = 0$  [21]. The closer the doxyl unit is situated towards the headgroup region of the lipid bilayer, the larger the order parameter. When comparing LUVs and nanodiscs, SMALPs, DIBMALPs, and SMA-SBLPs yielded a higher order parameter than polymer-free liposomes. This effect was more pronounced for the 16DSPC spin label probing the center of the lipid bilayer than for the 5DSPC spin label near the carbonyl region.

**Table 1**

CW EPR simulation results of 5DSPC spectra in DMPC LUVs and nanodiscs.

5DSPC								
$T/^\circ\text{C}$	LUVs		SMALPs		DIBMALPs		SMA-SBLPs	
	$S_{zz}$	$\tau_c/\text{ns}$	$S_{zz}$	$\tau_c/\text{ns}$	$S_{zz}$	$\tau_c/\text{ns}$	$S_{zz}$	$\tau_c/\text{ns}$
15	0.66	27.7	0.70	21.3	0.70	27.4	0.70	26.6
23	0.61	9.7	0.67	15.1	0.67	16.2	0.66	16.2
35	0.57	5.9	0.63	8.6	0.61	8.3	0.62	7.9

**Table 2**

CW EPR simulation results of 16DSPC spectra in DMPC LUVs and nanodiscs.

16DSPC								
$T/^\circ\text{C}$	LUVs		SMALPs		DIBMALPs		SMA-SBLPs	
	$S_{zz}$	$\tau_c/\text{ns}$	$S_{zz}$	$\tau_c/\text{ns}$	$S_{zz}$	$\tau_c/\text{ns}$	$S_{zz}$	$\tau_c/\text{ns}$
15	0.25	6.5	0.36	3.3	0.34	5.1	0.35	4.5
23	0.18	3.4	0.32	2.6	0.29	3.3	0.32	3.1
35	0.07	1.6	0.27	1.9	0.26	2.2	0.28	1.8

#### 4. Discussion

As shown in the results, we are able to correlate the temperature-dependent lipid characteristics detected by CW EPR with thermodynamic information obtained by DSC measurements. This enables us to get insight into the fundamentals of polymer/lipid interactions in nanodiscs which is much needed in this field of research. The successful preparation of DMPC nanodiscs with all three polymers is verified by DLS and TEM. In addition, DSC reveals that in all samples the lipid properties change as expected: (i) the main transition of DMPC broadens because of a decrease in the size of the cooperative unit reflecting a smaller particle size, and (ii) a small effect on  $T_m$  of DMPC is observed for all polymers. At the polymer/lipid ratio studied here, no drastic decrease in  $T_m$  was observed, as is the case for SMALPs made from the more hydrophobic copolymer SMA(3:1) [6]. In case of SMA-SB, a very small fraction of remaining liposomes was detected in the DSC traces as a sharp peak on top of the broad main transition, that, however, were not observed in DLS measurements (see Fig. 2A and B, top).

On the basis of the CW EPR results, a direct comparison of 16DSPC and 5DSPC for the same model membrane system yields a higher reorientational mobility for the doxyl unit placed at the end of the acyl chain (16DSPC), as highlighted in Scheme 1, leading to more isotropic spectra corresponding to decreased rotational correlation times  $\tau_c$  (compare Fig. 2A and Fig. S6B). Note that the temperature range across which  $\tau_c$  changes correlates with the broadness of the respective main transition peak determined by DSC. All three nanodisc systems exhibit a decreasing rotational mobility of both spin probes above  $T_m$ , as

concluded from both  $\tau_c$  and  $S_{zz}$ . Moreover, in a previous study of Stepien et al. focusing on nanodiscs encircled by membrane scaffold protein (MSP) [22], a more anisotropic motion of the doxyl unit was found through the diffusion tilt angle  $\beta$  in  $S_{zz}$  (discussed below). This trend was rationalized by the increased pressure exerted by the protein belt on the encircled lipid-bilayer patch. A similar effect found for the polymers studied here is depicted in Fig. 3 [18–21]. For spin-labeled lipids,  $\beta$  plays a crucial role as it significantly influences the shape of the CW EPR spectra [25] as well as the proportions for the diffusion tensor elements  $D_{\parallel}$  and  $D_{\perp}$ . 16DSPC possesses a smaller diffusion tilt angle in all three nanodiscs, which correlates with a more anisotropic motion of the respective doxyl unit.

Another feature already observed with MSP nanodiscs [22] is the change in the polarity profile, which can be characterized with the hyperfine coupling tensor  $A$  [30]. Its diagonal values are further used to calculate the apparent isotropic hyperfine coupling value  $a_{iso,app}$  (as described in the SI) to analyze the hydrophobicity in the local environment of the doxyl unit throughout the complete temperature series. Note that especially the measurements below  $T_m$  do not represent isotropic CW EPR spectra, emphasizing the “apparent” character of the  $a_{iso}$  values. In all DMPC nanodiscs, compared with LUVs, the water accessibility to the polar headgroup is significantly increased (schematically shown in Fig. 3), reflected in a higher hyperfine coupling value in the liquid-crystalline phase (Fig. 2B), whereas a hydrophobic barrier is formed in the center of the bilayer (see Fig. S6A) below  $T_m$ . Moreover, this water accessibility varies between the three different polymers SMA, DIBMA, and SMA-SB, as reflected in different interaction patterns between them and DMPC. This is particularly obvious in the case of SMA, which, as already shown in our previous study with small nitroxide radicals as guest molecules [13], induces a significant drop in the isotropic  $g$ -value for 16DSPC (see Fig. S7A). Note that the observation of a hydrophobic barrier in the center of MSP-based nanodiscs cannot be applied in general to all polymer-encapsulated systems as shown by the behavior of  $a_{iso,app}$  for 16DSPC (see Fig. S6A), again indicating that the type of polymer affects the polarity profile of the membrane itself.

For  $n$ DSPC spin-labels (with  $n = 5, 16$  in our study),  $S_{zz}$  reports only on the respective segment of the hydrocarbon chain to which the nitroxide fragment is attached. Thus, it is a segmental order parameter and does not reflect the order of the whole chain. The closer the doxyl unit is located to the polar headgroup of the lipid, the more tightly

packed are their respective segments in the fatty acid chains (see Scheme 1). The decrease of  $S_{zz}$  with increasing temperature correlates with the phase behavior determined via DSC independent from the respective model membrane system. Note that all tested nanodisc systems lead to an increase in the order parameter compared with DMPC liposomes. This effect is least pronounced for DIBMALPs (but still of the same magnitude as both SMALPs and SMA-SBLPs) [20], which form larger nanodiscs and, consequently, contain a lower percentage of lipid molecules that are in vicinity to the polymer rim. Moreover, DIBMA displays weaker interactions with the attached spin probe, thus leading to a reduced change in  $S_{zz}$  [21].

## 5. Conclusions

In this work, we analyzed CW EPR spectra of 16DSPC and 5DSPC incorporated in DMPC nanodiscs and compared them to both spin-labeled lipids in liposomes. We found that:

- all polymers induced broadening of the DMPC main transition while maintaining a similar  $T_m$ ,
- with all polymers, the water accessibility of the near-headgroup region and the center of the membrane changed,
- the segmental order parameter was increased in all studied nanodisc systems compared with LUVs, and
- $S_{zz}$  of DMPC in DIBMALPs appeared to be slightly less affected than with both other polymers probably due to DIBMA not bearing phenyl groups.

All of these observations are schematically summarized in Fig. 3. They indicate that the polymers exhibit different influences on the polar and apolar lipid regions, which should be considered when preparing polymer-solubilized lipids for protein studies or other in vitro investigations involving lipidic model membranes. CW EPR has long been known to be a valuable method to obtain insights into the ordering, rotational mobility, and water accessibility of lipids in large vesicles and we here show that it can even help understand slight differences in the local nanodisc structure induced by varying the applied polymer for encapsulation. While DSC measurements indicate a rather small macroscopic impact of the polymers on the lipids, several effects exerted by the different polymers on the level of the lipid molecules were

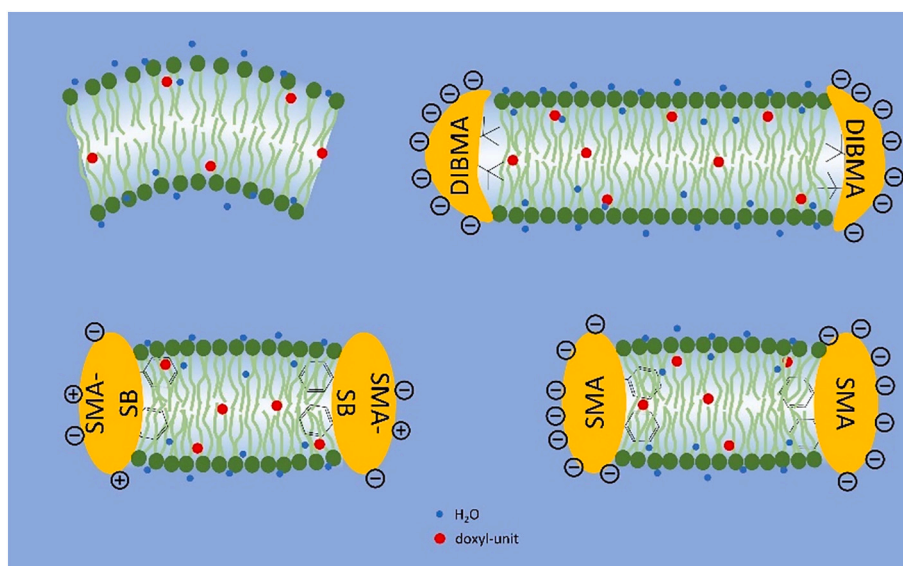


**Fig. 3.** Schematic comparison of the local structures in DMPC liposomes (upper left-hand side) and the three nanodisc systems SMALPs, DIBMALPs, and SMA-SBLPs. The location of the doxyl units is highlighted as red dots as well as the respective side groups of the polymer chain that reach inside the lipid bilayer system. Differences in water penetration of all bilayer systems are indicated by exemplary water molecules (blue dots).

observed with CW EPR spectroscopy, which allows characterization of heterogeneity in lipid mobility and local structuring.

### Author contributions

M.H., J.E., F.S., C.V., S.K., and D.H. conceived and planned research; M.H. and M.D. prepared samples; M.H., J.E., and F.S. performed experiments; M.H., J.E., F.S., and D.H. analyzed data; J.E. and F.S. carried out spectral simulations; M.H., J.E., F.S., and D.H. wrote the publication.

### Declaration of competing interest

The authors declare no competing financial interest.

Matthias Hoffmann reports financial support was provided by German Chemical Industry Association (VCI). Jana Eisermann reports financial support was provided by Alexander von Humboldt Foundation.

### Acknowledgments

M.H. thanks the German Chemical Industry Association (VCI) for financial support in form of the Kekulé scholarship. J.E. thanks the Alexander von Humboldt Foundation for financial support through a Feodor Lynen Research Fellowship. This work was supported by the Deutsche Forschungsgemeinschaft (DFG) in Research Training Group (RTG) 2670, "Beyond Amphiphilicity".

We thank Annekatrin Rother and Gerd Hause for their support in obtaining TEM micrographs. We thank PD Dr. Annette Meister for access to a plasma cleaner and general helpful discussions.

### Appendix A. Supplementary data

The Supporting Information is available online. (Nanodisc characterization with DLS/TEM, DSC of pure polymers, CW EPR simulation routine, comparison of simulated and measured spectra, further simulation results). Supplementary data to this article can be found online at doi:<https://doi.org/10.1016/j.bbmem.2021.183681>.

### References

- [1] J.M. Dörr, S. Scheidelaar, M.C. Koorengel, J.J. Dominguez, M. Schäfer, C.A. van Walree, J.A. Killian, The styrene-maleic acid copolymer: a versatile tool in membrane research, *Eur. Biophys. J.* 45 (2016) 3–21.
- [2] S.C. Lee, N.L. Pollock, Membrane proteins: is the future disc shaped? *Biochem. Soc. Trans.* 44 (2016) 1011–1018.
- [3] N. Österlund, J. Luo, S.K.T.S. Wärmländer, A. Gräslund, Membrane-mimetic systems for biophysical studies of the amyloid-beta peptide, *Biochim. Biophys. Acta, Proteins Proteomics* 1867 (2019) 492–501.
- [4] M. Overduin, M. Esmaili, Structures and interactions of transmembrane targets in native nanodiscs, *SLAS Discov.* 24 (2019) 943–952.
- [5] T.J. Knowles, R. Finka, C. Smith, Y.P. Lin, T. Dafforn, M. Overduin, Membrane proteins solubilized intact in lipid containing nanoparticles bounded by styrene maleic acid copolymer, *J. Am. Chem. Soc.* 131 (2009) 7484–7485.
- [6] A.O. Oluwole, B. Danielczak, A. Meister, J.O. Babalola, C. Vargas, S. Keller, Solubilization of membrane proteins into functional lipid-bilayer nanodiscs using a diisobutylene/maleic acid copolymer, *Angew. Chem. Int. Ed.* 56 (2017) 1919–1924.
- [7] S. Scheidelaar, M.C. Koorengel, J.D. Pardo, J.D. Meeldijk, E. Breukink, J. A. Killian, Molecular model for the solubilization of membranes into nanodiscs by styrene maleic acid copolymers, *Biophys. J.* 108 (2015) 279–290.
- [8] R. Cuevas Arenas, J. Klingler, C. Vargas, S. Keller, Influence of lipid bilayer properties on nanodisc formation mediated by styrene/maleic acid copolymers, *Nanoscale* 8 (2016) 15016–15026.
- [9] B. Danielczak, A. Meister, S. Keller, Influence of Mg(2+) and Ca(2+) on nanodisc formation by diisobutylene/maleic acid (DIBMA) copolymer, *Chem. Phys. Lipids* 221 (2019) 30–38.
- [10] A. Grethen, A.O. Oluwole, B. Danielczak, C. Vargas, S. Keller, Thermodynamics of nanodisc formation mediated by styrene/maleic acid (2:1) copolymer, *Sci. Rep.* 7 (2017) 11517.
- [11] A.O. Oluwole, J. Klingler, B. Danielczak, J.O. Babalola, C. Vargas, G. Pabst, S. Keller, Formation of lipid-bilayer nanodiscs by diisobutylene/maleic acid (DIBMA) copolymer, *Langmuir* 33 (2017) 14378–14388.
- [12] S. Scheidelaar, M.C. Koorengel, C.A. van Walree, J.J. Dominguez, J.M. Dörr, J. A. Killian, Effect of polymer composition and pH on membrane solubilization by styrene-maleic acid copolymers, *Biophys. J.* 111 (2016) 1974–1986.
- [13] J. Eisermann, M. Hoffmann, F.A. Schöffmann, M. Das, C. Vargas, S. Keller, D. Hinderberger, Molecular-level interactions of nanodisc-forming copolymers dissected by EPR spectroscopy, *Macromol. Chem. Phys.* 222 (11) (2021) 1–14, 2100051.
- [14] T. Ravula, S.K. Ramadugu, G. Di Mauro, A. Ramamoorthy, Bioinspired, size-tunable self-assembly of polymer-lipid bilayer nanodiscs, *Angew. Chem. Int. Ed.* 56 (2017) 11466–11470.
- [15] A.A.A. Smith, H.E. Autzen, B. Faust, J.L. Mann, B.W. Muir, S. Howard, A. Postma, A.J. Spakowitz, Y. Cheng, E.A. Appel, Lipid nanodiscs via ordered copolymers, *Chem.* 6 (2020) 2782–2795.
- [16] W. Mosslehy, N. Voskoboinikova, A. Colbasevici, A. Ricke, D. Klose, J.P. Klare, A. Y. Mulikdjanian, H.J. Steinhoff, Conformational dynamics of sensory rhodopsin II in nanolipoprotein and styrene-maleic acid lipid particles, *Photochem. Photobiol.* 95 (2019) 1195–1204.
- [17] J.J. Dominguez Pardo, J.M. Dörr, M.F. Renne, T. Ould-Braham, M.C. Koorengel, M.J. van Steenberg, J.A. Killian, Thermotropic properties of phosphatidylcholine nanodiscs bounded by styrene-maleic acid copolymers, *Chem. Phys. Lipids* 208 (2017) 58–64.
- [18] A.P. Bali, I.D. Sahu, A.F. Craig, E.E. Clark, K.M. Burridge, M.T. Dolan, C. Dabney-Smith, D. Konkolewicz, G.A. Lorigan, Structural characterization of styrene-maleic acid copolymer-lipid nanoparticles (SMALPs) using EPR spectroscopy, *Chem. Phys. Lipids* 220 (2019) 6–13.
- [19] M.C. Orwick, P.J. Judge, J. Procek, L. Lindholm, A. Graziadei, A. Engel, G. Gröbner, A. Watts, Detergent-free formation and physicochemical characterization of nanosized lipid-polymer complexes: Lipodisq, *Angew. Chem. Int. Ed.* 51 (2012) 4653–4657.
- [20] N. Voskoboinikova, E.G. Margheritis, F. Kodde, M. Rademacher, M. Schowe, A. Budke-Gieseke, O.E. Psathaki, H.J. Steinhoff, K. Cosentino, Evaluation of DIBMA nanoparticles of variable size and anionic lipid content as tools for the structural and functional study of membrane proteins, *Biochim. Biophys. Acta Biomembr.* 2021 (1863) 183588.
- [21] A. Colbasevici, N. Voskoboinikova, P.S. Orekhov, M.E. Bozdaganyan, M. G. Karlova, O.S. Sokolova, J.P. Klare, A.Y. Mulikdjanian, K.V. Shaitan, H. J. Steinhoff, Lipid dynamics in nanoparticles formed by maleic acid-containing copolymers: EPR spectroscopy and molecular dynamics simulations, *Biochim. Biophys. Acta Biomembr.* 2020 (1862) 183207.
- [22] P. Stepien, A. Polit, A. Wisniewska-Becker, Comparative EPR studies on lipid bilayer properties in nanodiscs and liposomes, *Biochim. Biophys. Acta* 1848 (2015) 60–66.
- [23] M. Isabel Collado, F.M. Goni, A. Alonso, D. Marsh, Domain formation in sphingomyelin/cholesterol mixed membranes studied by spin-label electron spin resonance spectroscopy, *Biochemistry* 44 (2005) 4911–4918.
- [24] S. Stoll, A. Schweiger, EasySpin, a comprehensive software package for spectral simulation and analysis in EPR, *J. Magn. Reson.* 178 (2006) 42–55.
- [25] D. Marsh, Distinct populations in spin-label EPR spectra from nitroxides, *J. Phys. Chem. B* 122 (2018) 6129–6133.
- [26] S. Ali, S. Minchey, A. Janoff, E. Mayhew, A differential scanning calorimetry study of phosphocholines mixed with paclitaxel and its bromoacylated taxanes, *Biophys. J.* 78 (2000) 246–256.
- [27] D.A. Erilov, R. Bartucci, R. Guzzi, A.A. Shubin, A.G. Maryasov, D. Marsh, S. A. Dzuba, L. Sportelli, Water concentration profiles in membranes measured by ESEEM of spin-labeled lipids, *J. Phys. Chem. B* 109 (2005) 12003–12013.
- [28] D. Kurad, G. Jeschke, D. Marsh, Lipid membrane polarity profiles by high-field EPR, *Biophys. J.* 85 (2003) 1025–1033.
- [29] M.R. Vartorelli, A.S. Garay, D.E. Rodrigues, Spin-labeled stearic acid behavior and perturbations on the structure of a gel-phase-lipid bilayer in water: 5-, 12- and 16-SASL, *J. Phys. Chem. B* 112 (2008) 16830–16842.
- [30] H.J. Steinhoff, Multi-frequency EPR spectroscopy studies of the structure and conformational changes of site-directed spin labelled membrane proteins, in: G. Pifat-Mrzljak (Ed.), *Supramolecular Structure and Function* vol. 8, Springer, New York, 2004, pp. 157–177.

## **A Nanoscale Model System for the Human Myelin Sheath**

Matthias Hoffmann, David Haselberger, Tommy Hofmann, Lisa Müller, Kevin Janson, Annette Meister, Manabendra Das, Carolyn Vargas, Sandro Keller, Panagiotis L. Kastritis, Carla Schmidt and Dariush Hinderberger

*Biomacromolecules* **2021**, accepted for publication.

Reprinted with permission from *Biomacromolecules*, 2021, M. Hoffmann, D. Haselberger, T. Hofmann, L. Müller, K. Janson, A. Meister, M. Das, C. Vargas, S. Keller, P. L. Kastritis, C. Schmidt and D. Hinderberger, A Nanoscale Model System for the Human Myelin Sheath. Copyright 2021 American Chemical Society.

# A Nanoscale Model System for the Human Myelin Sheath

Matthias Hoffmann,<sup>1,2</sup> David Haselberger,<sup>1,2</sup> Tommy Hofmann,<sup>1,3</sup> Lisa Müller,<sup>4</sup> Kevin Janson,<sup>1,3</sup> Annette Meister,<sup>1,3</sup> Manabendra Das,<sup>5</sup> Carolyn Vargas,<sup>5-8</sup> Sandro Keller,<sup>5-8</sup> Panagiotis L. Kastritis,<sup>1,3</sup> Carla Schmidt,<sup>1,3</sup> Dariush Hinderberger<sup>1,2,\*</sup>

1 Interdisciplinary Research Center HALOmem, MLU Halle-Wittenberg, Charles Tanford Protein Center, Kurt-Mothes-Str. 3a, 06120 Halle (Saale), Germany.

2 Institute of Chemistry, Martin Luther University (MLU) Halle-Wittenberg, Von-Danckelmann-Platz 4, 06120 Halle (Saale), Germany.

3 Institute of Biochemistry and Biotechnology, Charles Tanford Protein Center, Martin Luther University (MLU) Halle-Wittenberg, Kurt-Mothes-Str. 3a, 06120 Halle (Saale), Germany.

4 Institute of Pharmacy, MLU Halle-Wittenberg, Wolfgang-Langenbeck-Str. 4, 06120 Halle (Saale), Germany.

5 Molecular Biophysics, Technische Universität Kaiserslautern (TUK), Erwin-Schrödinger-Str. 13, 67663 Kaiserslautern, Germany.

6 Biophysics, Institute of Molecular Biosciences (IMB), NAWI Graz, University of Graz, Humboldtstr. 50/III, 8010 Graz, Austria.

7 Field of Excellence BioHealth, University of Graz, 8010 Graz, Austria.

8 BioTechMed-Graz, 8010 Graz, Austria.

**KEYWORDS** *Lipid nanodiscs, myelin, EPR spectroscopy, lipid quantification*

---

Neurodegenerative disorders are among the most common diseases in modern society. However, the molecular bases of diseases such as multiple sclerosis or Charcot-Marie-Tooth disease remain far from being fully understood. Research in this field is limited by the complex nature of native myelin and by difficulties in obtaining good *in vitro* model systems of myelin. Here, we introduce an easy-to-use model system of the myelin sheath that can be used to study myelin proteins in a native-like yet well-controlled environment. To this end, we present myelin-mimicking nanodiscs prepared through one of the amphiphilic copolymers styrene/maleic acid (SMA), diisobutylene/maleic acid (DIBMA), and styrene/maleimide sulfobetaine (SMA-SB). These nanodiscs were tested for their lipid composition using chromatographic (HPLC) and mass spectrometric (MS) methods and, utilizing spin probes within the nanodisc, their comparability with liposomes was studied. In addition, their binding behavior with bovine myelin basic protein (MBP) was scrutinized to ensure that the nanodiscs represent a suitable model system of myelin. Our results suggest that both SMA and SMA-SB are able to solubilize the myelin-like (cytoplasmic) liposomes without preferences for specific lipid headgroups or fatty acyl chains. In nanodiscs of both SMA and SMA-SB (called SMA(-SB)-lipid particles, short SMALPs or SMA-SBLPs, respectively) the polymers restrict the lipids' motion in the hydrophobic center of the bilayer. The head groups of the lipids, however, are sterically less hindered in nanodiscs when compared with liposomes. Myelin-like SMALPs are able to bind bovine MBP which can stack the lipid bilayers like in native myelin, showing the usability of these simple, well-controlled systems in further studies of protein-lipid interactions of native myelin.

---

## Introduction

In our society, medicine is frequently confronted with neurodegenerative diseases such as multiple sclerosis or the Charcot-Marie-Tooth disease which are caused in part by myelination deficiency.<sup>1-3</sup> For early-stage research of diseases connected to demyelination a variety of potential model systems is currently used in molecular-level studies<sup>4-8</sup>. All of them have their advantages and disadvantages and lead to a significant reduction of complexity compared to native myelin. This has the drawback that in studies of interactions between myelin lipids and myelin proteins in these model systems it is hard to know if and

how the findings can be transferred to the behavior in native myelin. However, such an understanding is essential and fundamental for a deeper understanding of pathological conditions in patients.

At the molecular level, the myelin sheath wraps around the axons of nerve cells of vertebrates.<sup>2</sup> Its main function is the insulation of the axon from electrical activity to increase the rate of signal transmission.<sup>2</sup> Thus, the membrane action potential is transmitted with high efficiency by saltatory conduction.<sup>9</sup> To achieve this insulating function, the myelin sheath mainly consists of lipid bilayers (lipid content 70-80 %<sup>10</sup>) that are tightly compacted by several

proteins.<sup>11-13</sup> Mutations, posttranslational modifications, and deficiencies in these proteins can lead to demyelination and neurodegenerative diseases.<sup>3, 11</sup>

The rather new class of polymer-encapsulated nanodiscs,<sup>14-15</sup> which are stackable and flat, fulfills the requirements for representing a myelin sheath model system, e.g. to contain all major lipids and proteins abundant in human myelin, including high amounts of cholesterol, and others listed in the SI. In addition, the polymeric nature of the used amphiphiles prevents penetration of the bilayer which could affect lipid properties or denature incorporated proteins. The main downside to most of the known polymers that are able to solubilize lipid membranes is their strong absorption in the UV range which is useful for protein studies.<sup>16</sup> To overcome this and other challenges, new polymers are developed in the field of research.<sup>16-20</sup>

In this work, we show how nanoscale models for myelin lipid bilayer membranes with the composition of the central nervous system (CNS) or peripheral nervous system (PNS) cytosolic leaflet can be achieved (see SI for details on criteria) by solubilization of myelin-like liposomes of the cytosolic CNS and PNS lipid composition with the well-known polymers styrene/maleic acid (SMA 2:1)<sup>21</sup> and diisobutylene/maleic acid (DIBMA)<sup>16</sup> as well as the new polymer styrene/maleimide sulfobetaine (SMA-SB).<sup>22-23</sup> The solubilization of these lipid mixtures is remarkably challenging because of the high amount of negatively charged, unsaturated phospholipids and the exceptionally high cholesterol content.<sup>24-26</sup> After preparation, the nanodiscs were investigated regarding their lipid composition using HPLC and MS, their lipid properties with continuous wave electron paramagnetic resonance (CW EPR), and their interactions with the model protein bMBP, which is known to act as “molecular glue” between two myelin layers in both PNS and CNS.<sup>11</sup> The achievement of lipid nanodiscs with the challenging lipid compositions of PNS and CNS myelin can in general be viewed as paving the way for more complex lipid model membrane systems on the one hand, and in this specific case allows for future studies on protein-lipid interactions in myelin and factors enabling or even enforcing myelin formation or degradation, even using native-like combinations of myelin proteins in a realistic yet highly controlled lipid environment.

## Materials and Methods

### Materials

The three polymers poly-(styrene-maleic acid) (SMA 2:1 hydrolyzed from styrene/maleic anhydride (Xiran SZ30010)), poly-(diisobutylene-alt-maleic acid) (DIBMA) and poly-(styrene-maleimide sulfobetaine) (SMA-SB) were synthesized following a protocol published previously.<sup>22</sup> HPLC-grade chloroform (CHCl<sub>3</sub>) and methanol (MeOH) as well as the buffer salts were purchased from Carl Roth (Karlsruhe, Germany, tris buffer salt >99.3 % and NaCl >99.7 %). Aqueous ammonia was bought from Grüssing (Filsun, Germany). All used lipids were purchased

from Avanti Polar Lipids (Alabaster, AL, USA). The model protein bMBP (≥90 %) was purchased from Sigma (St. Louis, MO, USA).

### Preparation of polymer solutions and polymer-lipid samples

Polymer stock solutions were prepared as previously described.<sup>22-23</sup> An appropriate amount of either SMA or SMA-SB was dissolved in saline tris buffer (50 mM tris, 300 mM NaCl, pH 7.4 in Millipore MilliQ water with a specific resistance of  $\rho = 18.2 \text{ M}\Omega \text{ cm}$ ) to yield mass concentrations of 25 mg/mL (SMA) or 15 mg/mL (SMA-SB) at room temperature followed by heating combined with ultra-sonicating for 30 min at 70 °C. After cooling down, both polymer stock solutions were stable for two weeks at room temperature. DIBMA stock solutions were prepared as described before.<sup>16</sup> In short, Sokalan CP9 (BASF, Ludwigshafen, Germany) was dialyzed against tris buffer and the DIBMA concentration was checked via refractive index with an Abbemat 450 (Anton Paar, Graz, Austria) using a literature<sup>16</sup> value for  $dn/dc$ .

Preparation of myelin-like nanodiscs was conducted as follows: the lipids containing either no or 3.3 mol% spin label lipid (5DSPC or 16DSPC, replacing PC lipids in part) were dissolved in CHCl<sub>3</sub>/MeOH 2:1 (vol/vol), mixed in lipid compositions resembling cytosolic CNS (cholesterol:PE:PS:PC:SM:PI 44:27:13:11:3:2) or PNS (cholesterol:PE:PS:PC:SM:PI 37:22:19:9:9:4) myelin.<sup>27-28</sup> Subsequently, the solvent was evaporated in a gentle stream of nitrogen to obtain a thin dry lipid layer. Tris buffer was added, and the total lipid concentration was adjusted to somewhat above 3 mM. The lipids were allowed to suspend at 45 °C while ultra-sonicating the sample for at least 10 min. Subsequently, the resulting liposomes were extruded (35 times) through a 400 nm polycarbonate membrane. We have chosen to use liposomes larger than 100 nm to increase the size difference between nanodiscs and remaining liposomes and, thus, to improve the chromatographic separation in the next step. Prepared liposomes were mixed with polymer solutions to various polymer to lipid ratios at a final lipid concentration of 3 mM and, subsequently, incubated at 45 °C for 16 h while shaking.

### Separation of nanodiscs and remaining liposomes

During solubilization of liposomes of a myelin-like lipid composition, the resulting nanodiscs had to be separated from remaining liposomes which could hinder downstream characterization techniques. For this, 500  $\mu\text{L}$  of the 3 mM lipid/polymer suspensions were injected onto a Superose 6 Increase 10/300 GL size exclusion chromatography (SEC) column (GE Healthcare Bio-Sciences AB, Uppsala, Sweden) mounted to an Äkta pure (GE Healthcare Bio-Sciences AB) chromatography system. The following size exclusion chromatography was conducted using saline tris buffer (50 mM tris, 300 mM NaCl, pH 7.4) for elution with a flow rate of 0.5 mL/min. After discarding approximately 7.5 mL (5 mL injection loop purging and discarding of the first 2.5 mL which is

0.1 column volumes (CVs)) fractions of 500  $\mu\text{L}$  each were collected until 1.1 CVs were eluted. Detection during chromatography was conducted with UV absorbance detectors operating at 254 nm for samples containing SMA or SMA-SB and at 220 nm for DIBMA. The fractions within UV absorbance peaks were further studied with dynamic light scattering to ensure the presence of particles in the size range typical for lipid nanodiscs.

#### Dynamic light scattering (DLS)

DLS experiments were conducted on a Litesizer 500 (Anton Paar) either with a 70  $\mu\text{L}$  3 mm  $\times$  3 mm Micro Quartz cuvette (Hellma, Müllheim, Germany) or disposable cuvettes of 500  $\mu\text{L}$ , the latter for characterization of SEC fractions. The irradiation wavelength was  $\lambda = 658$  nm while the detection angle was maintained at 90° (side scattering) or 175° (back scattering) at constant temperature of 20 °C if not stated otherwise. Prior to each measurement, the sample was allowed to equilibrate for at least 1 min. Data obtained from DLS measurements was evaluated directly using the Kalliope software (Anton Paar).

#### Transmission electron microscopy (TEM)

TEM samples were prepared by spreading 5  $\mu\text{L}$  of the (polymer-)lipid suspensions after chromatographic separation of remaining liposomes and dilution with an equal amount of tris buffer onto freshly glow discharged grids with carbon support film (300 mesh) on copper (Quantifoil Micro Tools, Großlobichau, Germany). After 30-45 s excess suspension was blotted up using filter paper. The grids were washed three times with MilliQ water. 5  $\mu\text{L}$  of 2 % aqueous uranyl acetate solution was placed onto the grid and also blotted up after 1 min. After preparation the samples were dried for at least 24 h. All TEM samples were examined with a Zeiss EM 900 transmission electron microscope (Carl Zeiss Microscopy, Jena, Germany). In addition, the best sample was also imaged using a Glacios 200 kV cryo-electron transmission microscope (Thermo Fisher Scientific, Eindhoven, Netherlands). The respective images were acquired on a Falcon 3EC direct electron detector in linear mode with a total dose of 30  $\text{e}^-/\text{\AA}^2$ , and a magnification of 92000 X, resulting in a pixel size of 1.567  $\text{\AA}/\text{pixel}$ .

#### Extraction of lipids with organic solvent

For lipid quantification and mass spectrometric analysis, lipids of the prepared suspensions were extracted to  $\text{CHCl}_3/\text{MeOH}$  following the protocol of Bligh and Dyer.<sup>29</sup> In short, to the volume of the aqueous suspension MeOH (2.5x volume) and  $\text{CHCl}_3$  (1.25x volume) were added and the mixture was shaken for 2 min. Again,  $\text{CHCl}_3$  (1.25x volume) was added followed by shaking for 30 s. Additional water was added (1.25x volume) and once again the mixture was shaken for 30 s. The layers were allowed to separate and the lower layer containing mainly  $\text{CHCl}_3$ , MeOH, and nonpolar lipids was collected and the solvents were evaporated in a gentle stream of nitrogen.

#### Lipid quantification with high performance liquid chromatography (HPLC)

Lipids in nanodisc and liposome samples were quantitatively analyzed using an HPLC method customized from the literature.<sup>30</sup> The measurement system contained a LC Net II/ADC Interface Box, a PU-980 pump, a LG-2080-02 gradient mixer and a DG-2080-53 3-line degasser (all from JASCO Deutschland, Pfungstadt, Germany) as well as a LiChrospher Si 60 (5  $\mu\text{m}$ ) LiChro-CART 125-4 column (Merck, Darmstadt, Germany) and a SEDEX 55 ELS detector (SEDERE, Alfortville, France). Prior to sample measurements, stock solutions containing all lipids in appropriate ratios were prepared to calibrate the quantification (see **Figure S5 and S6**). 20  $\mu\text{L}$  sample were injected for each measurement. Elution was conducted at 1 mL/min with a solvent gradient of (A) 80/19.5/0.5  $\text{CHCl}_3/\text{MeOH}/\text{NH}_3\text{,aq}$  (32 %) and (B) 60/34/5.5/0.5  $\text{CHCl}_3/\text{MeOH}/\text{H}_2\text{O}/\text{NH}_3\text{,aq}$  (32 %) (all solvent mixtures in vol%) following literature.<sup>30</sup> During elution, the solvent gradient was adjusted linearly as follows (here shown as relative content of solvent A): 0-14 min 100 %  $\rightarrow$  0 %; 14-23 min 0 %; 23-24 min 0 %  $\rightarrow$  100 %; and 24-25 min 100 %.

#### Mass spectrometry (MS)

Lipids were extracted from the nanodiscs and spotted onto a 10 x 10 cm silica gel 60 thin layer chromatography (TLC) plate F254 (Merck). TLC separation was performed in  $\text{CHCl}_3/\text{MeOH}/\text{H}_2\text{O}$  (65:25:4) as mobile phase. After separation, TLC plates were air-dried and stained with a 0.03 % (w/v) Coomassie Brilliant blue G250 solution in 20 % (v/v) MeOH and 80 %  $\text{H}_2\text{O}$ . Visible spots were removed from the carrier and stained lipids (data not shown).

For lipid quantification, dried lipids were dissolved in 20  $\mu\text{L}$  of 80 % MeOH/20 %  $\text{CHCl}_3$  (v/v) and 2  $\mu\text{L}$  of a 100 times diluted stock of SPLASH Lipidomix Mass Spec standard (Sigma-Aldrich) in 80 % MeOH/20 %  $\text{CHCl}_3$  was added to each sample.

Mass spectra were acquired on a Q Exactive Plus Hybrid Quadrupole-Orbitrap Mass Spectrometer (Thermo Fisher Scientific, Waltham, MA, USA) equipped with a Nanospray Flex ion source (Thermo Fisher Scientific). 5  $\mu\text{L}$  of sample were loaded into borosilicate offline emitter coated with gold/palladium (Thermo Fisher Scientific).

MS settings were as follows: capillary voltage,  $\pm 2.5$  to 2.8 kV; capillary temperature, 250 °C; resolution, 70000; RF-lens level, 50; scan range of MS spectra, 400-1600  $m/z$ ; ion mode, positive (for PC lipids) or negative (for PE/PS/PI lipids); maximal injection time, 100 ms; automatic gain control target,  $2 \cdot 10^6$ ; microscans, 1; target resolution, 100000.

Tandem MS settings: maximal injection time, 100 ms; automatic gain control target,  $5 \cdot 10^5$ ; microscans, 1; target resolution, 70000; fragmentation type, HCD; mass selection window, 1  $m/z$ ; Top20 automatic precursor selection for 1 min; selected precursors were excluded for 30 s.

Acquired mass spectra were analyzed manually using the lipid maps tools (<http://www.lipid-maps.org/tools/>).

#### Continuous wave electron paramagnetic resonance (CW EPR) spectroscopy

CW EPR spectroscopy was used to further characterize the impact of surrounding polymers on the lipids while being able to differentiate between different polarities or restricted rotational motions. To this end, spin-labeled lipids (5DSPC or 16DSPC, 3.3 mol% of total lipid) were incorporated in the liposomes (and, therefore, the nanodiscs solubilized from the liposomes) substituting only phosphocholine lipids. To ensure a good signal to noise ratio the aqueous suspensions after SEC were concentrated using centrifugation filters (Amicon Ultra 4 with a molecular weight cutoff of 30 kDa, Merck Millipore, Billerica, MA, USA) at  $3220\times g$  until a volume of 200-300  $\mu\text{L}$  was reached. After centrifugation, the presence of nanodiscs in the resulting suspensions were checked using DLS once again. 10-15  $\mu\text{L}$  of the sample were filled into micropipettes (BLAUBRAND intraMark, Wertheim, Germany) and capped with capillary tube sealant (CRITOSEAL Leica, Wetzlar, Germany).

X-band CW EPR spectroscopic measurements were performed with the Miniscope MS5000 (magnettech, Freiberg Instruments, Freiberg, Germany) benchtop spectrometer. Temperature control was achieved by connecting the H04 temperature control unit (magnettech) and, thus, temperature series were recorded between 0-70 °C. All spectra were measured with a modulation amplitude of 0.1 mT and a microwave power of 3.63 mW. The range of the magnetic field was adjusted to the width of measured spectra and set between 332.5 and 347.5 mT.

Analysis of the recorded CW EPR spectra was conducted using MatLab (R2017a, v. 9.2) in combination with the EasySpin toolbox (v. 5.2.28) for EPR spectroscopy.<sup>31</sup> Spectra of liposomes (for both 16DSPC and 5DSPC) and all other systems containing 5DSPC were simulated with a single component using the model of anisotropic Brownian motion with an axial symmetry and orienting potential (see Supporting Information for further information).<sup>32-33</sup> In nanodisc systems containing 16DSPC, inclusion of a second component was necessary to achieve an acceptable agreement between simulated and experimental spectra.

#### Differential scanning calorimetry (DSC)

To analyze the impact of the three polymers on macroscopic lipid phase transitions, DSC was used without chromatographic separation of liposomes, since both lipid mixtures did not show any phase transitions in liposomes. Prior to all measurements, the samples as well as the reference buffer solution was degassed under vacuum while stirring. DSC measurements were performed using a MicroCal VP-DSC differential scanning calorimeter (MicroCal, Northampton, MA, USA). In all experiments, 5 heating/cooling cycles were measured to assure sample stability and

reproducibility from which one representative heating curve (heating rate 60 K h<sup>-1</sup> between 5 and 95 °C) was chosen. Further evaluation of the DSC results involved subtraction of regularly collected buffer/buffer baselines as well as subtraction of off-set values, if necessary.

## **Results and Discussion**

### Preparation of myelin-like nanodiscs

The successful preparation of myelin-like nanodiscs requires knowledge of the optimal polymer/lipid ratio for optimal solubilization.<sup>21</sup> To achieve this, the solubilization efficiency of the three polymers towards myelin-like liposomes was tested with DLS by measuring autocorrelation functions as exemplarily shown in **Figure 1A**. For all other autocorrelation functions see **Figure S1**. Solubilization of the liposomes goes along with a decrease in the size of the scattering particles and, thus, with a shift of the autocorrelation function to shorter correlation times.<sup>16, 21</sup> In previous studies using polymer nanodiscs, the solubilization efficiency was tested determining either the size of particles,<sup>16, 21</sup> the turbidity of the sample,<sup>15</sup> or other methods.<sup>16-17, 21</sup> Here, both of the former methods were found unsuitable for detecting the presence of nanodiscs because only partial solubilization of the complex lipid mixtures could be achieved. The decreased solubilization efficiency is easily explained by the lipid mixtures used here.<sup>24-26</sup> It is known that solubilization works best with saturated short-chain lipids such as DMPC and if unsaturated lipids are used, solubilization efficiency is reduced.<sup>21, 25</sup> This is thought to be due to an increased lateral pressure within the lipid bilayer, which impedes the penetration of the amphiphilic polymers into liposomes.<sup>24-25</sup> In addition, lipid mixtures studied here contain large amounts of cholesterol, which is also known to increase the lateral pressure of the bilayer<sup>34</sup> and, furthermore, causes the bilayer to phase-separate into ordered and disordered domains.<sup>35</sup> This phase separation may hinder the complete solubilization process as well, given that domain formation is possible in liposomes but probably not in the size-restricted nanodiscs because of the much smaller number of lipids they contain.

All optimal polymer/lipid ratios (*w/w*) for the solubilization approach used here are shown in **Table S1**. As can be concluded from DLS measurements (see **Figure S1**), SMA and SMA-SB showed substantial shifts in the autocorrelation function, whereas DIBMA exhibited only minor effects. While for solubilization of CNS liposomes only small polymer/lipid ratios were necessary in the case of SMA (1.5/1) and SMA-SB (2/1), solubilization of PNS liposomes was most effective when all three polymers were added in the highest amount suitable for the following SEC, *i.e.* at a ratio of polymer/lipid of 5/1.

Since the liposomes cannot be solubilized completely, the nanodiscs have to be separated from the remaining liposomes. In this study, the separation was conducted by SEC.

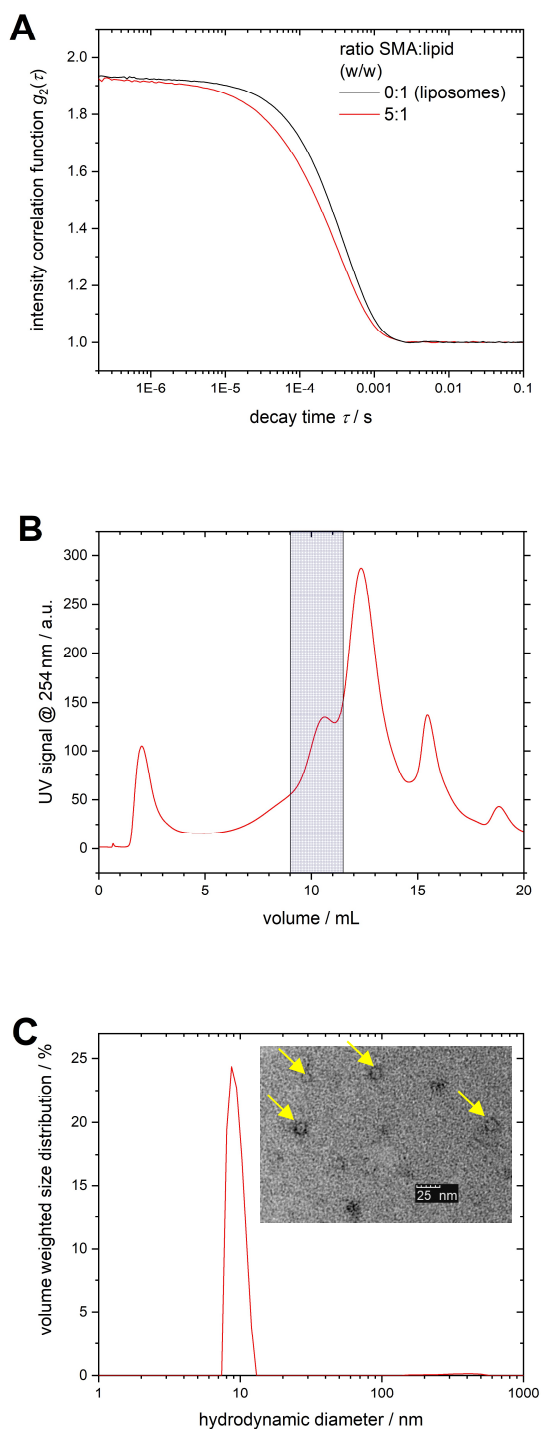


**Figure 1.** Preparation of myelin-like SMALPs containing lipids of the cytosolic PNS myelin composition. **(A)** Intensity correlation functions before and after addition of SMA to PNS liposomes (here, a lipid concentration of 1 mM was used); **(B)** size exclusion chromatogram of the resulting mixture of liposomes, SMA, and SMALPs with marked fractions containing nanodiscs conducted with a flow rate of 0.5 mL/min; **(C)** size characterization of PNS SMALPs with DLS side scattering at 20 °C, the inset in **(C)** shows a section of a corresponding TEM micrograph with nanodiscs marked by yellow arrows.

The detailed chromatographic separation and purification of all nanodisc-forming systems can be found in the SI. Comparison of all three polymers leads to the conclusion that only in lipid/SMA systems an additional peak appears in the chromatograms originating from nanodiscs. For both SMA-SB and DIBMA, possible nanodisc peaks are overlaid by a peak of pure polymer.

After SEC, all collected fractions that showed UV absorption were further tested for their particle size using DLS. If particles in the range of lipid nanodiscs (5–30 nm) were found, the respective fractions were combined (compare **Figure 1C** and **Figure S3**). The nanodisc sizes observed in DLS correlate well with the elution volume of the samples in the SEC when comparing all polymers. Note that in all fractions remaining liposomes were detected even after SEC. This may be the result of a low separation efficiency of the SEC but, since the chromatograms did not show a significantly increased baseline, an equilibrium between nanodiscs and liposomes, even after separation, is more probable. From literature it is known that polymer-encapsulated nanodiscs show fast lipid exchange among each other and in combination with monolayers.<sup>36–38</sup> A similar but somewhat slower lipid exchange would probably be observed between nanodiscs and liposomes, too. Thermodynamically, the driving force for solubilization of liposomes to nanodiscs is described using transfer free energies of both the polymer or the lipid molecules.<sup>39–40</sup>  $\Delta G_{\text{lipid}}$  is positive, that is the lipids prefer their initial bilayer state within the liposome, while  $\Delta G_{\text{polymer}}$  is negative, *i.e.*, the polymers prefer surrounding the nanodisc rather than being adsorbed to liposomes.<sup>21, 39–40</sup> In case of the complex lipid mixtures, used in this study, the magnitudes of both transfer free energies could be in a range which allows an equilibrium between nanodiscs and liposomes containing polymer to be detectable. This is plausible especially for mixtures containing a high amount of cholesterol because in liposomes these lipid mixtures are known to form ordered domains. In nanodiscs, by contrast, their size restrictions probably inhibit the formation of sizeable domains and, thus,  $\Delta G_{\text{lipid}}$  could be significantly more positive. For future applications of myelin-like nanodiscs, a further thermodynamic evaluation will be necessary, which could be conducted using *e.g.*  $^{31}\text{P}$  NMR spectroscopy.<sup>39–40</sup>

From these lipid/polymer suspensions, TEM samples were prepared by diluting them to 50 % of their initial concentration and ensuing preparation steps (see Materials and Methods). TEM micrographs were collected to confirm the presence of nanodiscs after separation of remaining liposomes.

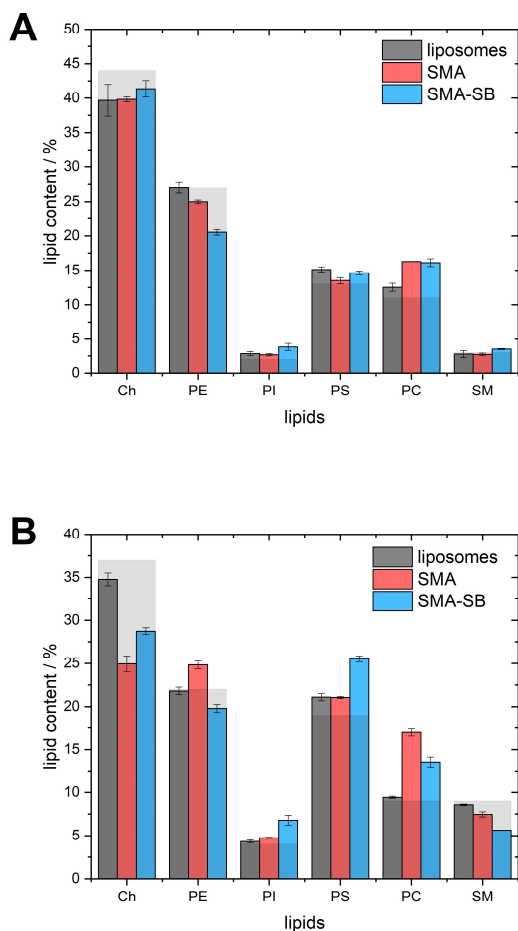


**Figure 2.** Lipid composition of myelin-like nanodiscs as detected with HPLC after extraction with  $\text{CHCl}_3/\text{MeOH}$ ; (A), cytosolic CNS lipid mixture, (B), cytosolic PNS lipid mixture. Light gray columns represent the theoretical lipid composition used for liposome preparation. The lipids are shown in order of their appearance in the chromatograms and error bars represent the standard error of three independent experiments.

The TEM micrographs (see **Figure S4** in the Supporting Information) of all samples show the successful preparation of myelin-like nanodiscs indicating similar sizes as detected by DLS (compare **Figure S3** and **Figure S4**). However, the three studied polymers differ in contrast. Nanodiscs of SMA and DIBMA yield clear micrographs with sufficient contrast, while nanodiscs containing SMA-SB appear to have lower contrast. This is probably due to the different ionic character of the polymers, as SMA and DIBMA are anionic, whereas SMA-SB is zwitterionic,<sup>22</sup> which may influence the binding affinity of the contrast agent uranyl acetate. To ensure constant staining for all polymers, we optimized the staining procedure and prepared the samples three times with each preparation being a double determination.

The whole preparation process is exemplarily shown for the system PNS lipids with SMA (polymer/lipid 5/1) in **Figure 1**.

### Analysis of lipid properties in myelin-like nanodiscs

After successful preparation of nanodiscs of myelin-like liposomes, their lipid contents were studied to ensure similarity with the well-known model system of liposomes. This is because, although the lipid vesicles were formed to resemble the myelin sheath composition, it is unknown if, during solubilization, nanodisc lipid composition was robustly recovered.

To elucidate compositional variation, the lipid composition of prepared myelin-like nanodiscs was studied with analytical HPLC regarding headgroup content (see **Figure S7**).<sup>30</sup> In **Figure 2** the composition of each system is shown in comparison to the lipid composition of liposomes prior to solubilization with the polymers. Only SMALPs and SMA-SBLPs are shown, as DIBMALPs yielded no reproducible results, which may be due to the low solubilization efficiency of DIBMA as was observed by CW EPR spectroscopy of incorporated spin labels discussed in the following chapters.

From **Figure 2** it can be concluded that the additional extraction steps<sup>29</sup> induce only minor changes in detected lipid compositions (compare the theoretical composition shown in light gray and liposomes, maximal deviation of  $-4.3\%$  for cholesterol in the CNS-like liposomes). Both SMA and SMA-SB solubilize all lipids in similar amount as they are present in the liposomes and only minor preferences are observed which is in accordance with literature.<sup>24,41</sup> Somewhat stronger deviations from liposomal compositions were found in the case of the PNS lipid mixture: while SMALPs appear to show a minor deficiency in cholesterol content ( $-10\%$  compared to liposomes) and a higher amount of PC ( $+7.5\%$ ), SMA-SB prefers to solubilize anionic lipids ( $+2.4\%$  for PI and  $+4.4\%$  for PS). The latter effect was also observed in the CNS lipid mixture but to a smaller extent ( $+1\%$  for PI). For other lipid mixtures containing even more negatively charged lipids, this solubilization preference of SMA-SB could be useful since the mainly used negatively charged polymers SMA and DIBMA showed repulsive interactions with anionic molecules.<sup>22,42-43</sup> However, deviations from the liposomal lipid compositions were only minor and, hence, myelin-like nanodiscs can be assumed to exhibit similar surface properties as myelin-like liposomes in general.

Besides the lipid composition in terms of surface charge, *i.e.*, the relative ratio of all headgroups, the polymers could prefer different lipid chain compositions as well. To study lipid chain composition, we used mass spectrometry after extraction and TLC. TLC (data not shown) was conducted to minimize overlap of lipid species with similar mass in the acquired mass spectra. The results of MS analysis of all systems are shown in **Figure S9**.

For PE, PS, and PI, all myelin-like nanodiscs exhibited similar chain compositions as observed in liposomes of the same lipid mixture with maximal deviations of approximately  $\pm 30\%$ . For PC lipids, in contrast, deviations are found depending on the polymer and the lipid mixture (see **Figure S9C** and **D**). These stronger

deviations can be attributed to the poor signal/noise ratio of PC lipids in this experiment resulting from polymeric contamination that could not be removed. For all but few exceptions all lipids were found in both liposomes and nanodiscs of all three polymers. Therefore, it can be concluded, that SMA, SMA-SB, and DIBMA do not exhibit pronounced preferences for distinct types of lipid chains.

Besides lipid preferences, the polymers were also compared concerning their lipid solubilization efficiency. As can be concluded from **Figure S1**, SMA and SMA-SB exhibited strong effects on the diffusional correlation time, that is correlated to the mean size of the particles, as observed with DLS, whereas DIBMA did not change the mean diffusion coefficient of the scattering particles. As an additional indicator of solubilization efficiency, 16DSPC was added to the lipid mixture as spin probe. By measuring CW EPR spectra of all nanodisc systems after equal sample treatment below power saturation the spin probe concentration and, thus, the lipid concentration can be compared by measuring the double integral (DI) of the spectra.<sup>44-45</sup> This, obviously, is possible only because none of the polymers exhibits strong preferences for either distinct lipid headgroups or distinct lipid chains. In addition, the comparability of all samples was ensured by concentrating them to similar volumes prior to measurement as well as by working with low microwave power to prevent power saturation.<sup>44-45</sup> However, it was not possible to prepare all samples completely equal and small preferences in lipid solubilization were observed before. Therefore, the normed double integral values shown in **Figure S10** have to be considered to be an approximation of lipid content. From measured double integral values, it can be concluded that only SMA and SMA-SB are capable of solubilizing PNS and CNS lipid mixtures to a suitable extent. DIBMA, in contrast, did not solubilize either of the two lipid mixtures within the experimental procedures applied in this study to an extent usable for most applications. Thus, DIBMA will be excluded from the following discussion. Nevertheless, temperature-dependent CW EPR spectroscopic measurements were also performed with DIBMALPs and are shown in the Supporting Information (see **Figures S14** and **S22**).

CW EPR spectroscopy also enables us to unravel changes in lipid environment induced by the polymers at different positions within the bilayer.<sup>46-49</sup> For this, spin labeled lipids were introduced bearing a doxyl moiety either in terminal position (16DSPC) or near the carbonyl group (5DSPC) of the *sn*-2 chain. A different position of the unpaired electron spin allows detecting hydration and rotational mobility in a distinct section of the bilayer.<sup>46-49</sup> In this work, temperature-dependent EPR spectra were measured between 0 and 70 °C of all studied nanodisc systems as well as myelin-like liposomes and simulated with the model of Brownian motion with axial symmetry (see Supporting Information for further details and **Ta-**

**bles S2-S13, Figure S18, and Figure S26** for simulation results). The temperature-dependent spectra and comparison of measured and simulated spectra are shown in **Figures S11-S17** and **Figures S19-S25**.

First, from the observed CW EPR spectra, it is obvious that only minor differences between the CNS and the PNS lipid composition were found for all studied systems. The hydration, as concluded from simulated <sup>14</sup>N hyperfine coupling constants  $a_{iso}$  (see **Figure S18** and **Figure S26**), as well as the rotational behavior (**Figure 3** as well as **Figure S18** and **Figure S26**) remained similar when comparing both CNS and PNS composition for each model system. Subsequently, in the following all results apply for both systems if not stated otherwise.

Second, due to use of 16- and 5DSPC, the nanodisc systems can be compared to liposomes of a similar composition to study the impact of each polymer onto (i) the core of the bilayer and (ii) the interface between hydrophobic chain and hydrophilic head-group, respectively.<sup>46-49</sup>

For (i), 16DSPC was introduced into the lipid mixture prior to liposome solubilization. From the data shown in **Figure S18** it can be concluded, that all studied model systems exhibit axial rotation with temperature-dependent  $\tau_c$ ,  $S_{zz}$  and  $a_{iso}$ . The rotational correlation time  $\tau_c$  decreases with temperature. Addition of either of the two polymers SMA or SMA-SB induces an increase of  $\tau_c$ . Furthermore, the rotational motion of 16DSPC changes its anisotropy  $T_{rot}$ <sup>50</sup> with increasing temperature in myelin-like liposomes while in both polymer-encapsulated nanodiscs it remains nearly constant over the whole temperature range studied. Thus, both polymers hindered a more isotropic motion of the lipid chains. The CW EPR spectra were simulated using the least number of spectral components possible, that is one for liposomes and one or two for both SMALPs and SMA-SBLPs depending on temperature. Inclusion of a second component characterized by a higher hydration and lower rotational mobility, *i.e.*, increased  $a_{iso}$  as well as higher  $\tau_c$  compared to the main component found for all systems, respectively, in both nanodisc systems was necessary to achieve a reasonable fit to the experimental data. However, the respective additional components of both polymers differ in their temperature stability, rotational restrictions, and polarity of their environment (see **Figure S18**). Complex spectra with correlated  $a_{iso}$  and rotational behavior causes a hindered separation of the simulation parameters. The decreased  $a_{iso}$  shown in **Figure S18**, therefore, has to be considered most probably an artifact resulting from simulation of the motional regime of the spin probe which is especially difficult to simulate in combination with environmental polarity and an additional component. However, if this is a real effect, it could in the future be studied further using hyperfine spectroscopy in D<sub>2</sub>O solvent, for example.

For lipid bilayers surrounded by SMA, an additional component between approximately 0 °C and 34 °C is

needed in the analysis, which exhibits increased  $\tau_c$  combined with a higher order parameter and a more polar spin label environment when compared with myelin-like liposomes (see **Figure S18**). 16DSPC in SMA-SBLPs had to be simulated with an additional component between 0 °C and 55 °C (CNS) or 64 °C (PNS) which is denoted by even stronger rotational restrictions combined with increased order but an environmental polarity in between liposomes and SMALPs (see **Figure S18**). In contrast to 16DSPC in SMALPs, the spectra of 16DSPC in SMA-SBLPs at 0 °C and 5 °C can be simulated using only the additional component and, therefore, differ substantially from the spectra found in liposomes.

The additional spectral component, featuring increased polarity and hydration in each model system, can be consistently explained with the addition of the amphiphilic polymers, *i.e.*, SMA<sup>14, 43</sup> and SMA-SB,<sup>22-23</sup> that change polarity directly plus disrupt the bilayer structure by providing the basis for increased water penetration into the core of the membrane.<sup>15-16, 51</sup> On the other hand, increased restrictions of spin label rotational mobility can either be the result of a polymer-induced formation of a condensed lipid phase<sup>23, 52</sup> or by lipid-polymer interactions with the surrounding polymer itself.<sup>15, 48, 51</sup> To study this effect, we performed DSC measurements of SMALPs and SMA-SBLPs of both lipid compositions prior to separation of the liposomes.

$C_p$  peaks in the DSC results would indicate a lipid phase transition, and as is observable in **Figure S27**, in our DSC experiments there are no  $C_p$  peaks over the whole temperature range. Furthermore, when studying 5DSPC in the same systems, no additional spectral component is necessary for suitable fit of simulation to the experimental spectra.

From the combination of CW EPR and DSC, it can be concluded that the observed spectral component with increased rotational restrictions and polarity has to be induced by direct interactions between the polymers and the lipids. Subsequently, the main difference between both polymers is probably induced by different nanodisc sizes. The prepared myelin-like SMALPs of both lipid compositions exhibited larger diameters as observed with DLS and TEM than SMA-SBLPs. The interfacial area between the polymer and lipids depends on the particle diameter. This correlates with the effects visible in the additional component observed in the CW EPR spectra. However, it is possible that the observed interactions originate from a temperature-dependent size increase of the nanodiscs. Such an increasing size was observed only for myelin-like SMALPs, while SMA-SBLPs exhibited a nearly constant size as determined by DLS (see **Figure S28** and **Figure S29**).

Addition of 5DSPC to the lipid mixtures prior to liposome solubilization, enables the study of the interfacial region between lipid headgroups and chains.<sup>46-49</sup> The simulation results of temperature-dependent CW EPR spectra are shown in **Figure S26**. They indicate only minor effects when compared with results

of 16DSPC simulation which is due to the already reduced rotational mobility of the spin label.<sup>32, 48</sup> However, a change in polarity was found for SMA in comparison with liposomes at elevated temperatures. SMA shows a decreased  $a_{iso}$  between 30 °C and 65 °C compared with liposomes, which declines again around 70 °C. This could be the result of SMALPs being more hydrophobic. The differences in  $a_{iso}$ , however, are only minor. Thus, this interpretation has to be reviewed using hyperfine spectroscopic methods in future studies. The rotational correlation time  $\tau_c$  was affected to a small extent by the surrounding polymer, in contrast to the observations in the membrane core. Nevertheless, differences between liposomes and both nanodisc systems emerge when comparing the anisotropy of rotation  $T_{rot}$ .<sup>50</sup> All three systems, in general, exhibited strong anisotropic motion. With increasing temperature,  $T_{rot}$  of both 5DSPC in SMALPs and in SMA-SBLPs deviates from  $T_{rot}$  found in liposomes to a more isotropic rotational behavior. This effect was more pronounced in the case of SMA-SB-encapsulated lipid nanodiscs, which is probably due to SMA-SB being more apolar<sup>22</sup> and, hence, preferably interacting with the hydrophobic core instead of the whole bilayer. Thus, less rotational restrictions were exerted by SMA-SB in the only weakly interacting hydrophilic part of the bilayer. As the hydrophobic-hydrophilic interfacial region remains sterically demanding and the lipids are unable to leave the bilayer, the rotation becomes more isotropic instead of becoming faster. Changes in  $T_{rot}$ , as observed here, are caused by significant differences in rotational behavior while a similar  $\tau_c$  is maintained within the dataset (compare with Ref. <sup>48</sup>). Our results, thus, have to be considered a clear argument for changing rotational restrictions, that is an increased wiggling motion of the spin label in-plane compared to liposomes.

From studying myelin-like nanodiscs in comparison with liposomes, it can be concluded, that a variation of labeling position within the bilayer yields vastly contrary results. While both polymers induced similar effects in both the membrane core as well as the carbonyl-near region, respectively, the deviations from liposomes were more pronounced in SMA-SBLPs. Addition of the polymer induced increased rotational restrictions in the membrane core that were accompanied by an increase in polarity and hydration, while the rotational anisotropy in the more polar regions of the membrane was reduced. Both findings lead to a model depicted in **Figure 5** which combines a compression effect in the hydrophobic parts with a small loosening effect in the hydrophilic parts of the membrane. SMA exhibits the same effects to a smaller extent, which is due to (i) a larger diameter of the nanodiscs resulting in a reduced interaction area between polymer and lipids in relation to lipid number and (ii) a higher polarity of the SMA polymer in comparison to SMA-SB, which enables SMA to bind both the hydrophilic and the hydrophobic areas of the lipid membrane while SMA-SB interacts to a smaller extent with the headgroups than SMA.

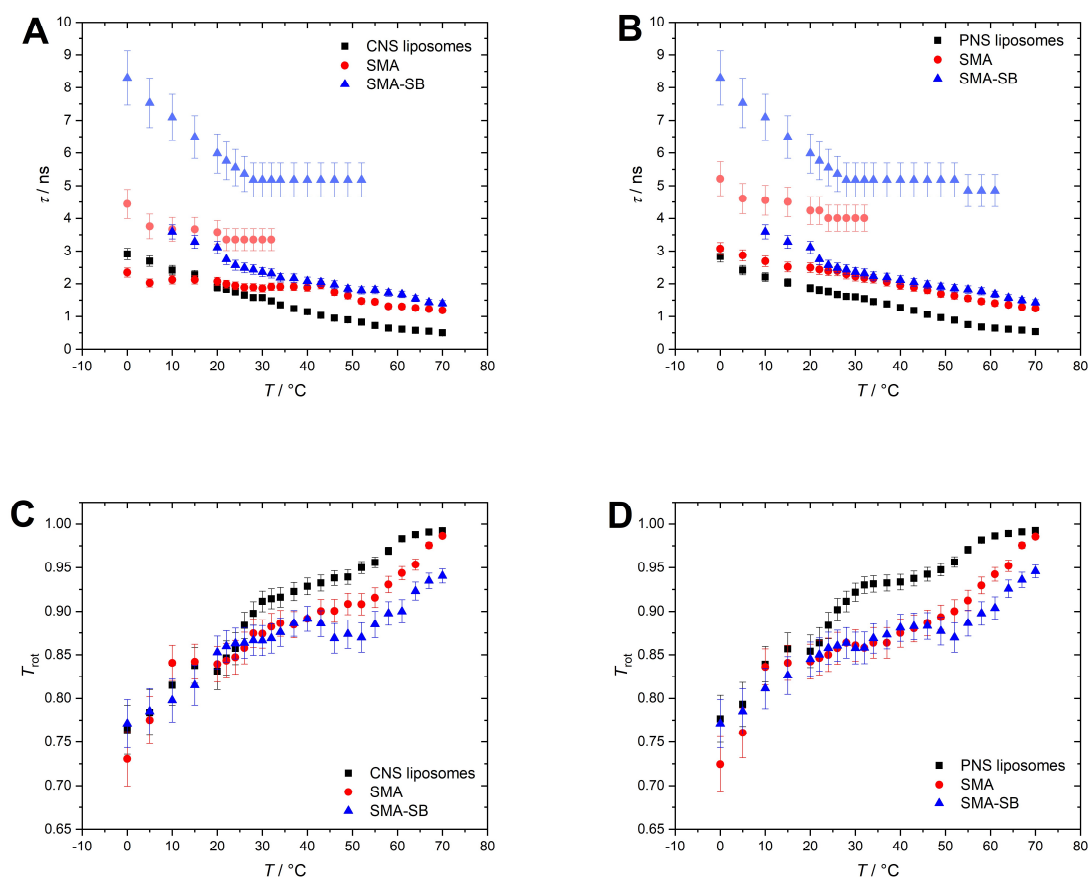


**Figure 3.** Simulation results of CW EPR spectra of 16DSPC (A/B) and 5DSPC (C/D) in liposomes and nanodiscs of the cytosolic CNS (A/C) and PNS (B/D) myelin composition. Shown are the rotational correlation time  $\tau_c$  (A/B) of 16DSPC and the rotational anisotropy  $T_{rot}$  (C/D) of 5DSPC. The spectral component of slow rotation appearing in X-band CW EPR spectra of SMALPs and SMA-SBLPs is presented in brightened colors to set it apart from the fast-rotating component.

#### Suitability of myelin-like nanodiscs as model system for protein studies

Successful preparation of nanodiscs with a (near) native lipid composition is only the first step necessary for *in vitro* myelin research. Generally, the suitability of the prepared systems for mimicking cytosolic myelin requires further investigations. To this end, we added myelin basic protein (MBP) to the myelin-like nanodiscs to test for MBP-membrane interaction and induced self-assembly. MBP is abundant in both CNS and PNS cytosolic myelin, and we have ample experience in the characterization of MBP in different charge variants in LUVs.<sup>12,53</sup> As a suitable model protein, here we used bovine MBP<sup>28</sup> which presents a similar amino acid sequence as human MBP.<sup>54</sup>

In the myelin sheath, MBP is incorporated into the multilayer system between both cytosolic leaflets of opposed bilayers.<sup>11-12</sup> Since MBP acts as “molecular glue”, holding together two lipid bilayers,<sup>11-12</sup> it induces association of multiple lipid particles. Therefore, its interactions with lipid model systems can be observed by light scattering techniques. To ensure comparability of all measurements, we added the same amount of bMBP to each sample resulting in

equal protein concentration but differing lipid concentration and, thus, different lipid/protein ratio.

First, DLS of the nanodiscs with and without addition of bMBP was measured. The resulting size distributions for SMALPs of both PNS and CNS myelin-like nanodiscs are shown in **Figure 4** (for both other polymers and comparison with pure bMBP see **Figure S30**). In the case of SMALPs, addition of bMBP has a strong effect on the size of scattering particles. The small nanodiscs disappear while new particles of hydrodynamic diameters of more than 1  $\mu\text{m}$  appear. While the vanishing of the small particles probably was induced by larger particles, which scatter much more strongly, the large particles additionally observed must be the result of aggregated nanodiscs. The bMBP alone exhibited a small fraction of aggregated protein. Those large particles, however, did not scatter to a similar extent as the mixtures of SMALPs and bMBP. Furthermore, mixtures of bMBP and the polymer without lipids do not contain particles of similar size (see **Figure S30**). Therefore, the observed interactions cannot originate from unspecific coulombic interactions between anionic polymer

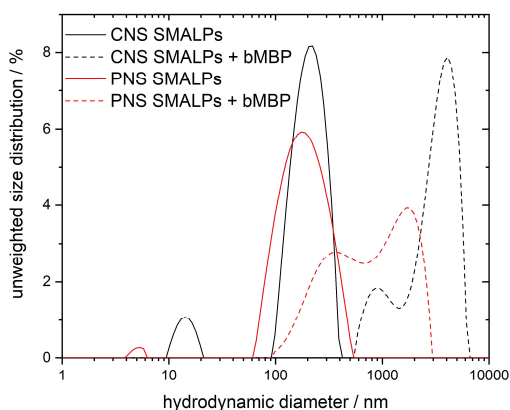


**Figure 4.** Size distribution of SMALPs of the cytosolic CNS and PNS myelin lipid composition with and without bMBP as observed with DLS measurements.

and cationic bMBP alone. For SMA-SBLPs, by contrast, no observable size change of the lipid particles is induced by the protein (see **Figure S30**).

From DLS measurements, it can be concluded, that only in myelin-like SMALPs bMBP can execute its native function of stacking lipid bilayers to a noticeable extent.

By measuring CW EPR spectra of myelin-like nanodiscs containing 16DSPC or 5DSPC with bMBP it is possible to study the protein's effect on the bound lipids. The spectra of all nanodisc samples are shown in **Figure S31** and **Figure S32** in the Supporting Information.

We found that addition of the protein induced no changes in lipid mobility and hydration for all studied systems. One would typically assume in CW EPR studies of interactions between penetrating proteins and lipids that an additional spectral component after addition of the protein becomes observable.<sup>55</sup> This is not the case here after addition of bMBP. However, bMBP had an effect on the spectral intensity in some cases. When the protein is added to myelin-like nanodiscs the double integral value has to be reduced to 50 % of the pure systems due to dilution. In both SMALP systems and SMA-SBLPs containing PNS lipids the double integral was reduced even further to 30–40 % of the nanodiscs without protein while for DIBMALPs and CNS SMA-SBLPs it remained approximately at 50 %.

A decrease in spectral intensity can be induced by increased spin exchange interaction between the spin probes.<sup>56</sup> If this interaction becomes strong enough, *i.e.*, the spin probes collide directly, the spectral peaks can become broad enough to be indiscernible from the baseline. This effect could be induced by guest molecules such as proteins which preferably bind lipids or reject them if the model system is spatially confined.

In case of myelin-like SMALPs, the size of the nanodiscs limited the space available for the lipids to approximately 10 nm. bMBP as a positively charged protein is known to preferably bind to negatively charged lipid surfaces.<sup>28, 57</sup> Subsequently, it probably gathers negatively charged lipids in inhomogeneous membranes like the studied myelin-like composition. The used spin label lipids bear zwitterionic PC headgroups. Thus, it is possible that bMBP repelled or ignored the PC spin labels to some extent which is in accordance with literature showing weak interaction between bMBP and PC lipids.<sup>28, 57</sup> If the protein did not bind the spin probe lipids, they accumulate at the rim of the nanodisc and, hence, likely interact more frequently among themselves, which causes a broadening of the peaks.

While the addition of bMBP to myelin-like nanodiscs did not directly affect the mobility and hydration of the spin-labeled lipids, they could be pushed to the rim of the nanodisc and exhibit strong peak broadening which, thus, have decreased intensity. This indication of protein binding to the lipids was only found for myelin-like SMALPs and SMA-SBLPs containing PNS lipids. This may be due to a slightly higher binding affinity of bMBP to the more anionic PNS lipid mixture.

In conclusion, we have shown that myelin-like nanodiscs encapsulated by SMA are the only model systems that are able to bind bMBP in a native way. SMA-SBLPs only bind the protein if the lipid composition resembles the cytosolic PNS, which may be the result of changed lipid properties as discussed before. However, in PNS SMA-SBLPs bMBP was not able to stack the nanodiscs. The resulting model is depicted in **Figure 5**.

## Conclusions

In this study, we present the preparation of myelin-like nanodiscs with SMA containing either PNS or CNS cytosolic lipids. The study and optimization of the solubilization process was conducted using DLS. Since solubilization was incomplete and liposomes remained, they had to be separated by SEC after which the nearly pure nanodiscs could be characterized further.

The myelin-like nanodiscs were studied regarding their lipid composition, the properties of the myelin lipids and their suitability to be used as model system for natural myelin in lab scale.

Our results suggest that the preparation in acceptable amount is possible with the polymers SMA and SMA-SB. Both polymers do not show any preference for distinct lipid headgroups or chains. However, only myelin-like SMALPs present lipid-protein interactions with the model protein bMBP while maintaining the protein's natural function.

By including the spin-labeled lipids 16DSPC and 5DSPC in our solubilization, we were able to characterize the effects of both SMA and SMA-SB on the lipids within the myelin-like nanodiscs either in the

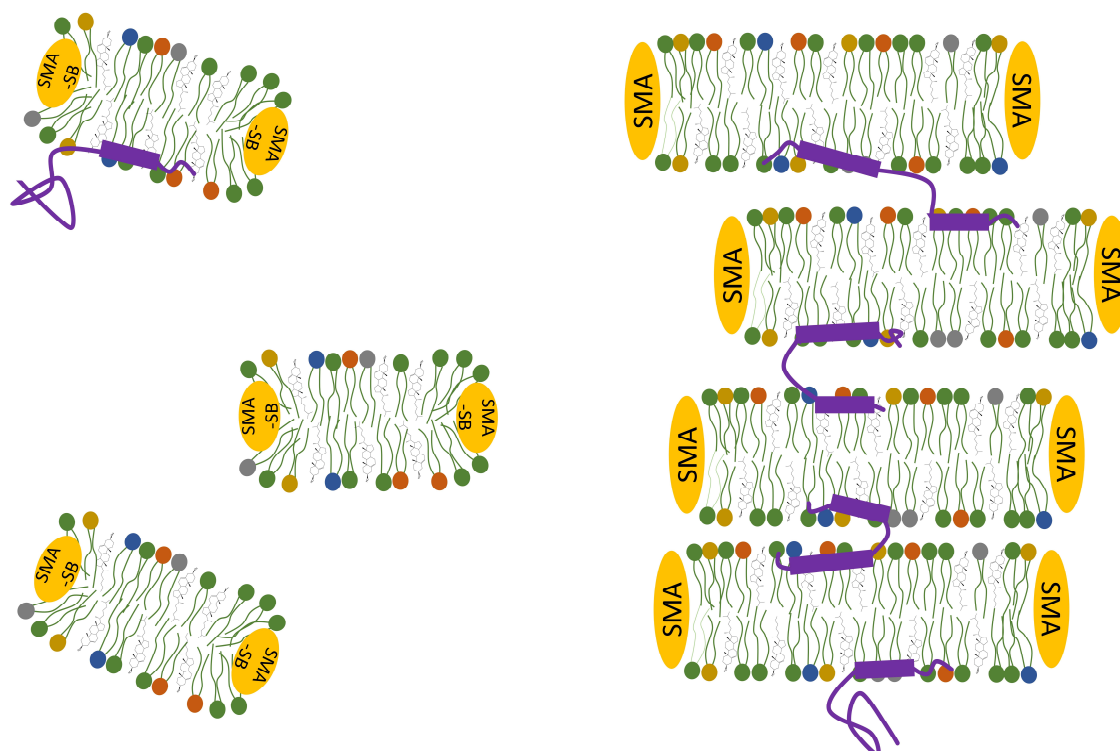


**Figure 5.** Suitability of SMALPs and SMA-SBLPs as model system for human myelin. While SMALPs of both cytosolic CNS and PNS lipid composition can bind bMBP and aggregate, only the PNS-like SMA-SBLPs can bind bMBP but, however, do not show aggregation. Note the different constraint both polymers exert onto the lipids as observed with CW EPR measurements. The myelin-like lipid composition is indicated by differently colored phospholipids as well as cholesterol. The sizes in this scheme are not to scale and size differences are exaggerated.

hydrophobic center of the bilayer or near the carbonyl groups. We find that both polymers exert steric constraints onto the hydrophobic part of the lipids while a small loosening effect is observable for the carbonyl-near membrane region. Both effects were significantly more pronounced in SMA-SBLPs and may have prevented the membrane stacking by bMBP. The third amphiphilic polymer in this study, DIBMA, was not able to solubilize myelin-like liposomes in a usable extent.

In future studies, the preparation process described herein will be further optimized and different proteins will be studied in combination with the myelin-like lipid composition. The model system presented here enables further structural studies of partly disordered myelin proteins such as MBP<sup>11</sup> with a variety of methods, *i.e.* solution and solid state NMR spectroscopy.<sup>17,58</sup> Even SMA-SB and DIBMA could be suitable for solubilization with different experimental parameters. The composition of the nanodiscs could be optimized using both cytosolic and extracellular lipids. If it is possible to prepare nanodiscs containing both the extracellular and the cytosolic leaflet this would enable even more nature-like research such as mimicking myelin with all major lipids and proteins in combination. When considering that the lipid composition of PNS and CNS myelin is challenging to be solubilized by polymers, our work shows

that more complex lipid model membrane systems are in general accessible through polymer-encapsulated nanodiscs. We can furthermore study protein-lipid interactions in myelin and factors driving myelin formation or degradation using combinations of myelin proteins in a highly controlled lipid environment resembling myelin's cytoplasmic leaflet.

## ASSOCIATED CONTENT

### Supporting Information.

The Supporting Information is available free of charge at <http://pubs.acs.org>.

Details on CW EPR simulation and lipids, optimal polymer/lipid ratios, further DLS data, chromatograms, TEM micrographs, HPLC calibration, MS data, CW EPR data including spectra and simulation results, and DSC data

## AUTHOR INFORMATION

### Corresponding Author

\* E-mail address: [dariush.hinderberger@chemie.uni-halle.de](mailto:dariush.hinderberger@chemie.uni-halle.de)

Telephone number: +49 345 55-25230

Fax number: +49 345 55-27576

### Present Addresses

David Haselberger: Institute of Physics, Martin Luther University (MLU) Halle-Wittenberg, Betty-Heimann-Str. 7, 06120 Halle (Saale), Germany.

## Author Contributions

M.H., T.H., L.M., M.D., C.V., S.K., P.L.K., C.S., and D.Hi. conceived and planned research; M.H., D.Ha., and M.D. contributed to sample preparation; M.H., D.Ha., T.H., and L.M. performed experiments; M.H., D.Ha., T.H., L.M., K.J., A.M., and D.Hi. analyzed data; M.H. carried out spectral simulations; M.H., T.H., L.M., K.J., S.K., P.L.K., C.S., and D.Hi. wrote the publication.

## Funding Sources

M.H. thanks the Fonds der Chemischen Industrie (FCI) for a Kekulé scholarship. T.H. and C.S. acknowledge funding from the Federal Ministry for Education and Research (BMBF, 03Z22HN22) and the European Regional Development Funds (EFRE, ZS/2016/04/78115). P.L.K. was supported by the Federal Ministry for Education and Research (BMBF, ZIK program) (Grant nos. 03Z22HN23 and 03COV04), the European Regional Development Funds for Saxony-Anhalt (grant no. EFRE: ZS/2016/04/78115), funding by Deutsche Forschungsgemeinschaft (DFG) (project number 391498659, RTG 2467) and the Martin-Luther University of Halle-Wittenberg. A.M. and P.L.K. were supported by International Graduate School AGRIPOLY, funded by the European Regional Development Fund (ERDF) and the Federal State Saxony-Anhalt with a scholarship to K.J.

## ACKNOWLEDGMENT

We thank Annkatrin Rother, Gerd Hause, and Farzad Hamdi for their support in conducting electron microscopy (EM) and Fotis Kyrilis for his support in EM and SEC experiments.

## ABBREVIATIONS

5DSPC, 1-palmitoyl-2-stearoyl-(5-doxyl)-*sn*-glycero-3-phosphocholine, 16DSPC, 1-palmitoyl-2-stearoyl-(16-doxyl)-*sn*-glycero-3-phosphocholine, bMBP, bovine myelin basic protein, CNS, central nervous system, CV, column volume, CW EPR, continuous wave electron paramagnetic resonance, DI, double integral, DIBMA, diisobutylene/maleic acid copolymer, DLS, dynamic light scattering, DSC, differential scanning calorimetry, HPLC, high performance liquid chromatography, LPs, lipid particles (used in combination with the three polymers), MBP, myelin basic protein, MS, mass spectrometry, NMR, nuclear magnetic resonance, PC, phosphatidylcholine lipids, PE, phosphatidylethanolamine lipids, PI, phosphatidylinositol lipids, PS, phosphatidylserine lipids, PNS, peripheral nervous system, SEC, size exclusion chromatography, SM, sphingomyelin lipids, SMA, styrene/maleic acid copolymer, SMA-SB, styrene/maleic amide sulfobetaine copolymer, TEM, transmission electron microscopy, TLC, thin layer chromatography.

## REFERENCES

1. Lassmann, H., Mechanisms of white matter damage in multiple sclerosis. *Glia* **2014**, *62* (11), 1816-1830.
2. Nave, K. A.; Werner, H. B., Myelination of the nervous system: mechanisms and functions. *Annu. Rev. Cell. Dev. Biol.* **2014**, *30*, 503-533.
3. Niemann, A.; Berger, P.; Suter, U., Pathomechanisms of mutant proteins in Charcot-Marie-Tooth disease. *Neuromolecular Med.* **2006**, *8* (1-2), 217-241.
4. Fraser, P. E.; Deber, C. M., Surface accessibility of <sup>13</sup>C-labeled lysine residues in membrane-bound myelin basic protein. *J. Biol. Chem.* **1984**, *259* (14), 8689-8692.
5. Sedzik, J.; Blaurock, A. E.; Höchli, M., Lipid/Myelin Basic Protein Multilayers A Model for the Cytoplasmic Space in Central Nervous System Myelin. *J. Mol. Biol.* **1984**, *174*, 385-409.
6. Shanshiashvili, L. V.; Suknidze, N. C.; Machaidze, G. G.; Mikeladze, D. G.; Ramsden, J. J., Adhesion and clustering of charge isomers of myelin basic protein at model myelin membranes. *Arch. Biochem. Biophys.* **2003**, *419* (2), 170-177.
7. Walker, A. G.; Rumsby, M. G., The induction of liposome aggregation by myelin basic protein. *Neurochem. Int.* **1985**, *7*, 441-447.
8. Yurlova, L.; Kahya, N.; Aggarwal, S.; Kaiser, H. J.; Chiantia, S.; Bakhti, M.; Pewzner-Jung, Y.; Ben-David, O.; Futerman, A. H.; Brügger, B.; Simons, M., Self-segregation of myelin membrane lipids in model membranes. *Biophys. J.* **2011**, *101* (11), 2713-2720.
9. Hartline, D. K., What is myelin? *Neuron Glia Biol.* **2008**, *4* (2), 153-163.
10. Boggs, J. M.; Moscarello, M. A., Structural organization of the human myelin membrane. *Biochim. Biophys. Acta* **1978**, *515*, 1-21.
11. Bakhti, M.; Aggarwal, S.; Simons, M., Myelin architecture: zipper membranes tightly together. *Cell. Mol. Life Sci.* **2014**, *71* (7), 1265-1277.
12. Tzakos, A. G.; Kursula, P.; Theodorou, V.; Troganis, A.; Tselios, T.; Svarnas, C.; Matsoukas, J.; Apostolopoulos, V.; Gerotheranassis, I. P., Structure and function of the myelin proteins: current status and perspectives in relation to multiple sclerosis. *Curr. Med. Chem.* **2005**, *12*, 1569-1587.
13. Raasakka, A.; Ruskamo, S.; Kowal, J.; Han, H.; Baumann, A.; Myllykoski, M.; Fasano, A.; Rossano, R.; Riccio, P.; Bürck, J.; Ulrich, A. S.; Stahlberg, H.; Kursula, P., Molecular structure and function of myelin protein P0 in membrane stacking. *Sci. Rep.* **2019**, *9* (1), 642.
14. Knowles, T. J.; Finka, R.; Smith, C.; Lin, Y. P.; Dafforn, T.; Overduin, M., Membrane proteins solubilized intact in lipid containing nanoparticles bounded by styrene maleic acid copolymer. *J. Am. Chem. Soc.* **2009**, *131*, 7484-7485.
15. Scheidelaar, S.; Koorengevel, M. C.; Pardo, J. D.; Meeldijk, J. D.; Breukink, E.; Killian, J. A., Molecular model for the solubilization of membranes into nanodisks by styrene maleic acid copolymers. *Biophys. J.* **2015**, *108* (2), 279-290.
16. Oluwole, A. O.; Danielczak, B.; Meister, A.; Babalola, J. O.; Vargas, C.; Keller, S., Solubilization of Membrane Proteins into Functional Lipid-Bilayer Nanodiscs Using a Diisobutylene/Maleic Acid Copolymer. *Angew. Chem. Int. Ed.* **2017**, *56* (7), 1919-1924.
17. Ravula, T.; Ramadugu, S. K.; Di Mauro, G.; Ramamoorthy, A., Bioinspired, Size-Tunable Self-Assembly of Polymer-Lipid Bilayer Nanodiscs. *Angew. Chem. Int. Ed.* **2017**, *56* (38), 11466-11470.
18. Yasuhara, K.; Arakida, J.; Ravula, T.; Ramadugu, S. K.; Sahoo, B.; Kikuchi, J. I.; Ramamoorthy, A., Spontaneous Lipid Nanodisc Formation by Amphiphilic Polymethacrylate Copolymers. *J. Am. Chem. Soc.* **2017**, *139* (51), 18657-18663.
19. Hardin, N. Z.; Ravula, T.; Di Mauro, G.; Ramamoorthy, A., Hydrophobic Functionalization of Polyacrylic Acid as a Versatile Platform for the Development of Polymer Lipid Nanodiscs. *Small* **2019**, *15* (9), 1804813.
20. Ravula, T.; Ramamoorthy, A., Synthesis, Characterization, and Nanodisc Formation of Non-ionic Polymers. *Angew. Chem. Int. Ed.* **2021**, *60*, 1-5.
21. Grethen, A.; Oluwole, A. O.; Danielczak, B.; Vargas, C.; Keller, S., Thermodynamics of nanodisc formation mediated by styrene/maleic acid (2:1) copolymer. *Sci. Rep.* **2017**, *7* (1), 11517.
22. Eisermann, J.; Hoffmann, M.; Schöffmann, F. A.; Das, M.; Vargas, C.; Keller, S.; Hinderberger, D., Molecular-Level Interactions of Nanodisc-Forming Copolymers Dissected by EPR Spectroscopy. *Macromol. Chem. Phys.* **2021**, *accepted manuscript*.
23. Hoffmann, M.; Eisermann, J.; Schöffmann, F. A.; Das, M.; Vargas, C.; Keller, S.; Hinderberger, D., Influence of Different Polymer Belts on Lipid Properties in Nanodiscs Characterized by CW EPR Spectroscopy. *Biochim. Biophys. Acta Biomembranes* **2021**, *submitted manuscript*.

24. Dörr, J. M.; Scheidelaar, S.; Koorengel, M. C.; Dominguez, J. J.; Schäfer, M.; van Walree, C. A.; Killian, J. A., The styrene-maleic acid copolymer: a versatile tool in membrane research. *Eur. Biophys. J.* **2016**, *45* (1), 3-21.
25. Oluwole, A. O.; Klingler, J.; Danielczak, B.; Babalola, J. O.; Vargas, C.; Pabst, G.; Keller, S., Formation of Lipid-Bilayer Nanodiscs by Diisobutylene/Maleic Acid (DIBMA) Copolymer. *Langmuir* **2017**, *33* (50), 14378-14388.
26. Smith, A. A. A.; Autzen, H. E.; Faust, B.; Mann, J. L.; Muir, B. W.; Howard, S.; Postma, A.; Spakowitz, A. J.; Cheng, Y.; Appel, E. A., Lipid Nanodiscs via Ordered Copolymers. *Chem* **2020**, *6* (10), 2782-2795.
27. Inouye, H.; Kirschner, D. A., Membrane interactions in nerve myelin: determination of surface charge from biochemical data. *Biophys. J.* **1988**, *53*, 247-260.
28. Widder, K.; Träger, J.; Kerth, A.; Harauz, G.; Hinderberger, D., Interaction of Myelin Basic Protein with Myelin-like Lipid Monolayers at Air-Water Interface. *Langmuir* **2018**, *34* (21), 6095-6108.
29. Bligh, E. G.; Dyer, W. J., A rapid method of total lipid extraction and purification. *Can. J. Biochem. Physiol.* **1959**, *37*, 911-917.
30. Becart, J.; Chevalier, C.; Biesse, J. P., Quantitative analysis of phospholipids by HPLC with a light scattering evaporating detector - application to raw materials for cosmetic use. *J. High Resolut. Chromatogr.* **1990**, *13*, 126-129.
31. Stoll, S.; Schweiger, A., EasySpin, a comprehensive software package for spectral simulation and analysis in EPR. *J. Magn. Reson.* **2006**, *178* (1), 42-55.
32. Colbasevici, A.; Voskoboinikova, N.; Orekhov, P. S.; Bozdaganyan, M. E.; Karlova, M. G.; Sokolova, O. S.; Klare, J. P.; Mulki-djanian, A. Y.; Shaitan, K. V.; Steinhoff, H. J., Lipid dynamics in nanoparticles formed by maleic acid-containing copolymers: EPR spectroscopy and molecular dynamics simulations. *Biochim. Biophys. Acta Biomembr.* **2020**, *1862* (5), 183207.
33. Marsh, D., Distinct Populations in Spin-Label EPR Spectra from Nitroxides. *J. Phys. Chem. B* **2018**, *122* (23), 6129-6133.
34. Aye, M. A.; Levitan, I., Paradoxical impact of cholesterol on lipid packing and cell stiffness. *Front. Biosci.* **2016**, *21*, 1245-1259.
35. Veatch, S. L.; Keller, S. L., Miscibility phase diagrams of giant vesicles containing sphingomyelin. *Phys. Rev. Lett.* **2005**, *94* (14), 148101.
36. Danielczak, B.; Keller, S., Collisional lipid exchange among DIBMA-encapsulated nanodiscs (DIBMALPs). *Eur. Polym. J.* **2018**, *109*, 206-213.
37. Danielczak, B.; Keller, S., Lipid exchange among polymer-encapsulated nanodiscs by time-resolved Förster resonance energy transfer. *Methods* **2020**, *180*, 27-34.
38. Hazell, G.; Arnold, T.; Barker, R. D.; Clifton, L. A.; Steinke, N. J.; Tognoloni, C.; Edler, K. J., Evidence of Lipid Exchange in Styrene Maleic Acid Lipid Particle (SMALP) Nanodisc Systems. *Langmuir* **2016**, *32* (45), 11845-11853.
39. Vargas, C.; Arenas, R. C.; Frotscher, E.; Keller, S., Nanoparticle self-assembly in mixtures of phospholipids with styrene/maleic acid copolymers or fluorinated surfactants. *Nanoscale* **2015**, *7* (48), 20685-20696.
40. Cuevas Arenas, R.; Klingler, J.; Vargas, C.; Keller, S., Influence of lipid bilayer properties on nanodisc formation mediated by styrene/maleic acid copolymers. *Nanoscale* **2016**, *8* (32), 15016-26.
41. Medina-Carmona, E.; Varela, L.; Hendry, A. C.; Thompson, G. S.; White, L. J.; Boles, J. E.; Hiscock, J. R.; Ortega-Roldan, J. L., A quantitative assay to study the lipid selectivity of membrane-associated systems using solution NMR. *Chem. Commun.* **2020**, *56* (78), 11665-11668.
42. Danielczak, B.; Meister, A.; Keller, S., Influence of Mg(2+) and Ca(2+) on nanodisc formation by diisobutylene/maleic acid (DIBMA) copolymer. *Chem. Phys. Lipids* **2019**, *221*, 30-38.
43. Scheidelaar, S.; Koorengel, M. C.; van Walree, C. A.; Dominguez, J. J.; Dörr, J. M.; Killian, J. A., Effect of Polymer Composition and pH on Membrane Solubilization by Styrene-Maleic Acid Copolymers. *Biophys. J.* **2016**, *111* (9), 1974-1986.
44. Gerlock, J. L., Determination of Free Radicals in Polymer Films by Electron Spin Resonance Spectrometry. *Anal. Chem.* **1983**, *55*, 1520-1522.
45. Bauer, D. R.; Gerlock, J. L., ESR Studies of Photooxidation and Stabilization of Polymer Coatings. In *Advanced ESR Methods in Polymer Research*, Schlick, S., Ed. John Wiley & Sons, Inc.: Hoboken, 2006; pp 255-278.
46. Kurad, D.; Jeschke, G.; Marsh, D., Lipid Membrane Polarity Profiles by High-Field EPR. *Biophys. J.* **2003**, *85*, 1025-1033.
47. Vartorelli, M. R.; Garay, A. S.; Rodrigues, D. E., Spin-labeled Stearic Acid Behavior and Perturbations on the Structure of a Gel-Phase-Lipid Bilayer in Water: 5-, 12- and 16-SASL. *J. Phys. Chem. B* **2008**, *112*, 16830-16842.
48. Stepien, P.; Polit, A.; Wisniewska-Becker, A., Comparative EPR studies on lipid bilayer properties in nanodiscs and liposomes. *Biochim. Biophys. Acta* **2015**, *1848* (1 Pt A), 60-66.
49. Erilov, D. A.; Bartucci, R.; Guzzi, R.; Shubin, A. A.; Maryasov, A. G.; Marsh, D.; Dzuba, S. A.; Sportelli, L., Water Concentration Profiles in Membranes Measured by ESEEM of Spin-Labeled Lipids. *J. Phys. Chem. B* **2005**, *109*, 12003-12013.
50. Eisermann, J.; Prager, L.; Hinderberger, D., Solvent and concentration effects on highly defined, colloid-like ionic clusters in solution. *Phys. Chem. Chem. Phys.* **2018**, *20* (3), 1421-1430.
51. Jamshad, M.; Grimard, V.; Idini, I.; Knowles, T. J.; Dowle, M. R.; Schofield, N.; Sridhar, P.; Lin, Y. P.; Finka, R.; Wheatley, M.; Thomas, O. R.; Palmer, R. E.; Overduin, M.; Govaerts, C.; Ruyschaert, J. M.; Edler, K. J.; Dafforn, T. R., Structural analysis of a nanoparticle containing a lipid bilayer used for detergent-free extraction of membrane proteins. *Nano Res.* **2015**, *8* (3), 774-789.
52. Kleinschmidt, J. H.; Mahaney, J. E.; Thomas, D. D.; Marsh, D., Interaction of Bee Venom Melittin with Zwitterionic and Negatively Charged Phospholipid Bilayers: A Spin-Label Electron Spin Resonance Study. *Biophys. J.* **1997**, *72*, 767-778.
53. Kattinig, D. R.; Bund, T.; Boggs, J. M.; Harauz, G.; Hinderberger, D., Lateral self-assembly of 18.5-kDa myelin basic protein (MBP) charge component-C1 on membranes. *Biochim. Biophys. Acta* **2012**, *1818* (11), 2636-2647.
54. Harauz, G.; Musse, A. A., A tale of two citrullines - structural and functional aspects of myelin basic protein deimination in health and disease. *Neurochem. Res.* **2007**, *32* (2), 137-158.
55. Marsh, D., Electron spin resonance in membrane research: protein-lipid interactions. *Methods* **2008**, *46* (2), 83-96.
56. Schneider, D. J.; Freed, J. H., Calculating Slow Motional Magnetic Resonance Spectra. In *Biological Magnetic Resonance*, Berliner, L. J.; Reuben, J., Eds. Plenum Press: New York, 1989; Vol. 8, Spin Labeling - Theory and Applications, pp 1-76.
57. Polverini, E.; Arisi, S.; Cavatorta, P.; Berzina, T.; Cristofolini, L.; Fasano, A.; Riccio, P.; Fontana, M. P., Interaction of Myelin Basic Protein with Phospholipid Monolayers: Mechanism of Protein Penetration. *Langmuir* **2003**, *19*, 872-877.
58. Pointer-Keenan, C. D.; Lee, D. K.; Hallok, K.; Tan, A.; Zand, R.; Ramamoorthy, A., Investigation of the interaction of myelin basic protein with phospholipid bilayers using solid-state NMR spectroscopy. *Chem. Phys. Lipids* **2004**, *132* (1), 47-54.

## 5 Discussion

The papers published in my doctorate studies cover different approaches of influencing lipids in supramolecular model systems by applying intramolecular or external constraints onto the lipid molecules.

Paper [P2] deals with the observation of characteristics of monolayers at the air/water interface containing a model ether and ester lipid, PHPC and DPPC, in comparison. The data presented in this publication is closely connected to earlier work shown in [P1]. The two studied lipids differ in the linkage between their *sn*-2 chain and the glycerol backbone. While DPPC contains two acyl chains, as is typical for phospholipids in most biological systems, PHPC comprises one ester bond in the *sn*-1 position and an ether bond in the *sn*-2 position. This somewhat small structural difference was found to induce a major rearrangement of the glycerol backbone in aqueous suspensions.<sup>53</sup>

The results collected in this dissertation suggest a similar effect in monolayers at the air/water interface. While the surface pressure isotherms of both lipids are comparable, additional measurements of IRRA spectra revealed different chain tilt angles in the liquid condensed lipid phase accompanied by an increased hydration of both the phosphate and the carbonyl group in PHPC. Furthermore, the methylene groups directly adjacent to the carbonyl moiety in *sn*-1 position, which is present in both lipids, are significantly more disordered in PHPC than in DPPC, *i.e.*, *gauche* conformers broaden the observable CH<sub>2</sub> wagging progression bands. The monolayer study presented in this thesis results similar lipid properties as in the bilayer system and is therefore discussed closely related to the bulk system.<sup>53</sup>

First, it is remarkable that a substitution of a carbonyl group with a methylene segment, that is the change from ester to ether bond, which presumably yields a more apolar glycerol region, causes increased hydration of the respective part of the lipid. In addition to hydrational changes, the ether linkage causes an altered ordering of the glycerol-near methylene segments. All of the observed differences between PHPC and DPPC are achievable only by rearranging the glycerol backbone in the lipid molecules. In diester lipids, such as DPPC, the glycerol is known to be orientated approximately perpendicular to the interface between lipid headgroups and the water in both bilayer and condensed monolayer systems.<sup>59-60,98</sup> In PHPC, in contrast, the ether bond in *sn*-2 position causes the glycerol backbone to be aligned approximately parallel to the bilayer (or monolayer) plane.<sup>53</sup> A similar effect is already known for phospholipids with altered chain positions, *i.e.*, 1,3-diacyl or 1,3-diamido phospholipids.<sup>99-100</sup> Intriguingly, a change as small as introducing an ether bond causes similar changes to the overall lipid orientation as interchanging the position of a whole chain and the headgroup on the glycerol backbone.

As a consequence, the water accessibility of the polar part of the lipid changes. This results in an altered lateral density in the headgroup region which could influence interactions with peripheral guest molecules such as peripheral membrane proteins.

Since not only the polar part of the lipid is affected by the structural changes but also the hydrophobic chains' tilt angle, the ether linkage influences the whole monolayer (or bilayer) of PHPC. The structural adaption of the whole lipid molecule probably has implications for native membranes in biological systems containing high amounts of ether lipids, such as membranes of extremophiles.<sup>44-46</sup> While both lipids and proteins in extremophile organisms adapted to their environment,<sup>46,101</sup> changes in the membrane structure have to be accompanied by adjustment of the membrane proteins.

This work is meant to cover the structural changes in the model system of the synthetic ether and ester lipids PHPC and DPPC. Thus, the obtained results are not directly applicable to natural systems, which contain a variety of different lipids including various headgroups, chain lengths, and degrees of saturation, and even membrane-spanning TELs.<sup>44-46</sup> To increase the relevance for biological systems, both model compounds are additionally studied in mixtures at the air/water interface.

Langmuir monolayers represent an excellent model system for the study of lipid/lipid interactions in mixtures.<sup>6</sup> The thermodynamics of miscibility are easily accessible through the measurement of compression isotherms on a film balance and can be complemented by epi-fluorescence microscopy and spectroscopic measurements such as IRRAS.<sup>6,102-103</sup> In the investigations presented here, the lipids PHPC and DPPC were found to be non-ideally miscible over the complete observed surface pressure range. However, in isotherms of PHPC/DPPC mixtures an additional kink or plateau in the isotherms was visible, that did not appear in isotherms of the pure lipids. The combination of fluorescence microscopy of PHPC/DPPC mixtures and IRRAS using PHPC and chain-perdeuterated DPPC-*d*<sub>62</sub> revealed that the additional plateaus were not caused by additional lipid phases induced by immiscibility. Both lipids undergo the main transition from liquid expanded to liquid condensed phase coherently but a delayed transition of the headgroup phosphates could be the cause of the plateau.

The non-ideal miscibility of PHPC and DPPC found in this study is probably caused by structural differences between both lipids as discussed before. Different glycerol backbone orientations of both lipids have to result in slight changes in the overall molecular shape of the lipids. Asymmetries between mixture components is known to result in non-ideal mixing behavior and even in immiscibility in extreme cases.<sup>104-105</sup>

The miscibility studies in this simple model system containing only two synthetic components highlight the importance of understanding lipid/lipid interactions for complex lipid mixtures. In nature, a variety of different compounds is involved in lipid membranes including phospholipids, sterols, and membrane proteins.<sup>43,46,101</sup> All molecules incorporated in the membrane contribute to its unique function and behavior and even small changes within the molecules can have a tremendous impact on the supramolecular system.

The second project presented here consists of two papers that deal with the interactions between amphiphilic copolymers and DMPC ([P4]) or myelin-like lipid mixtures ([P5]). [P3] provides the basis for this study by presenting the interactions between the same polymers and small molecules. In general, we took the same

approach for both lipid systems. We prepared liposomes of the respective lipids and added one of the studied copolymers, that are SMA,<sup>5,9,81</sup> DIBMA,<sup>13</sup> and SMA-SB. The mixtures of liposomes and polymer were then shaken for 16 hours at elevated temperature, *i.e.*, at 30 °C for DMPC and at 45 °C for the myelin-like liposomes. The successful formation of nanodiscs was examined by DLS measurement and for the best samples by electron microscopy.

The main goal of this project was to unravel the impact the polymers had on the lipids through shielding the hydrophobic lipid chains against the surrounding water. In the case of DMPC, this could be done by measuring DSC thermograms as was conducted for SMA and DIBMA before.<sup>13,81</sup> In [P4], the DSC results were additionally compared with temperature-dependent CW EPR spectroscopic measurements characterizing motional restrictions and hydrational changes within the bilayer in two different positions.<sup>12,20-23,106</sup> To this end, two lipid spin probes were introduced into the system, respectively, that are 1-palmitoyl-2-stearoyl-(5-doxyl)-*sn*-glycero-3-phosphocholine (5DSPC) and 1-palmitoyl-2-stearoyl-(16-doxyl)-*sn*-glycero-3-phosphocholine (16DSPC). The use of these spin probes allows probing the lipid properties in the center of the bilayer or near the carbonyls, separately, while avoiding major disturbances of the lipids.<sup>20-23</sup> We, first, studied the influence of the three copolymers on well-known DMPC bilayers in paper [P4] and, subsequently, characterized additional effects introduced by complex lipid mixtures in [P5], as is shown in the following.

The ability of SMA and DIBMA to solubilize DMPC liposomes is well-established.<sup>8-9,13</sup> From DSC experiments discussed in the literature, it is also known that both polymers exhibit different stress onto the bilayer due to aromatic side chains being able to penetrate the lipid chain region in contrast to aliphatic side chains.<sup>13</sup> CW EPR spectroscopy of lipids labeled in different chain positions revealed a general increase of motional restrictions caused by the polymers.<sup>12,83,107-108</sup> In paper [P4], we present the temperature-dependent CW EPR spectra of 5DSPC and 16DSPC in nanodiscs encapsulated by the established polymers SMA and DIBMA, and the new polymer SMA-SB.

Evaluation of the DSC thermograms of all nanodiscs in comparison with DMPC liposomes revealed a distinct broadening of the main melting transition of the DMPC gel phase to the fluid crystalline phase. This broadening has to be attributed to the decreased size of the cooperative unit of the transition due to the smaller size of the particles.<sup>13</sup> Furthermore, the main transition temperature  $T_m$  of DMPC liposomes was maintained in all studied nanodiscs. Additional measurement and simulation of CW EPR spectra showed clear impact of all three polymers on the segmental order parameter in both probed chain positions in accordance with literature, that is, all polymers increased the order of the lipid bilayer.<sup>12,83,107-108</sup> Solubilization of DMPC by the polymers also caused changes in lipid hydration. While the chain terminations, as probed with 16DSPC, were less hydrated in nanodiscs compared to liposomes, the carbonyl-near region experienced a higher degree of hydration. Changes of the hydration imply altered water accessibility of the lipid chains which is caused by the

surrounding polymers. Connected to the increased order, that is more pronounced in the bilayer center, the higher lateral density in the bilayer inhibits water penetration into the membrane core.

The additional constraints onto the bilayer that are caused by the encapsulating polymers were found to be slightly more pronounced for both styrene-containing polymers SMA and SMA-SB, which, again, supports literature conclusions.<sup>8,13</sup> The results of this research paper, therefore, support former evidence for aromatic polymer side chains being able to penetrate the bilayer, while aliphatic side chains, such as in DIBMA, had only minor effects. In addition, an ordering effect of all studied polymers has to be considered over large temperature ranges when applying nanodiscs for lipid and protein research.

In paper [P5], the study of polymer/lipid interactions was expanded to complex lipid mixtures resembling the cytosolic leaflet of the PNS or CNS myelin sheath.

The lipid mixtures used in this study consist of natural lipids, that were bought as purified extracts from pig brain (phosphatidylethanolamine, phosphatidylcholine, phosphatidylserine, and sphingomyelin) or bovine liver (phosphatidylinositol), as well as ovine cholesterol (44 % in CNS and 37 % in PNS).<sup>97</sup> Thus, the phospholipids were mainly unsaturated and contained various chain lengths. Recreating the known lipid compositions of cytosolic myelin, the applied lipid mixtures contained 15 % or 23 % negatively charged lipids for CNS- or PNS-resembling mixtures, respectively.<sup>24</sup> As mentioned in the theoretical chapter of this thesis, the composition of both studied lipid mixtures hinders efficient solubilization of liposomes by the amphiphilic copolymers used here.<sup>8,86</sup> However, it was possible to prepare nanodiscs from liposomes containing the lipids listed above with SMA and SMA-SB, although no complete solubilization could be achieved. DIBMA, in contrast, was not able to solubilize the studied lipid mixtures in an amount suitable for the use as myelin model system. To discriminate between not solubilized liposomes and newly formed nanodiscs, the liposomes had to be separated via size exclusion chromatography.

After formation of the nanodiscs, their lipid composition was studied using HPLC and MS. From the resulting data, it can be concluded that both SMA and SMA-SB preserve the liposomes' lipid composition in good approximation. Only minor preferences of SMA for phosphocholines and of SMA-SB for anionic lipids were observed. MS enabled the determination of the polymers' preferences for distinct chain lengths or degrees of unsaturation. We could show that in nanodiscs encapsulated by SMA or SMA-SB similar lipid chains were present as in liposomes. Concluding these experiments, the lipid composition of the prepared nanodiscs remains similar allowing further investigation of the lipid properties within the bilayer.

CW EPR spectroscopy using 5DSPC and 16DSPC revealed similar effects as in DMPC nanodiscs. While the polymers caused motional restrictions in the membrane core, they did not affect the rotational correlation time of 5DSPC to a similar extent. However, the anisotropy of rotation of the doxyl moiety near the lipids' carbonyl groups changed due to solubilization, *i.e.*, the probe's rotation became more isotropic in nanodiscs at elevated temperatures compared with liposomes. Interestingly, the center

of the bilayer was strongly influenced by the polymers depending on temperature. At low temperatures, an additional spectral component was necessary for simulating the measured spectra. This component featured a higher hydration accompanied by restricted motion. With increasing temperature, this spectral component vanished. Using DSC, we were able to rule out polymer-induced lipid transitions as a cause for this behavior. The conclusive interpretation we drew was that lipid/polymer interactions were responsible for the observed behavior. This means that at low temperatures the lipids interacted strongly with the surrounding polymer belt, which is detected by increased hydration and decreased mobility. With increasing temperature, this interaction got weaker.

Combination of the results from [P4] and [P5] leads to the following model for the main interaction patterns of the copolymers SMA, SMA-SB, and DIBMA with enclosed lipids. If the polymer's hydrophobic side chains are aromatic, they are able to penetrate the lipid chain region of the solubilized bilayer, which is supported by literature results.<sup>8,13</sup> In addition, the hydrophobicity of the whole polymer probably governs the approximate interaction area between the lipids and the polymer. The most hydrophobic polymer, SMA-SB, preferred interaction with the bilayer core where it had the strongest effects on the lipid mobility. SMA presented a similar, but weaker, impact on the lipids. DIBMA, as the third studied polymer, exerted less restrictions on DMPC bilayers than both aromatic polymers (compare reference 13). However, DIBMA was not able to solubilize more complex lipid mixtures to a suitable extent. The impact of polymer hydrophobicity is presented graphically in **Figure 5.1**.

Following the characterization of lipid properties, the myelin-like nanodiscs were further investigated for their ability to serve as a model system for the human myelin sheath. To this end, the protein bMBP was added which is known to act as a “molecular glue” between the cytosolic leaflets of native myelin.<sup>95-97</sup> It binds two opposing bilayers and, therefore, sticks the membranes together.<sup>95-97</sup> In the nanodisc system containing a myelin-like lipid composition of either the cytosolic PNS or CNS leaflet, it should be

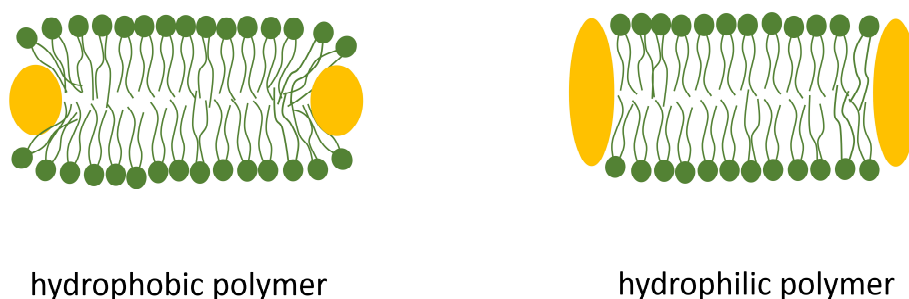


**Figure 5.1.** Schematic representation of lipid/polymer interactions depending on the polymer's hydrophobicity as discussed in the text. Polymer (yellow) and lipids are depicted in an abstract form disregarding the complexity of lipid mixtures including various chain lengths, headgroups, and degrees of saturation as well as cholesterol content.

able to stack the prepared nanodiscs. Using DLS and CW EPR spectroscopy, we found stacking of the nanodiscs in a native-like manner for myelin-like SMALPs. This was concluded from an increase in particle size and lipid/protein interactions as observed via broadened CW EPR spectra.

In this final part of the project, successful MBP-induced aggregation of the nanodiscs supported the potential of using myelin-like nanodiscs as a model system mimicking the human myelin sheath.

Comparison of all projects presented in this thesis reveals several similarities. Both the compression of monolayers at the air/water interface as well as manipulating temperature parallel to IRRA or CW EPR spectroscopic measurements provides the basis for understanding lipid phase transitions. The coupled IRRAS measurements or CW EPR spectroscopy enable complementary investigation of lipid order and hydration, both being featured in ordered/disordered transitions of the lipids as investigated in this thesis.<sup>26,109-110</sup> The results discussed before suggest quite similar effects occurring in monolayers and bilayers caused by a small intramolecular change within the lipid or by constraints exerted by exogenous polymers regarding hydrational properties of the lipids. As could be shown, the water accessibility of the lipids' chains was strongly dependent on the headgroup and chain geometry, on the one hand, and on surrounding molecules exerting steric restrictions on different parts of the lipid in the studied nanodisc systems, on the other hand.

The preparation of myelin-like nanodiscs from natural lipid mixtures containing mainly brain lipids and cholesterol combines all of the above presented topics. The lipid mixture used comprised ester and ether lipids, *i.e.*, they contained plasmalogens as was shown by MS measurements in [P5], highlighting the study of mixtures between these different phospholipids as was shown in [P2], exemplarily conducted with synthetic ester and ether lipids. In addition, the outcomes of the temperature-dependent study of DMPC nanodiscs in paper [P4] could be expanded with lipid/lipid interactions occurring in the complex myelin-like lipid mixtures and, therefore, contributes to the field of research with an easily accessible approach while preserving a natural-like system.

## 6 Conclusions and Outlook

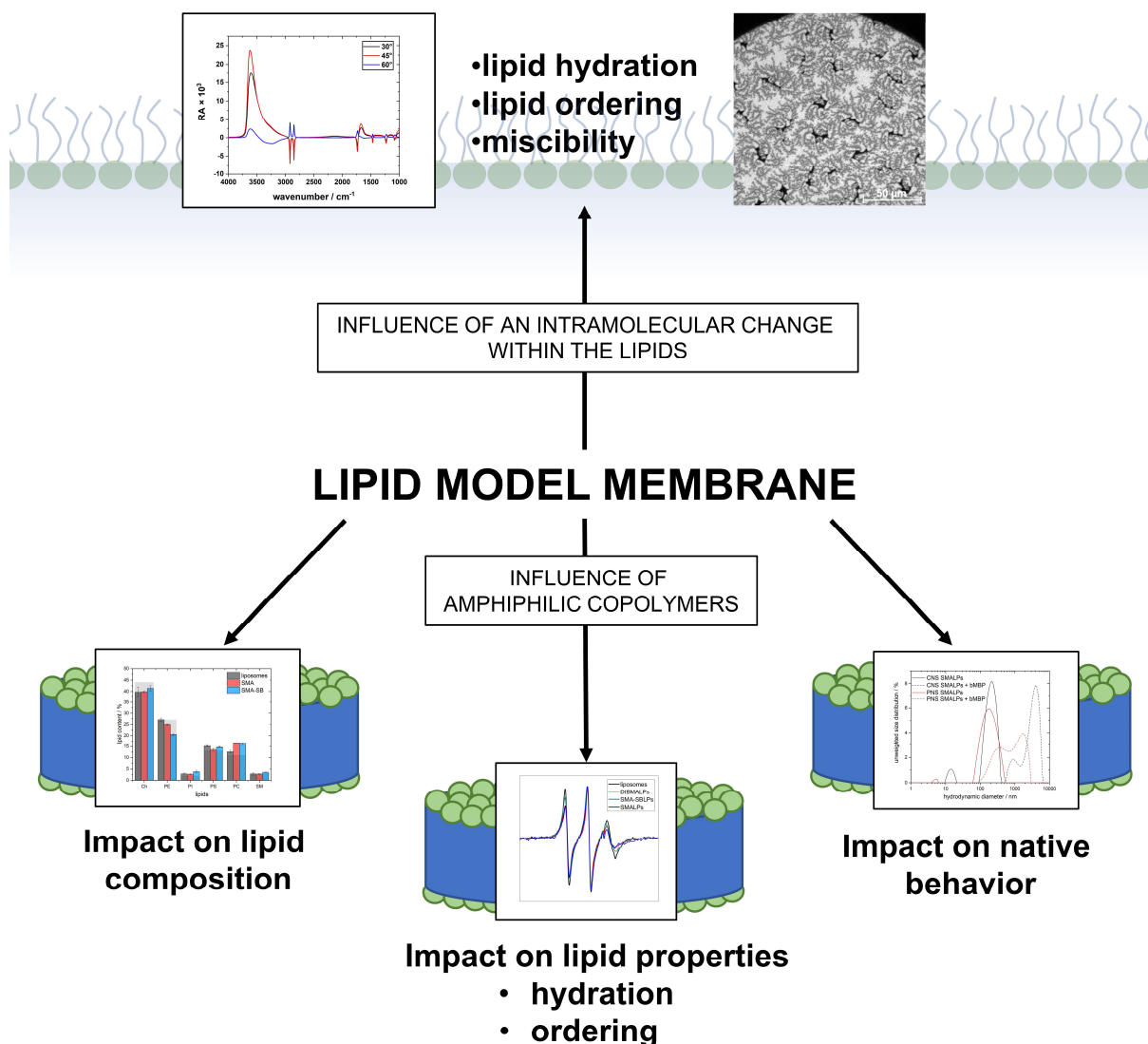


**Figure 6.1.** Graphical representation of the research done during the work for this thesis. The approach of, first, characterizing the influence of a molecular change within the lipids and, second, the impact of exogenous polymers on the properties of the supramolecular nanodiscs merge to a view on lipid model membranes from different perspectives.

During the work in my doctorate, I investigated a variety of factors influencing the lipid behavior in monolayers and bilayers. The study of systems of increasing complexity allowed stepwise interpretation of the impact of, first, an intramolecular change within the lipids forming the investigated supramolecular assembly and, second, amphiphilic copolymers surrounding different lipid bilayers resulting in polymer-encapsulated nanodiscs. The general approach used in this thesis is depicted graphically in **Figure 6.1**.

The comparative study of monolayers at the air/water interface containing the model lipids DPPC and PHPC in [P2] revealed major structural changes of the whole lipids

caused by a change as small as substituting the ester bond in *sn*-2 position with an ether linkage. This minor molecular difference resulted in rearrangement of the glycerol region, accompanied by hydrational changes of carbonyl and phosphate group, and by altered lipid chain tilt angle. Several mixtures of DPPC and PHPC showed non-ideal miscibility involving a coherent compression-dependent phase transition of the lipid chains followed by a headgroup transition.

This first part of the thesis shows that even small molecular changes of the lipids can affect the properties of the macroscopic model system formed by them. For increased biological significance, similar studies could elucidate the effect of natural ether lipids which are abundant in extremophiles, Archaea, and even in some human tissues.<sup>44-46,50-52</sup>

The second project presented here deals with the formation of nanodiscs from either model liposomes consisting of DMPC or myelin-like liposomes containing natural lipids in a composition resembling parts of the human myelin sheath. Here, the polymers as exogenous molecules exert additional constraints onto the lipid bilayer that influence the properties of the whole supramolecular assembly, as well.

In the context of this work, the main objective was to unravel different effects of the polymers on two regions of the lipid bilayer: the membrane center and the carbonyl-near chain region. Combining the results of [P4] and [P5] with the groundwork discussed in [P3], it can be concluded that two main properties of the polymers govern the mode of interaction with small molecules and lipids.

Firstly, the charge and hydrophobicity of the polymers play a role. The polymer's charge and its resulting zeta potential is the main property influencing interactions with small molecules and its hydrophobicity determines the interaction area between polymer and lipids in nanodiscs containing the studied complex lipid mixtures. SMA and DIBMA interact with other molecules mainly via coulombic forces, while the mode of action of the zwitterionic SMA-SB is driven mainly by weaker interactions with small molecules, such as hydrophobic forces (see [P3]). Incorporation of a myelin-like lipid bilayer leads to SMA covering a larger area of the lipids and SMA-SB interacting preferably with the hydrophobic membrane core. DIBMA in contrast was not able to solubilize the investigated complex lipid mixtures to a suitable extent. In addition, the charge of the polymer is involved in the first contact between solubilized liposomes and the polymer during nanodisc formation. In [P5] it could be shown by comparing the lipid preferences of SMA and SMA-SB that the charge difference between both polymers causes only minor differences in solubilized lipids. Interestingly, SMA-SB was able to solubilize slightly more anionic lipids compared with their abundance in the precursor liposomes and in SMALPs. For the studied lipid composition this effect was minor but it highlights the importance of using polymers of different charge adjusted to the lipid mixture that should be solubilized.

Secondly, the nature of the hydrophobic side chains governs the magnitude of the steric impact the polymers exert on the enclosed bilayer and presumably their ability to insert into the membrane during nanodisc formation. Polymers containing aromatic side chains, e.g., SMA and SMA-SB, were found to penetrate the bilayer to a higher

extent than polymers bearing aliphatic side chains such as DIBMA. In DMPC nanodiscs, this effect led to slightly stronger ordering of the lipids in SMALPs and SMA-SBLPs compared with DIBMALPs. In the study of myelin-like nanodiscs, this effect was not observable due to DIBMA not being able to solubilize the liposomes, in the first place. Because SMA solubilized the highest amount of lipids despite the polymer being negatively charged, the inability of DIBMA in nanodisc formation is probably mainly due to its inability to penetrate the already highly ordered myelin membrane.

In general, the addition of amphiphilic copolymers to liposomes can lead to changes in the membrane's water accessibility, lipid order, and lipid mobility as shown in both discussed papers [P4] and [P5]. The influence of the used polymer has to be considered by researchers for discussing the biological relevance of the observed results. However, polymer-encapsulated nanodiscs represent one of the best accessible model systems for lipid and membrane protein research. Possible differences between natural systems and nanodiscs are not fully understood and have to be studied further. In many cases deviations from natural characteristics are even compensated by the advantages of using nanodisc-forming polymers, such as avoiding detergents in protein purification or the ability to mimic natural system like the myelin sheath.

Paper [P5] presents a possible application of nanodiscs in protein research in detail. We could show that the myelin protein bMBP was able to aggregate myelin-like nanodiscs in a presumably native-like manner. This paper covers the basics of preparing a model system that could be refined to mimic the whole human myelin sheath. To this end, several other proteins could be incorporated and the asymmetrical membrane composition of the cytosolic and the extracellular leaflet of the myelin membrane should be addressed. Furthermore, bMBP represents a peripheric membrane protein.<sup>97</sup> To this point, the studied myelin-like nanodiscs were not used to characterize transmembrane proteins, yet. A suitable candidate for future research is the myelin protein P0, which contains a transmembrane helix and both an intra- and extracellular domain and connects three myelin bilayers via protein/lipid and protein/protein interactions.<sup>111</sup>

In conclusion, this thesis contributes to several research fields including the monolayer studies of ether lipids, characterization of interaction mechanisms between lipids and polymers in nanodiscs, and the introduction of a model system resembling the human myelin sheath, as is presented schematically in **Figure 6.1**. The results gathered during this dissertation highlight the importance of understanding properties of the systems of interest that may be considered as trivial by many researchers studying protein functions and seeking applicability despite the lipids' properties and restrictions having an immediate effect on incorporated transmembrane proteins, for instance. While many principles of influences on lipid properties could be elucidated here, every result evokes a variety of new questions that this outlook cannot fully cover, which, of course, is the main driving force in science.

## 7 References

1. Chan, Y. H. M.; Boxer, S. G., Model membrane systems and their applications. *Curr. Opin. Chem. Biol.* **2007**, *11* (6), 581-587.
2. Lewis, R. N. A. H.; Prenner, E. J.; Kondejewski, L. H.; Flach, C. R.; Mendelsohn, R.; Hodges, R. S.; McElhaney, R. N., Fourier Transform Infrared Spectroscopic Studies of the Interaction of the Antimicrobial Peptide Gramicidin S with Lipid Micelles and with Lipid Monolayer and Bilayer Membranes. *Biochem.* **1999**, *38*, 15193-15203.
3. Österlund, N.; Luo, J.; Wärmländer, S. K. T. S.; Gräslund, A., Membrane-mimetic systems for biophysical studies of the amyloid-beta peptide. *Biochim. Biophys. Acta Proteins Proteom.* **2019**, *1867* (5), 492-501.
4. Peetla, C.; Stine, A.; Labhasetwar, V., Biophysical Interactions with Model Lipid Membranes: Applications in Drug Discovery and Drug Delivery. *Mol. Pharm.* **2009**, *6* (5), 1264-1276.
5. Dörr, J. M.; Scheidelaar, S.; Koorengevel, M. C.; Dominguez, J. J.; Schäfer, M.; van Walree, C. A.; Killian, J. A., The styrene-maleic acid copolymer: a versatile tool in membrane research. *Eur. Biophys. J.* **2016**, *45* (1), 3-21.
6. Blume, A., Lipids at the air–water interface. *ChemTexts* **2018**, *4* (1), 3.
7. Blume, A.; Kerth, A., Peptide and protein binding to lipid monolayers studied by FT-IRRA spectroscopy. *Biochim. Biophys. Acta Biomembr.* **2013**, *1828* (10), 2294-2305.
8. Scheidelaar, S.; Koorengevel, M. C.; Dominguez Pardo, J.; Meeldijk, J. D.; Breukink, E.; Killian, J. A., Molecular model for the solubilization of membranes into nanodisks by styrene maleic Acid copolymers. *Biophys. J.* **2015**, *108* (2), 279-290.
9. Knowles, T. J.; Finka, R.; Smith, C.; Lin, Y. P.; Dafforn, T.; Overduin, M., Membrane Proteins Solubilized Intact in Lipid Containing Nanoparticles Bounded by Styrene Maleic Acid Copolymer. *J. Am. Chem. Soc.* **2009**, *131*, 7484-7485.
10. Jamshad, M.; Grimard, V.; Idini, I.; Knowles, T. J.; Dowle, M. R.; Schofield, N.; Sridhar, P.; Lin, Y. P.; Finka, R.; Wheatley, M.; Thomas, O. R. T.; Palmer, R. E.; Overduin, M.; Govaerts, C.; Ruysschaert, J. M.; Edler, K. J.; Dafforn, T. R., Structural analysis of a nanoparticle containing a lipid bilayer used for detergent-free extraction of membrane proteins. *Nano Res.* **2015**, *8* (3), 774-789.
11. Kopf, A. H.; Dörr, J. M.; Koorengevel, M. C.; Antoniciello, F.; Jahn, H.; Killian, J. A., Factors influencing the solubilization of membrane proteins from Escherichia coli membranes by styrene-maleic acid copolymers. *Biochim. Biophys. Acta Biomembr.* **2020**, *1862* (2), 183125.
12. Colbasevici, A.; Voskoboinikova, N.; Orekhov, P. S.; Bozdaganyan, M. E.; Karlova, M. G.; Sokolova, O. S.; Klare, J. P.; Mulkidjanian, A. Y.; Shaitan, K. V.; Steinhoff, H. J., Lipid dynamics in nanoparticles formed by maleic acid-containing copolymers: EPR spectroscopy and molecular dynamics simulations. *Biochim. Biophys. Acta Biomembr.* **2020**, *1862* (5), 183207.
13. Oluwole, A. O.; Danielczak, B.; Meister, A.; Babalola, J. O.; Vargas, C.; Keller, S., Solubilization of Membrane Proteins into Functional Lipid-Bilayer Nanodiscs Using a Diisobutylene/Maleic Acid Copolymer. *Angew. Chem. Int. Ed.* **2017**, *56* (7), 1919-1924.
14. Dilworth, M. V.; Findlay, H. E.; Booth, P. J., Detergent-free purification and reconstitution of functional human serotonin transporter (SERT) using

- diisobutylene maleic acid (DIBMA) copolymer. *Biochim. Biophys. Acta Biomembr.* **2021**, 1863 (7), 183602.
15. Spector, A. A.; Yorek, M. A., Membrane lipid composition and cellular function. *J. Lipid Res.* **1985**, 26 (9), 1015-1035.
  16. van der Veen, J. N.; Kennelly, J. P.; Wan, S.; Vance, J. E.; Vance, D. E.; Jacobs, R. L., The critical role of phosphatidylcholine and phosphatidylethanolamine metabolism in health and disease. *Biochim. Biophys. Acta Biomembr.* **2017**, 1859 (9 Pt B), 1558-1572.
  17. Akutsu, H.; Ikematsu, M.; Kyogoku, Y., Molecular Structure and Interaction of Dipalmitoyl Phosphatidylcholine in Multilayers. Comparative Study with Phosphatidylethanolamine. *Chem. Phys. Lipids* **1981**, 28, 149-158.
  18. Ali, S.; Minchey, S.; Janoff, A.; Mayhew, E., A Differential Scanning Calorimetry Study of Phosphocholines Mixed with Paclitaxel and Its Bromoacylated Taxanes. *Biophys. J.* **2000**, 78, 246-256.
  19. Lewis, R. N. A. H.; McElhaney, R. N., Membrane lipid phase transitions and phase organization studied by Fourier transform infrared spectroscopy. *Biochim. Biophys. Acta Biomembr.* **2013**, 1828 (10), 2347-2358.
  20. Erilov, D. A.; Bartucci, R.; Guzzi, R.; Shubin, A. A.; Maryasov, A. G.; Marsh, D.; Dzuba, S. A.; Sportelli, L., Water Concentration Profiles in Membranes Measured by ESEEM of Spin-Labeled Lipids. *J. Phys. Chem. B* **2005**, 109, 12003-12013.
  21. Kurad, D.; Jeschke, G.; Marsh, D., Lipid Membrane Polarity Profiles by High-Field EPR. *Biophys. J.* **2003**, 85, 1025-1033.
  22. Stepien, P.; Polit, A.; Wisniewska-Becker, A., Comparative EPR studies on lipid bilayer properties in nanodiscs and liposomes. *Biochim. Biophys. Acta Biomembr.* **2015**, 1848 (1 Pt A), 60-66.
  23. Vartorelli, M. R.; Garay, A. S.; Rodrigues, D. E., Spin-labeled Stearic Acid Behavior and Perturbations on the Structure of a Gel-Phase-Lipid Bilayer in Water: 5-, 12- and 16-SASL. *J. Phys. Chem. B* **2008**, 112, 16830-16842.
  24. Inouye, H.; Kirschner, D. A., Membrane Interactions in Nerve Myelin: II. Determination of Surface Charge from Biochemical Data. *Biophys. J.* **1988**, 53, 247-260.
  25. Mendelsohn, R.; Mao, G.; Flach, C. R., Infrared reflection-absorption spectroscopy: Principles and applications to lipid-protein interaction in Langmuir films. *Biochim. Biophys. Acta Biomembr.* **2010**, 1798 (4), 788-800.
  26. Mendelsohn, R.; Brauner, J. W.; Gericke, A., External Infrared Reflection Absorption Spectrometry of Monolayer Films at the Air-Water Interface. *Annu. Rev. Phys. Chem.* **1995**, 46, 305-334.
  27. Flach, C. R.; Gericke, A.; Mendelsohn, R., Quantitative Determination of Molecular Chain Tilt Angles in Monolayer Films at the Air/Water Interface: Infrared Reflection/Absorption Spectroscopy of Behenic Acid Methyl Ester. *J. Phys. Chem. B* **1997**, 101, 58-65.
  28. Schrettl, S.; Stefaniu, C.; Schwieger, C.; Pasche, G.; Oveisi, E.; Fontana, Y.; Fontcuberta i Morral, A.; Reguera, J.; Petraglia, R.; Corminboeuf, C.; Brezesinski, G.; Frauenrath, H., Functional carbon nanosheets prepared from hexayne amphiphile monolayers at room temperature. *Nat. Chem.* **2014**, 6 (6), 468-476.
  29. Schwieger, C.; Chen, B.; Tschierske, C.; Kressler, J.; Blume, A., Organization of T-shaped facial amphiphiles at the air/water interface studied by infrared reflection absorption spectroscopy. *J. Phys. Chem. B* **2012**, 116 (40), 12245-12256.

30. Schwieger, C.; Meister, A.; Daum, S.; Blume, A.; Bacia, K., Binding of the GTPase Sar1 to a Lipid Membrane Monolayer: Insertion and Orientation Studied by Infrared Reflection-Absorption Spectroscopy. *Polymers* **2017**, *9* (11), 612.
31. Barth, A.; Zscherp, C., What vibrations tell us about proteins. *Q. Rev. Biophys.* **2002**, *35* (4), 369-430.
32. Hoernke, M.; Mohan, J.; Larsson, E.; Blomberg, J.; Kahra, D.; Westenhoff, S.; Schwieger, C.; Lundmark, R., EHD2 restrains dynamics of caveolae by an ATP-dependent, membrane-bound, open conformation. *Proc. Natl. Acad. Sci. USA* **2017**, *114* (22), E4360–E4369.
33. Dicko, A.; Bourque, H.; Pézolet, M., Study by infrared spectroscopy of the conformation of dipalmitoylphosphatidylglycerol monolayers at the air–water interface and transferred on solid substrates. *Chem. Phys. Lipids* **1998**, *96*, 125-139.
34. Neuhaus, F.; Mueller, D.; Tanasescu, R.; Stefaniu, C.; Zaffalon, P. L.; Balog, S.; Ishikawa, T.; Reiter, R.; Brezesinski, G.; Zumbuehl, A., Against the rules: pressure induced transition from high to reduced order. *Soft Matter* **2018**, *14* (19), 3978-3986.
35. Jeschke, G.; Schlick, S.; Earle, K. A.; Budil, D. E., ESR Fundamentals. In *Advanced ESR Methods in Polymer Research*, Schlick, S., Ed. John Wiley & Sons: Hoboken, New Jersey, 2006; pp 1-98.
36. Scheffler, K.; Stegmann, H. P., *Elektronenspinresonanz - Grundlagen und Anwendung in der organischen Chemie*. Springer: Heidelberg, 1970.
37. Schweiger, A., Pulsed Electron Spin Resonance Spectroscopy: Basic Principles, Techniques, and Examples of Applications. *Angew. Chem. Int. Ed.* **1991**, *30* (3), 265-292.
38. Hinderberger, D. Polyelectrolytes and Their Counterions Studied by EPR Spectroscopy. Johannes-Gutenberg-Universität Mainz, Mainz, 2004.
39. van Doorslaer, S.; Murphy, D. M.; Schleicher, E.; Weber, S.; Hinderberger, D.; Drescher, M.; Bordignon, E.; Krstic, I.; Endeward, B.; Margraf, D.; Marko, A.; Prisner, T. F.; van Slageren, J., *EPR Spectroscopy Applications in Chemistry and Biology*. Springer: Heidelberg, 2012.
40. Antholine, W. E.; Bobst, A. M.; Chignell, C. F.; Dalton, L. R.; Hsia, J. C.; Hyde, J. S.; Keana, J. F. W.; Miller, W. G.; Piette, L. H.; Swartz, H. M., *Spin Labeling: Theory and Applications*. Academic Press: London, 1979; Vol. 2.
41. Berliner, L. J.; Butler, K. W.; Freed, J. H.; Gaffney, B. J.; Griffith, O. H.; Jost, P.; Krugh, T. R.; Lajzerowicz-Bonneteau, J.; Luckhurst, G. R.; McConnell, H. M.; Morrisett, J. D.; Nordio, P. L.; Seelig, J.; Smith, I. C. P., *Spin Labeling: Theory and Applications*. Academic Press: London, 1976; Vol. 1.
42. Isabel Collado, M.; Goni, F. M.; Alonso, A.; Marsh, D., Domain Formation in Sphingomyelin/Cholesterol Mixed Membranes Studied by Spin-Label Electron Spin Resonance Spectroscopy. *Biochem.* **2005**, *44*, 4911-4918.
43. Szlaza, W.; Zendran, I.; Zalesinska, A.; Tarek, M.; Kulbacka, J., Lipid composition of the cancer cell membrane. *J. Bioenerg. Biomembr.* **2020**, *52* (5), 321-342.
44. de Rosa, M.; Gambacorta, A.; Gliozzi, A., Structure, Biosynthesis, and Physicochemical Properties of Archaeobacterial Lipids. *Microbiol. Rev.* **1986**, *50*, 70-80.
45. Fuhrhop, J. H.; Wang, T., Bolaamphiphiles. *Chem. Rev.* **2004**, *104*, 2901-2937.

46. van de Vossenberg, J. L. C. M.; Driessen, A. J. M.; Konings, W. N., The essence of being extremophilic: the role of the unique archaeal membrane lipids. *Extremophiles* **1998**, *2*, 163-170.
47. Waite, M., Phospholipases. In *Biochemistry of Lipids, Lipoproteins and Membranes*, 2 ed.; Vance, D. E.; Vance, J. E., Eds. Elsevier: Amsterdam, 1991; pp 269-295.
48. Grit, M.; Zuidam, N. J.; Underberg, W. J. M.; Crommelin, D. J. A., Hydrolysis of Partially Saturated Egg Phosphatidylcholine in Aqueous Liposome Dispersions and the Effect of Cholesterol Incorporation on Hydrolysis Kinetics. *J. Pharm. Pharmacol.* **1993**, *45*, 490-495.
49. Kensil, C. R.; Dennis, E. A., Alkaline Hydrolysis of Phospholipids in Model Membranes and the Dependence on Their State of Aggregation. *Biochem.* **1981**, *20*, 6079-6085.
50. Benjamin, D. I.; Cozzo, A.; Ji, X.; Roberts, L. S.; Louie, S. M.; Mulvihill, M. M.; Luo, K.; Nomura, D. K., Ether lipid generating enzyme AGPS alters the balance of structural and signaling lipids to fuel cancer pathogenicity. *Proc. Natl. Acad. Sci. USA* **2013**, *110* (37), 14912-14917.
51. Braverman, N. E.; Moser, A. B., Functions of plasmalogen lipids in health and disease. *Biochim. Biophys. Acta* **2012**, *1822* (9), 1442-1452.
52. Leßig, J.; Fuchs, B., Plasmalogens in Biological Systems: Their Role in Oxidative Processes in Biological Membranes, their Contribution to Pathological Processes and Aging and Plasmalogen Analysis. *Curr. Med. Chem.* **2009**, *16*, 2021-2041.
53. Lewis, R. N. A. H.; Pohle, W.; McElhaney, R. N., The Interfacial Structure of Phospholipid Bilayers: Differential Scanning Calorimetry and Fourier Transform Infrared Spectroscopic Studies of 1,2-Dipalmitoyl-sn-Glycero-3-Phosphorylcholine and Its Dialkyl and Acyl-Alkyl Analogs. *Biophys. J.* **1996**, *70*, 2736-2746.
54. McIntosh, T. J.; McDaniel, R. V.; Simon, S. A., Induction of an Interdigitated Gel Phase in fully Hydrated Phosphatidylcholine Bilayers. *Biochim. Biophys. Acta* **1983**, *731*, 109-114.
55. Serrallach, E. N.; Dijkman, R.; de Haas, G. H.; Shipley, G. G., Structure and Thermotropic Properties of 1,3-Dipalmitoyl-glycero-2-phosphocholine. *J. Mol. Biol.* **1983**, *170*, 155-174.
56. Smith, E. A.; Dea, P. K., Differential Scanning Calorimetry Studies of Phospholipid Membranes: The Interdigitated Gel Phase. In *Applications of Calorimetry in a Wide Context*, Elkordy, A. A., Ed. IntechOpen: Rijeka, 2013; pp 407-444.
57. Arrondo, J. L. R.; Goni, F. M.; Macarulla, J. M., Infrared Spectroscopy of Phosphatidylcholines in Aqueous Suspension. A Study of the Phosphate Group Vibrations. *Biochim. Biophys. Acta* **1984**, *794*, 165-168.
58. Blume, A.; Hübner, W.; Messner, G., Fourier Transform Infrared Spectroscopy of <sup>13</sup>C=O-Labeled Phospholipids Hydrogen Bonding to Carbonyl Groups. *Biochem.* **1988**, *27*, 8239-8249.
59. Hauser, H.; Pascher, I.; Pearson, R. H.; Sundell, S., Preferred Conformation and Molecular Packing of Phosphatidylethanolamine and Phosphatidylcholine. *Biochim. Biophys. Acta* **1981**, *650*, 21-51.
60. Hauser, H.; Pascher, I.; Sundell, S., Preferred Conformation and Dynamics of the Glycerol Backbone in Phospholipids. An NMR and X-ray Single-Crystal Analysis. *Biochem.* **1988**, *27*, 9166-9174.

61. Brezesinski, G.; Dietrich, A.; Dobner, B.; Möhwald, H., Morphology and structures in double-, triple- and quadruple-chain phospholipid monolayers at the air/water interface. *Progr. Colloid Polym. Sci.* **1995**, *98*, 255-262.
62. Brezesinski, G.; Dietrich, A.; Struth, B.; Böhm, C.; Bouwman, W. G.; Kjaer, K.; Möhwald, H., Influence of ether linkages on the structure of double-chain phospholipid monolayers. *Chem. Phys. Lipids* **1995**, *76*, 145-157.
63. Lee, S. C.; Pollock, N. L., Membrane proteins: is the future disc shaped? *Biochem. Soc. Trans.* **2016**, *44* (4), 1011-1018.
64. Parmar, M. J.; De Marcos Lousa, C.; Muench, S. P.; Goldman, A.; Postis, V. L., Artificial membranes for membrane protein purification, functionality and structure studies. *Biochem. Soc. Trans.* **2016**, *44* (3), 877-882.
65. Tribet, C.; Audebert, R.; Popot, J. L., Amphipols: Polymers that keep membrane proteins soluble in aqueous solutions. *Proc. Natl. Acad. Sci. USA* **1996**, *93*, 15047-15050.
66. le Maire, M.; Champeil, P.; Moller, J. V., Interaction of membrane proteins and lipids with solubilizing detergents. *Biochim. Biophys. Acta* **2000**, *1508*, 86-111.
67. Rigaud, J. L.; Pitard, B.; Levy, D., Reconstitution of membrane proteins into liposomes: application to energy-transducing membrane proteins. *Biochim. Biophys. Acta* **1995**, *1231*, 223-246.
68. Poget, S. F.; Girvin, M. E., Solution NMR of membrane proteins in bilayer mimics: Small is beautiful, but sometimes bigger is better. *Biochim. Biophys. Acta Biomembr.* **2007**, *1768* (12), 3098-3106.
69. Tamm, L. K.; Liang, B., NMR of membrane proteins in solution. *Prog. Nucl. Magn. Reson. Spectrosc.* **2006**, *48* (4), 201-210.
70. Diller, A.; Loudet, C.; Aussenac, F.; Raffard, G.; Fournier, S.; Laguerre, M.; Grélard, A.; Opella, S. J.; Marassi, F. M.; Dufourc, E. J., Bicelles: A natural 'molecular goniometer' for structural, dynamical and topological studies of molecules in membranes. *Biochimie* **2009**, *91* (6), 744-751.
71. Hein, C.; Henrich, E.; Orbán, E.; Dötsch, V.; Bernhard, F., Hydrophobic supplements in cell-free systems: Designing artificial environments for membrane proteins. *Eng. Life Sci.* **2014**, *14* (4), 365-379.
72. Zoonens, M.; Popot, J. L., Amphipols for each season. *J. Membr. Biol.* **2014**, *247* (9-10), 759-796.
73. Bayburt, T. H.; Grinkova, Y. V.; Sligar, S. G., Self-Assembly of Discoidal Phospholipid Bilayer Nanoparticles with Membrane Scaffold Proteins. *Nano Lett.* **2002**, *2*, 853-856.
74. Hernández-Rocamora, V. M.; García-Montanes, C.; Rivas, G., Phospholipid Bilayer Nanodiscs: A Powerful Tool to Study the Structural Organization and Biochemical Reactivity of Proteins in Membrane-like Environments. *Curr. Top. Med. Chem.* **2014**, *14*, 2637-2646.
75. Denisov, I. G.; Sligar, S. G., Nanodiscs in Membrane Biochemistry and Biophysics. *Chem. Rev.* **2017**, *117* (6), 4669-4713.
76. Esmaili, M.; Brown, C. J.; Shaykhtudinov, R.; Acevedo-Morantes, C.; Wang, Y. L.; Wille, H.; Gandour, R. D.; Turner, S. R.; Overduin, M., Homogeneous nanodiscs of native membranes formed by stilbene-maleic-acid copolymers. *Nanoscale* **2020**, *12* (32), 16705-16709.
77. Ravula, T.; Hardin, N. Z.; Ramadugu, S. K.; Cox, S. J.; Ramamoorthy, A., Formation of pH-Resistant Monodispersed Polymer-Lipid Nanodiscs. *Angew. Chem. Int. Ed.* **2018**, *57* (5), 1342-1345.

78. Ravula, T.; Ramadugu, S. K.; Di Mauro, G.; Ramamoorthy, A., Bioinspired, Size-Tunable Self-Assembly of Polymer-Lipid Bilayer Nanodiscs. *Angew. Chem. Int. Ed.* **2017**, *56* (38), 11466-11470.
79. Scheidelaar, S.; Koorengevel, M. C.; van Walree, C. A.; Dominguez, J. J.; Dörr, J. M.; Killian, J. A., Effect of Polymer Composition and pH on Membrane Solubilization by Styrene-Maleic Acid Copolymers. *Biophys. J.* **2016**, *111* (9), 1974-1986.
80. Hall, S. C. L.; Tognoloni, C.; Price, G. J.; Klumperman, B.; Edler, K. J.; Dafforn, T. R.; Arnold, T., Influence of Poly(styrene-co-maleic acid) Copolymer Structure on the Properties and Self-Assembly of SMALP Nanodiscs. *Biomacromolecules* **2018**, *19* (3), 761-772.
81. Grethen, A.; Oluwole, A. O.; Danielczak, B.; Vargas, C.; Keller, S., Thermodynamics of nanodisc formation mediated by styrene/maleic acid (2:1) copolymer. *Sci. Rep.* **2017**, *7* (1), 11517.
82. Cunningham, R. D.; Kopf, A. H.; Elenbaas, B. O. W.; Staal, B. B. P.; Pfukwa, R.; Killian, J. A.; Klumperman, B., Iterative RAFT-Mediated Copolymerization of Styrene and Maleic Anhydride toward Sequence- and Length-Controlled Copolymers and Their Applications for Solubilizing Lipid Membranes. *Biomacromolecules* **2020**, *21* (8), 3287-3300.
83. Orwick, M. C.; Judge, P. J.; Procek, J.; Lindholm, L.; Graziadei, A.; Engel, A.; Gröbner, G.; Watts, A., Detergent-free formation and physicochemical characterization of nanosized lipid-polymer complexes: Lipodisq. *Angew. Chem. Int. Ed.* **2012**, *51* (19), 4653-4657.
84. Vargas, C.; Cuevas Arenas, R.; Frotscher, E.; Keller, S., Nanoparticle self-assembly in mixtures of phospholipids with styrene/maleic acid copolymers or fluorinated surfactants. *Nanoscale* **2015**, *7* (48), 20685-20696.
85. Cuevas Arenas, R.; Klingler, J.; Vargas, C.; Keller, S., Influence of lipid bilayer properties on nanodisc formation mediated by styrene/maleic acid copolymers. *Nanoscale* **2016**, *8* (32), 15016-15026.
86. Jakubec, M.; Barias, E.; Furse, S.; Govasli, M. L.; George, V.; Turcu, D.; Iashchishyn, I. A.; Morozova-Roche, L. A.; Halskau, O., Cholesterol-containing lipid nanodiscs promote an alpha-synuclein binding mode that accelerates oligomerization. *FEBS J.* **2021**, *288* (6), 1887-1905.
87. Cuevas Arenas, R.; Danielczak, B.; Martel, A.; Porcar, L.; Breyton, C.; Ebel, C.; Keller, S., Fast Collisional Lipid Transfer Among Polymer-Bounded Nanodiscs. *Sci. Rep.* **2017**, *7*, 45875.
88. Danielczak, B.; Keller, S., Collisional lipid exchange among DIBMA-encapsulated nanodiscs (DIBMALPs). *Eur. Polym. J.* **2018**, *109*, 206-213.
89. Danielczak, B.; Keller, S., Lipid exchange among polymer-encapsulated nanodiscs by time-resolved Förster resonance energy transfer. *Methods* **2020**, *180*, 27-34.
90. Grethen, A.; Glueck, D.; Keller, S., Role of Coulombic Repulsion in Collisional Lipid Transfer Among SMA(2:1)-Bounded Nanodiscs. *J. Membr. Biol.* **2018**, *251* (3), 443-451.
91. Krishnarajana, B.; Ravula, T.; Ramamoorthy, A., Detergent-free extraction, reconstitution and characterization of membrane-anchored cytochrome-b5 in native lipids. *Chem. Commun.* **2020**, *56* (48), 6511-6514.
92. Voskoboynikova, N.; Karlova, M.; Kurre, R.; Mulkidjanian, A. Y.; Shaitan, K. V.; Sokolova, O. S.; Steinhoff, H. J.; Heinisch, J. J., A Three-Dimensional Model of the Yeast Transmembrane Sensor Wsc1 Obtained by SMA-Based Detergent-

- Free Purification and Transmission Electron Microscopy. *J. Fungi* **2021**, *7* (2), 118.
93. Nave, K. A.; Werner, H. B., Myelination of the nervous system: mechanisms and functions. *Annu. Rev. Cell Dev. Biol.* **2014**, *30*, 503-533.
  94. Tzakos, A. G.; Kursula, P.; Theodorou, V.; Troganis, A.; Tselios, T.; Svarnas, C.; Matsoukas, J.; Apostolopoulos, V.; Gerothanassis, I. P., Structure and Function of the Myelin Proteins: Current Status and Perspectives in Relation to Multiple Sclerosis. *Curr. Med. Chem.* **2005**, *12*, 1569-1587.
  95. Bakhti, M.; Aggarwal, S.; Simons, M., Myelin architecture: zippering membranes tightly together. *Cell. Mol. Life Sci.* **2014**, *71* (7), 1265-1277.
  96. Harauz, G.; Musse, A. A., A tale of two citrullines-structural and functional aspects of myelin basic protein deimination in health and disease. *Neurochem. Res.* **2007**, *32* (2), 137-158.
  97. Widder, K.; Träger, J.; Kerth, A.; Harauz, G.; Hinderberger, D., Interaction of Myelin Basic Protein with Myelin-like Lipid Monolayers at Air-Water Interface. *Langmuir* **2018**, *34* (21), 6095-6108.
  98. Bayerl, T. M.; Thomas, R. K.; Penfold, J.; Rennie, A.; Sackmann, E., Specular reflection of neutrons at phospholipid monolayers: Changes of monolayer structure and headgroup hydration at the transition from the expanded to the condensed phase state. *Biophys. J.* **1990**, *57*, 1095-1098.
  99. Büldt, G.; de Haas, G. H., Conformational Differences between sn-3-Phospholipids and sn-2-Phospholipids: A Neutron and X-ray Diffraction Investigation. *J. Mol. Biol.* **1982**, *158*, 55-71.
  100. Fedotenko, I. A.; Stefaniu, C.; Brezesinski, G.; Zumbuehl, A., Monolayer properties of 1,3-diamidophospholipids. *Langmuir* **2013**, *29* (30), 9428-9435.
  101. Kumar, A.; Alam, A.; Tripathi, D.; Rani, M.; Khatoon, H.; Pandey, S.; Ehtesham, N. Z.; Hasnain, S. E., Protein adaptations in extremophiles: An insight into extremophilic connection of mycobacterial proteome. *Semin. Cell Dev. Biol.* **2018**, *84*, 147-157.
  102. Mattjus, P.; Bittman, R.; Slotte, J. P., Molecular Interaction and Lateral Domain Formation in Monolayers Containing Cholesterol and Phosphatidylcholines with Acyl- or Alkyl-Linked C16 Chains. *Langmuir* **1996**, *12*, 1284-1290.
  103. Dörfler, H. D., Mixing behavior of binary insoluble phospholipid monolayers. Analysis of the mixing properties of binary lecithin and cephalin systems by application of several surface and spreading techniques. *Adv. Colloid Interface Sci.* **1990**, *31*, 1-110.
  104. Dupuy, F.; Maggio, B., The hydrophobic mismatch determines the miscibility of ceramides in lipid monolayers. *Chem. Phys. Lipids* **2012**, *165* (6), 615-629.
  105. Mabrey, S.; Sturtevant, J. M., Investigation of phase transitions of lipids and lipid mixtures by high sensitivity differential scanning calorimetry. *Proc. Natl. Acad. Sci. USA* **1976**, *73*, 3862-3866.
  106. Marsh, D., Distinct Populations in Spin-Label EPR Spectra from Nitroxides. *J. Phys. Chem. B* **2018**, *122* (23), 6129-6133.
  107. Bali, A. P.; Sahu, I. D.; Craig, A. F.; Clark, E. E.; Burrige, K. M.; Dolan, M. T.; Dabney-Smith, C.; Konkolewicz, D.; Lorigan, G. A., Structural characterization of styrene-maleic acid copolymer-lipid nanoparticles (SMALPs) using EPR spectroscopy. *Chem. Phys. Lipids* **2019**, *220*, 6-13.
  108. Voskoboynikova, N.; Margheritis, E. G.; Kodde, F.; Rademacher, M.; Schowe, M.; Budke-Gieseck, A.; Psathaki, O. E.; Steinhoff, H. J.; Cosentino, K., Evaluation of DIBMA nanoparticles of variable size and anionic lipid content as

- tools for the structural and functional study of membrane proteins. *Biochim. Biophys. Acta Biomembr.* **2021**, 1863 (6), 183588.
109. Schindler, H.; Seelig, J., EPR spectra of spin labels in lipid bilayers. *J. Chem. Phys.* **1973**, 59 (4), 1841-1850.
  110. Sułkowski, W. W.; Pentak, D.; Nowak, K.; Sułkowska, A., The influence of temperature and pH on the structure of liposomes formed from DMPC. *J. Mol. Struct.* **2006**, 792-793, 257-264.
  111. Raasakka, A.; Ruskamo, S.; Kowal, J.; Han, H.; Baumann, A.; Myllykoski, M.; Fasano, A.; Rossano, R.; Riccio, P.; Bürck, J.; Ulrich, A. S.; Stahlberg, H.; Kursula, P., Molecular structure and function of myelin protein P0 in membrane stacking. *Sci. Rep.* **2019**, 9 (1), 642.

## 8 List of Abbreviations and Symbols

### 8.1 Abbreviations

5DSPC	1-palmitoyl-2-stearoyl-(5-doxyl)- <i>sn</i> -glycero-3-phosphocholine
16DSPC	1-palmitoyl-2-stearoyl-(16-doxyl)- <i>sn</i> -glycero-3-phosphocholine
bMBP	bovine myelin basic protein
CD	circular dichroism
CNS	central nervous system
CW EPR	continuous wave electron paramagnetic resonance
DIBMA	poly-(diisobutylene- <i>alt</i> -maleic acid)
DLS	dynamic light scattering
DMPC	1,2-dimyristoyl- <i>sn</i> -glycero-3-phosphocholine
DPPC	1,2-dipalmitoyl- <i>sn</i> -glycero-3-phosphocholine
DPPC- <i>d</i> <sub>62</sub>	1,2-dipalmitoyl- <i>d</i> <sub>62</sub> - <i>sn</i> -glycero-3-phosphocholine
DSC	differential scanning calorimetry
HPLC	high performance liquid chromatography
IR	infrared
IRRAS	infrared reflection absorption spectroscopy
MBP	myelin basic protein
MS	mass spectrometry
MSP	membrane scaffold protein
NMR	nuclear magnetic resonance
PC	phosphocholine
PHPC	1-palmitoyl-2- <i>O</i> -hexadecyl- <i>sn</i> -glycero-3-phosphocholine
PNS	peripheral nervous system
SEC	size exclusion chromatography
SMA	poly-(styrene- <i>co</i> -maleic acid)
SMA-SB	poly-(styrene- <i>co</i> -maleimide sulfobetaine)
TEL	tetraether lipid
TEM	transmission electron microscopy
UV	ultraviolet
xLP	polymer/lipid particle with x being either SMA, SMA-SB, or DIBMA

## 8.2 Symbols

$L_{\beta'}$	lamellar gel phase of lipids
$L_{\beta I}$	interdigitated gel phase of lipids
$L_c$	crystalline phase of lipids
$m_s$	electron spin quantum number
$P_{\beta'}$	rippled gel phase of lipids
$R$	reflectivity of the monolayer-covered interface
$RA$	reflectance-absorbance
$R_{ref}$	reflectivity of the surface without monolayer
$T_m$	main transition temperature of lipids

## 9 Acknowledgments

First of all, I thank Prof. Dariush Hinderberger for his excellent supervision and all scientific and personal discussions not only in the last two and a half years but also during my Master's studies. I want to thank him especially for all the scientific freedom I had during my work. This was just perfectly suited for my working methods and I very much appreciate how I was able to raise numerous new questions from every answer I got and that I could commit my work to such interesting topics.

Furthermore, I want to thank Prof. Heinz-Jürgen Steinhoff for being the second lecturer of this thesis.

In addition, my thanks go to all my collaborators and colleagues. In the first place, I want to thank Dr. Christian Schwieger and Dr. Simon Drescher for introducing me to the whole world of biophysical research and all fruitful discussions we had. Of the number of people, I worked with, I want to highlight Florian Schöffmann, Dr. Jana Eisermann, David Haselberger, and Annkatrin Rother. I am thankful for all input and teaching I got which made a dissertation possible in such a short time, in the first place. Besides the already mentioned people, I also want to thank Dr. Andreas Kerth, Andreas Kampe, Melanie Kampe, and all other colleagues for helping in every possible way and the outstanding working climate in the group.

Of course, this dissertation would not have been possible without the help of many other collaborators for which I am very thankful. From them, I want to mention especially Prof. Sandro Keller, Dr. Annette Meister, Kevin Janson, Dr. Tommy Hofmann, and Lisa Müller but this addresses also all other people who contributed to this work.

For all regards not work related I also want to give my special thanks to my friends outside my workgroup, especially Justus and Sarah Thümmeler.

At this point, I want to thank my family for all the support I got over the years enabling me to choose the subject of chemistry and to complete my studies. In particular, I thank my wife Jessi for supporting me in every facet in good days and keeping me sane in all other times for nearly one decade now.

At last, I want to thank the "Fonds der Chemischen Industrie" for the generous financial support in my work.

## 10 Academic Curriculum Vitae

### Persönliche Daten

Name	Matthias Hoffmann
Geburtsdatum	9. April 1995
Geburtsort	Gotha

### Akademischer Werdegang

- 2019-2022 Promotion  
Martin-Luther-Universität Halle-Wittenberg,  
bei Prof. D. Hinderberger („Komplexe selbstorganisierende Systeme“)
- 2016-2018 Masterstudium Chemie  
Martin-Luther-Universität Halle Wittenberg  
Abschluss: Master of Science (Durchschnittsnote 1,0)  
Thema der Masterarbeit:  
„Organisation, Phasenverhalten und Reaktivität von Azidolipid-Monoschichten  
an der Wasser-Luft-Grenzfläche“ (Note 1,0)
- 2013-2016 Bachelorstudium Chemie  
Martin-Luther-Universität Halle-Wittenberg  
Abschluss: Bachelor of Science (Durchschnittsnote 1,5)  
Thema der Bachelorarbeit:  
„Einfluss einer mizellaren Umgebung auf die Photoionisierung und  
Regeneration der Rotweinantioxidans Resveratrol“ (Note 1,7)
- 2005-2013  
Staatliches Gymnasium Arnoldischule Gotha  
Abschluss: Abitur (Durchschnittsnote 1,0)

### Auszeichnungen

- 2019-2021 Förderung durch den Fonds der Chemischen Industrie (FCI) im  
Rahmen eines Kekulé-Stipendiums
- 2017-2018 Deutschlandstipendium
- 2013 „Arnoldipreis“ für den Jahrgangsbesten des Abiturjahrgangs und  
GDCh-Preis für den jahrgangsbesten Abiturienten im Fach Chemie an der  
Arnoldischule Gotha

## Publikationen

- M. Hoffmann, D. Haselberger, T. Hofmann, L. Müller, K. Janson, A. Meister, M. Das, C. Vargas, S. Keller, P. L. Kastritis, C. Schmidt, D. Hinderberger, „A Nanoscale Model System for the Human Myelin Sheath“, *Biomacromolecules* **2021**, *22*, 3901-3912.
- M. Hoffmann, J. Eisermann, F. A. Schöffmann, M. Das, C. Vargas, S. Keller, D. Hinderberger, “Influence of Different Polymer Belts on Lipid Properties in Nanodiscs Characterized by CW EPR Spectroscopy”, *BBA Biomembranes* **2021**, *1863 (10)*, 183681.
- J. Eisermann, M. Hoffmann, F.A. Schöffmann, M. Das, C. Vargas, S. Keller, D. Hinderberger, „Molecular-level interactions of nanodisc-forming copolymers dissected by EPR spectroscopy“, *Macromol. Chem. Phys.* **2021**, *222*, 2100051.
- M. Hoffmann, S. Drescher, C. Schwieger, D. Hinderberger, „Influence of a Single Ether Bond on Assembly, Orientation, and Miscibility of Phosphocholine Lipids at the Air-Water Interface” *Phys. Chem. Chem. Phys.* **2021**, *23*, 5325-5339.
- M. Hoffmann; S. Drescher; C.H. Ihling; D. Hinderberger; C. Schwieger, „An azidolipid monolayer – transitions, miscibility, and UV reactivity studied by infrared reflection absorption spectroscopy” *Langmuir* **2020**, *36*, 12804-12815.
- C. Kerzig, M. Hoffmann, M. Goetz, „Resveratrol radical repair by vitamin C at the micelle-water interface: unexpected reaction rates explained by ion-dipole interactions” *Chem. Eur. J.* **2018**, *24*, 3038-3044.

Halle (Saale), 10. Februar 2022